Specific diagnostics needs for different machines

G. Kube
Deutsches Elektronen Synchrotron (DESY), Hamburg, Germany

Abstract
Beam diagnostics and instrumentation are an essential part of any accelerator. There is a large variety of parameters to be measured for observation of particle beams with the precision required to tune, operate, and improve the performance of the machine. However, depending on the type of accelerator, for the same parameter the working principle of a monitor may strongly differ, and thus the requirements for accuracy. This report will give an overview of selected types of accelerators in order to illustrate specific diagnostics needs which must be taken into account before designing a new instrument.

1 Introduction

Nowadays particle accelerators play an important role in a wide number of fields where a primary or secondary beam from an accelerator can be used for industrial or medical applications or for basic and applied research. The interaction of such beams with matter is exploited i) in order to analyse physical, chemical, or biological samples (example: particle-induced X-ray emission, PIXE), ii) for a modification of physical, chemical, or biological sample properties (example: sterilization), or iii) for fundamental research in basic subatomic physics. Table 1 shows a compilation of different accelerator applications [1] based on the year 2000. As can be seen, more than half of these accelerators are devoted to modification processes: ion implantation, surface modifications, industrial applications in the main for sterilization and polymerization.

Table 1: Worldwide inventory of particle accelerators in the year 2000 [1]

Category	Number
Ion implanters and surface modifications	7 000
Accelerators in industry	1 500
Accelerators in non-nuclear research	1 000
Radiotherapy	5 000
Medical isotope production	200
Hadron therapy	20
Synchrotron radiation sources	70
Nuclear and particle physics research	110
Total	15 000

In order to cover such a wide range of applications, different accelerator types are required. As an example, in art the Louvre museum utilizes the 2 MV tandem Pelletron accelerator AGLAE for ion beam analysis (IBA) studies [2]. Cyclotrons are often used to produce medical isotopes for positron emission tomography (PET) and single-photon-emission computed tomography (SPECT). For electron radiotherapy, mainly linear accelerators (linacs) are in operation, while cyclotrons or synchrotrons are additionally used for proton therapy [3]. Third-generation synchrotron light sources are electron synchrotrons, while the new fourth-generation light sources (free electron lasers) operating at short wavelengths are electron linac-based accelerators. Examples of these type of machines are SLAC/LCLS or DESY/FLASH and XFEL. Neutrino beams for elementary particle physics are produced with large proton synchrotrons, and in linear or circular colliders different species of particles are brought into collision. To give a few examples, this is realized with e^+e^- beams (SLAC/PEP II, KEK/KEKB, LNF/DAΦNE, BINP/VEPP4, CERN/LEP, and the future international linear collider ILC), with ep beams (DESY/HERA), with $p\bar{p}$ beams (FNAL/Tevatron), with pp beams (CERN/LHC), and with different ion–ion beams (BNL/RHIC: Au–Au, CERN/LHC: Pb–Pb). Reference [4] gives an overview of the large accelerator-based facilities together with proposals for the next generation of machines with emphasis on elementary particle physics.

As seen from this short list there exists a large number of accelerator types with different properties, and as a consequence the demands on beam diagnostics and instrumentation vary depending on machine type and application. To cover all these cases is out of the focus of this report. Linear and circular accelerators for high energy physics and synchrotron radiation applications are the primary concern, but nevertheless connections to other types of accelerators will be provided. However, before going into details, the first question to pose is about the beam parameters of interest and about the information that can be gained from their measurement.

1.1 Beam parameters and diagnostics

This section gives an overview of primary beam parameters together with examples for values which can be deduced. This list is far from complete, more details can be found in specific textbooks or lecture notes as in Refs. [5–7].

One of the first questions in the commissioning of a new accelerator is how many particles are in the machine, i.e., the *beam intensity* is one of the most important accelerator parameters. This can be a measurement of the bunch current (charge), of the dc current, or of both. With knowledge of the intensity it is possible to determine lifetime and coasting beam in circular machines, or transfer efficiencies in linacs and transfer lines.

One of the next questions which arises may be where these particles are located, i.e., the *position* of the beam centroid. Position measurements give access to a wide number of very important accelerator parameters. The most fundamental one is the determination of the beam orbit from which lattice parameters can be deduced. Position measurements are also required for tune measurements and the determination of the chromaticity; they are a fundamental part of feedback systems and more.

The next question might be how distribution of particles in space looks, i.e., the *beam profile* in both transversal and longitudinal dimensions are of interest. Beam size measurements are fundamental for the determination of the beam emittance; time resolved beam size studies give information about injection mismatch (betatron and dispersion matching) via the observation of turn-by-turn shape oscillations, or about dynamical processes as, for example, the study of beam blow up of individual bunches under collision in a particle collider. Furthermore beam halo diagnostics rely mainly on measurements of the transverse beam size.

Another parameter of interest is the *beam energy*, but mainly for users. In a lepton collider, for example, it defines the reaction energy which is available in order to produce new particles, while in synchrotron light sources (third-generation as well as free-electron-lasers — FELs) it defines the spectral characteristics of the emitted radiation.

In a collider the *luminosity* is the key parameter because it defines the count rate of the reaction channel under investigation. While an absolute online-luminosity determination is sometimes difficult to provide, the determination of a relative luminosity or simply a count rate which is proportional to it is a very important tool for the collision optimization (angle and position) of both beams via beam steering with local bumps.

In order to identify the position of beam losses, to prevent damage to the accelerator as well as to facility components, and to optimize the daily accelerator operation, *beam loss* monitors represent a very important diagnostics system.

In the next sections examples of these systems for different accelerator types will be given. Nevertheless, depending on the type of accelerator, there might be even more beam parameters of interest. In heavy-ion machines, for example, the determination of particle charge states and mass numbers are essential for the accelerator operation. However, these parameters are out of the focus of this report, more details can be found, e.g., in Refs. [6, 7].

1.2 General aspects of beam diagnostics

Depending on the operational mode of an accelerator there exist different requirements for beam diagnostics. Sometimes they cannot be fulfilled with only one device. As a consequence, two or more instruments are needed in order to measure the same beam parameter under different operational conditions because the dynamical range of a single device may not be sufficient.

One can roughly distinguish between two different modes of operation and summarize their impact on beam instrumentation:

1. diagnostics for accelerator (section) commissioning
   - applied in order to adjust the beam transport through different accelerator sections
   - required for the characterization of the beam behind each accelerator section
   - simple and robust devices with high sensitivity, allowing to operate with single or few bunches of low intensity
   - low or modest demands on accuracy
   - applications of beam disturbing methods are possible
2. diagnostics for standard operation
   - applied for precise beam characterization in order to control and improve the accelerator operation
   - required for the diagnosis of unwanted errors and to trigger interlocks
   - devices are typically based on more or less sophisticated schemes
   - high demands on accuracy
   - application of minimum beam disturbing schemes

As can be seen from this comparison even one accelerator already has specific diagnostics needs for different operational modes. However, the aim of this report is to compare the diagnostics requirements for different accelerators. Probably the most intuitive way to classify different accelerator types is to distinguish between linear and circular machines. The discussion of this way of classification is the subject of the next section.

1.3 Linear versus circular accelerators

In order to judge this way of classification, the basic differences of these accelerator concepts will be recalled in the following:

A linear accelerator has many accelerating cavities through which the beam passes once. One can consider a linac as an ‘open loop’ system in the sense that there exists no possibility for an orbit feedback, and everything depends on the start parameters. Furthermore a linac is a pulsed system. This means that the signals generated by the beam are a sequence of single events which may vary from shot to shot, a formation of an equilibrium state is not possible. In a linac, emittance and energy are a function of the location in the accelerator. Because the charge can be lost everywhere in the machine, many devices for transfer measurements are required. In case of beam loss in the machine the gun will supply charge until it is stopped, e.g., by an interlock.

In contrast to that a circular accelerator or storage ring has only a small number of accelerating cavities. It can be understood as a ‘closed loop’ system in the sense that there exists a periodical solution for the particle orbit, and an orbit feedback is possible. Owing to the closed loop behaviour resonances can occur in the system. A storage ring is a continuous wave (cw) system, the signals from the beam are repetitive and stable, in general, for many turns. It is possible that the beam reaches a kind of equilibrium state, and with it also the beam generated signals. Therefore high precision can be achieved by averaging, and the signals are typically treated in the frequency domain. Emittance and beam current are non- or slowly varying parameters. In case of a beam loss there are no particles in the storage ring until the beam is transferred again through the injector chain.

From the preceding comparison of these fundamental accelerator concepts it can be concluded that there are differences in the way beam generated signals are treated and processed. However, the beam diagnostics instruments which are used in both accelerator types are the same in the sense that there is no fundamental difference in the working principles of the monitor.

For deeper understanding, the next section considers the underlying physical principles of beam instrumentation. Based on that discussion a classification of diagnostics requirements for different accelerators will be worked out.

2 Beam monitors and underlying physical processes

The monitor concepts applied to particle beam diagnostics rely typically on one of the following physical processes:

- influence of the particle electromagnetic field,
- Coulomb interaction of charged particles penetrating matter,
- nuclear or elementary particle physics interactions,
- interactions of particles with photon beams.

In the following these processes are discussed in more detail, especially in view of the application in beam diagnostics for different types of particles.

2.1 Influence of the particle electromagnetic field

The influence of the particle electromagnetic field can be applied in two ways for beam diagnostic purposes.

Firstly the *non-propagating fields* can be used, i.e., the fields which are bound to the particle. The monitor principle relies on the electromagnetic influence of the moving charge on the environment (e.g., beam pipe). This influence is typically converted into a voltage or a current which can be measured on a low or high frequency scale. Examples of such types of monitors are beam transformers or pick-ups.

Secondly the *propagating fields* can be exploited, i.e., the fields which are not bound and propagate away from the moving particle as emitted photons. In this case the beam information is encoded in the photon intensity, and depending on the photon frequency (energy) it can be measured with various types of photon detectors with sensitivities ranging from the infrared up to the γ-ray region. Examples for such types of instruments are synchrotron radiation and optical transition radiation (OTR) monitors.

A comprehensive and illustrative discussion about the electromagnetic fields of a moving charged particle can be found, for example, in Ref. [8] and the report in these proceedings [9]. In both cases the contraction of the field components is widely exploited, i.e., the fact that for ultrarelativistic velocities the electric field is mainly transversal as illustrated in Fig. 1. The field contraction is characterized by the so-called Lorentz factor

$$\gamma = E/m_0c^2 \tag{1}$$

with E the total particle energy and m_0c^2 the rest mass energy. In the following the term *rest mass* will be used for the latter.

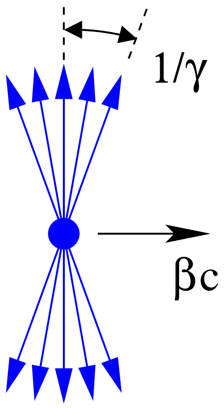

Fig. 1: Electric field lines of a uniformly moving charge with speed $v = \beta\, c$ as seen in in the laboratory frame

The proton is the lightest hadron and has a rest mass $m_p c^2 = 938.272$ MeV. Compared with this the electron e^- and its anti-particle, the positron e^+ are much lighter with $m_e c^2 = 0.511$ MeV (unless mentioned otherwise in the following, the name *electron* stands for both particles). Therefore, for a given total beam energy E, the field distribution of an electron is much more compressed than for a hadron. Figure 2 shows a comparison of the non–propagating transverse electric fields for an electron and a proton at a kinetic particle energy $E_{\text{kin}} = E - m_0 c^2 = 20$ GeV. As can be seen, the electron's transverse field component is more than 3 orders of magnitude larger, and the time interval during which the field is seen by an observer at a distance ρ away from the beam trajectory is about 3 orders shorter. From this comparison it can be concluded that a beam monitor based on the influence of the transverse electromagnetic field will have a much higher sensitivity to electrons than to hadrons, assuming the particles have the same energy.

The same holds for the case of propagating fields as can be seen from the calculated synchrotron radiation power shown in Fig. 3 for a proton and an electron. While the spectrum of electron synchrotron radiation extends up to the hard X-ray region, the proton spectrum has its maximum at centimetre wavelengths which are not of interest for standard applications and beam diagnostics purposes. Therefore for hadron beams the emission of synchrotron radiation emission (and also other radiation phenomena like transition radiation, diffraction radiation, Smith–Purcell radiation) is strongly suppressed. This has important consequences not only for beam diagnostics but also for particle beam dynamics as discussed later.

2.2 Coulomb interaction of charged particles penetrating matter

Charged particles penetrating matter transfer energy to the medium, either directly or indirectly, via the process of ionization or excitation of the constituent atoms. This can be observed as charged ions, for example in a gas counter, or as luminescent light. The techniques in use are therefore based on current measurements or on light observation by optical methods. Examples of such types of monitors are scintillators, viewing screens, and residual gas monitors.

The energy loss of particles in matter is described by the Bethe–Bloch equation. In the 'low energy approximation' it can be written as [10]

$$-\frac{\mathrm{d}E}{\mathrm{d}x} = 4\pi N_A\, r_e^2\, m_e c^2\, \frac{Z_t}{A_t}\, \rho_t\, \frac{Z_p^2}{\beta^2} \left[\ln \frac{2 m_e c^2 \gamma^2 \beta^2}{I} - \beta^2 \right] . \tag{2}$$

Equation (2) depends on some constants (N_A: Avogadro number; $m_e c^2$: electron rest mass; r_e: classical electron radius), on target material properties (ρ_t: material density; A_t, Z_t: atomic mass and nuclear charge; I: mean excitation energy), and on particle properties (Z_p: projectile charge; $\beta = v/c$: reduced particle speed). Figure 4 shows the energy loss for single charged particles in different target materials.

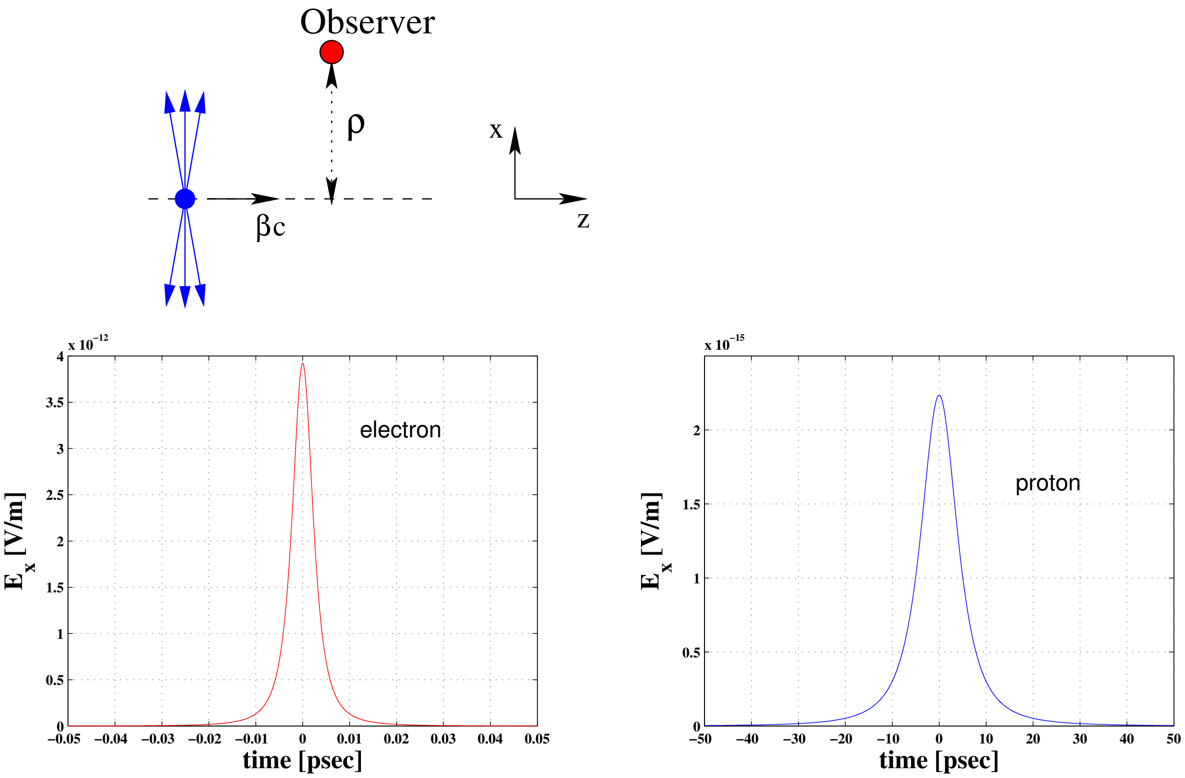

Fig. 2: Transverse electric field component for an electron (left) and a proton (right) moving uniformly with 20 GeV kinetic energy, as seen by an observer at a distance $\rho = 40$ mm away from the beam trajectory

The Bethe–Bloch equation is a quite accurate description of the energy loss of hadrons and heavy leptons (muons) in matter. From the structure of this equation it can be concluded that a high energy deposition in material is to be expected for particles with high charge Z_p and low velocity β. This is especially the case for heavy-ion beams. On the other hand, for the lighter electrons the energy loss due to electronic stopping is less pronounced, but they have an additional channel to lose their energy when traversing matter. Already at a few MeV particle energy radiative effects (i.e., the emission of bremsstrahlung) play an important role, see Fig. 4. The critical energy E_c defines that value where the energy loss due to bremsstrahlung and ionization is the same. It is approximately given by [10]

$$E_c = \frac{610 \text{ MeV}}{Z + 1.24} \quad \text{(solids and liquids)} , \qquad = \frac{710 \text{ MeV}}{Z + 0.92} \quad \text{(gases)} , \tag{3}$$

and for lead this value amounts to $E_c \approx 7.3$ MeV, cf. Fig. 4.

From this discussion it can be seen again that there is a difference in the monitor signal generation for hadron beams and for electron/positron beams.

2.3 Nuclear or elementary particle physics interactions

Nuclear or elementary particle physics interactions arise between beam particles and a fixed target, or in particle collisions of two counter-propagating beams. The signal of interest is a particle flux measured with nuclear or elementary particle physics detectors. With knowledge of the relevant reaction cross-section a beam quantity can be deduced. Examples of these types of monitors are beam loss and luminosity monitors. Also in this case hadrons and electrons behave differently.

Electrons are point-like objects. The interaction cross-section into their final states can be calculated very precisely in the frame of quantum electrodynamics (QED) resp. electroweak theory. They interact via the electroweak force, and electromagnetic showers typically have a rather short range.

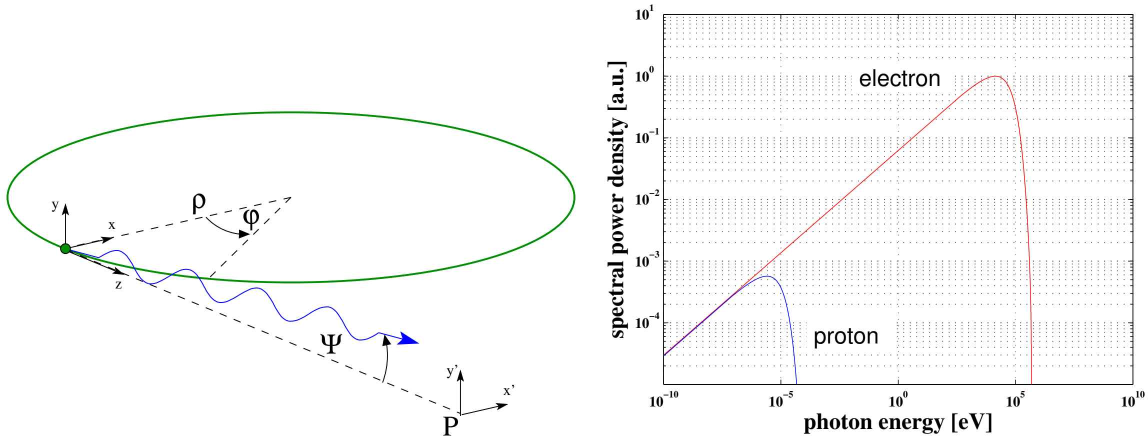

Fig. 3: Synchrotron radiation spectral power density for an electron and a proton, moving with 20 GeV kinetic energy on a circular orbit with radius $\rho = 370$ m. The visible spectral region extends from about 1.6 eV to 3.3 eV photon energy.

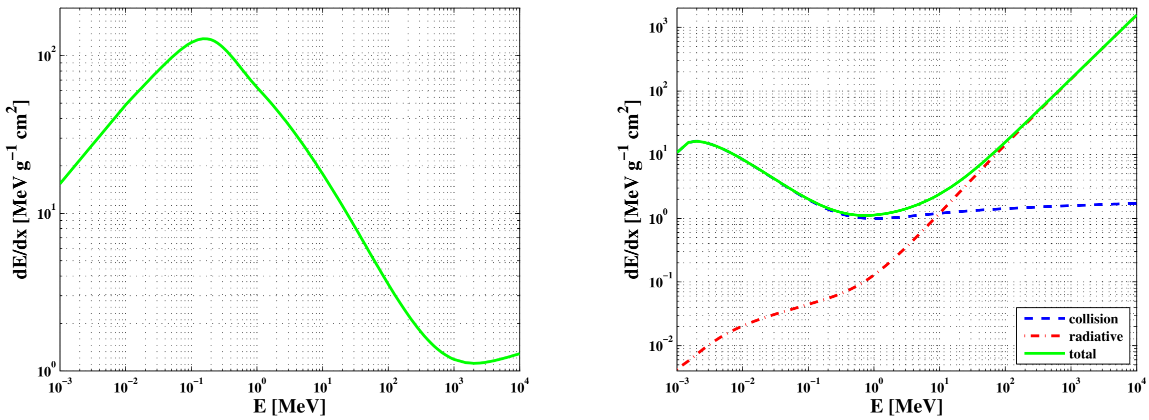

Fig. 4: Stopping power for protons (left) and electrons (right) in lead ($Z = 82$) as function of the projectile energy. According to Eq. (3) the critical energy is $E_c \approx 7.3$ MeV. The calculations were performed with the programs *pstar* and *estar* from Ref. [11].

In contrast to that hadrons have a constituent nature. The lightest one, the proton, is already a collection of quarks and gluons. Hadrons interact also via the strong force. The interaction cross-sections calculated in the frame of quantum chromodynamics (QCD) are less accurate. Protons with beam energies above a few GeV typically produce secondaries via hadronic showers, including pions, neutrals, muons etc. Hadronic showers typically have a longer range than electromagnetic ones.

2.4 Interaction of particles with photon beams

For the interaction of particles with photons a high power laser beam is usually scanned across the particle beam profile. Monitors based on this type of interaction are laser wire scanners or Compton polarimeters.

In the case of electron beams a flux of inverse Compton scattered photons is measured. The Compton differential cross-section is given by the Klein–Nishina formula [12]

$$\frac{\mathrm{d}\sigma}{\mathrm{d}\Omega} = \frac{r_e^2}{2} \left(\frac{\hbar\omega_s}{\hbar\omega_i}\right)^2 \left(\frac{\hbar\omega_s}{\hbar\omega_i} + \frac{\hbar\omega_i}{\hbar\omega_s} - \sin^2\theta\right) \tag{4}$$

with $r_e = e^2/m_e c^2$ the classical electron radius, $\hbar\omega_{i,s}$ the photon energy of the incident/scattered photon, and θ the polar angle. If light scattering on other beam particles is considered, the classical electron radius has to be replaced by the relevant particle radius which scales inversely proportional to the particle rest mass. As a consequence Compton scattering at heavier particles is strongly suppressed, and this type of monitor is applied only for electron beams.

For hadron and especially H^- beams a different mechanism is used, the laser photo neutralization. The cross-section for this process has its maximum at a photon wavelength of $\lambda \approx 900$ nm [13]. In this monitor a Nd:YAG laser beam ($\lambda = 1064$ nm, about 90% of maximum cross-section) is scanned across the H^- beam to photoneutralize narrow slices, i.e., the laser photons knock off electrons from the H^- ions. The liberated electrons are collected to provide a direct measurement of the beam profile. The process of laser photoneutralization is used not only for beam diagnostics purposes as a high power H^- beam profile monitor, but also for charge exchange injection in high intensity proton rings in order to replace conventionally used stripping foils [14].

2.5 Conclusion

The discussion in this section shows that there are fundamental differences in signal generation and underlying physical processes applied for beam instrumentation between an electron machine and a hadron machine. In some cases this requires completely different monitor concepts even for the measurement of the same beam parameter.

As a consequence, the emphasis in the following two sections will be on diagnostics for hadron accelerators, first for storage rings together with their injection chain and then for selected hadron machines. In the subsequent section the diagnostics for electron accelerators will be described. This includes diagnostics for lepton storage rings and for synchrotron light sources.

3 Diagnostics for hadron colliders and storage rings

There exist a number of large hadron colliders and storage rings in the world. Examples in Europe are the Large Hadron Collider (LHC) at CERN, the planned heavy-ion facility FAIR at GSI (Germany), and the Hadron Electron Ring Anlage (HERA) at DESY which was recently shut down.

The key parameter for each particle collider is the luminosity $\mathfrak{L}$. It quantifies the collider performance and relates the reaction cross-section (a property of the interaction itself) with the event rate which is the primary concern for the experiments:

$$\dot{N} = \mathfrak{L}\,\sigma\ . \tag{5}$$

However, apart from the necessity to measure the luminosity which requires an additional beam monitor, from the diagnostics point of view there is no difference between a collider and a storage ring. Therefore in the following no distinction will be made between these types of machines.

3.1 General considerations

In the following some general aspects of beam diagnostics will be discussed which are common for all high energy hadron machines and their injector chain.

First of all the high beam energy requires superconducting magnets to achieve the required dipole magnetic field for particle bending. In order to obtain superconductivity, the magnets have to be cooled down with the consequence that parts of the beam diagnostics instrumentation are located in the cold vacuum system. Furthermore, a superconducting environment requires reliable beam-loss monitors which are an integral part of a fast quench-protection system needed to avoid an uncontrolled transition from the superconducting to the normal-conducting state which may easily damage the magnets.

The second point is that these high particle energies cannot be reached in one single machine, i.e., a long injector chain is typically required in order to achieve the final beam energy. Figure 5 gives an overview of the ep collider HERA at DESY [15] with 920 GeV proton energy and 27.5 GeV electron energy together with the injector complex. However, a long injector chain means that there exist several pre–accelerators with beam properties which involve different requirements for beam diagnostics and instrumentation.

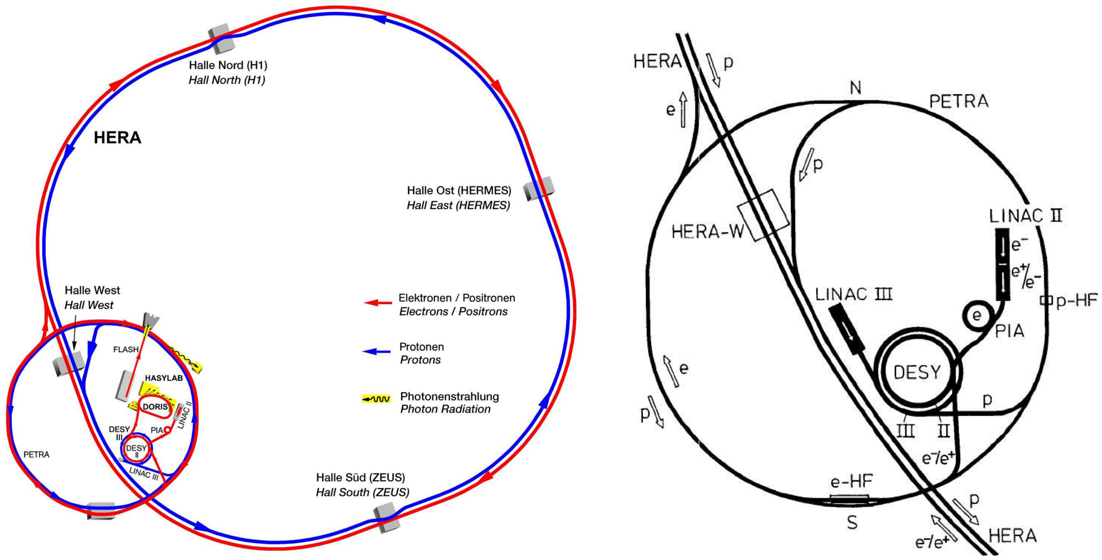

Fig. 5: Left: Overview of the DESY accelerator complex with the ep collider HERA. Right: HERA injector chain. The proton injection consists of Linac III, the DESY III injector synchrotron, and PETRA; the electron injection consists of Linac II, the positron intensity accumulator PIA, the DESY II injector synchrotron, and the PETRA ring which is used for both electrons and protons [15].

From the demands on the high energy storage ring it is possible to deduce directly several consequences for the injector chain.

In order to have sufficient counting rate in the colliding beam experiments it is necessary to achieve the optimum collider performance, i.e., the luminosity must be as high as possible. For two identical counter-propagating beams with equal horizontal and vertical emittance, the luminosity scales as

$$\mathfrak{L} \propto \frac{I^2}{\varepsilon} \,. \tag{6}$$

Here I is the particle current which should be as high as possible, and ε is the beam emittance which should be as small as possible. However, the beam emittance in a circular machine is strongly connected with the emission of synchrotron radiation. In a lepton accelerator the radiation emission leads to radiation damping on the one hand and quantum excitation (random excitation of oscillations) on the other hand [16, 17]. The consequence is the formation of an equilibrium emittance, i.e., the emittance is determined by the storage ring itself. In a hadron machine the situation is completely different. Owing to the large particle rest mass the synchrotron radiation emission is strongly suppressed. As a result the emittance is essentially determined already in the injector chain. This implies for the beam diagnostics that an accurate characterization of the beam is already required for the lowest energy machines. Furthermore only minimum-disturbing instrumentation can be used there: a beam distortion in the injector chain is irreversible and may result in an emittance blow-up in the final machine, involving a reduction of the collider luminosity which has to be avoided.

According to Liouville's theorem the normalized emittance ε_N is conserved during the acceleration process. However, it is the absolute emittance ε which defines the beam size (see Section 3.3.4) and which is therefore the parameter of interest. The relation between them is given by

$$\varepsilon = \frac{\varepsilon_N}{\beta\gamma} \qquad \text{where} \qquad \beta\gamma = \frac{pc}{m_0 c^2} \, . \tag{7}$$

Therefore the absolute emittance, and with it the achievable beam size, shrinks adiabatically during the acceleration process. To give an example, the LHC injector chain is considered: from the 50 MeV injector Linac II to the 450 GeV extraction from the SPS the absolute emittance shrinks by a factor of 1450, and the factor between Linac II and the LHC at full energy of 7 TeV amounts to 22 000. The consequence for beam diagnostics and instrumentation is that beam sizes and divergences are rather large at the beginning of the injector chain. As result a tight mesh of focusing magnets is required in order to transport the beam, and usually there is only restricted space for instrumentation.

Furthermore, at the low energies in the beginning of the injector chain the particle speed still changes with acceleration. This offers the possibility to use time-of-flight (TOF) measurements in some applications. Low energy particles also have a small magnetic rigidity, i.e., they are easy to bend. Therefore magnetic spectrometers can be used for momentum determination. However, space charge effects are pronounced at low energies and may influence particle dynamics and/or beam diagnostics measurements (especially for heavy-ion beams). Finally, according to the Bethe–Bloch equation (2) the energy deposition in matter is high for low energy particles. This may lead to a degradation or even the destruction of interceptive beam monitors like screens.

In the subsequent section the instrumentation of a hadron collider will be described together with its injector chain. For illustration the HERA injector accelerators which represent a standard injector chain for hadron accelerators are described. Starting from the linac a 'walk' along the injector complex will be done. Specific properties of the individual accelerators together with the consequences for beam diagnostics are discussed.

3.2 Source and injector linac

A widely used scheme for proton injector chains is to produce and accelerate negative hydrogen ions (H^-) and inject them into a circular accelerator where, by stripping to protons, the injection is not limited by Liouville's theorem. Figure 6 gives an overview of the 50 MeV H^- injector Linac III for HERA. In the following a short description of the subsystems is given. More details can be found, for example, in Ref. [18].

- H^- sources:
  Electron capture of vibrationally excited hydrogen molecules and subsequent dissociation into a neutral and negative ion results in the formation of an H^- beam. Two sources can be operated: either a 18 keV magnetron source or an RF-driven volume source.
- low energy beam transport (LEBT):
  The LEBT serves as matching section for the beam to the acceptance of the subsequent RFQ.
- radio frequency quadrupole (RFQ):
  The RFQ accelerates the beam from 18 keV up to 750 keV.
- medium energy beam transport (MEBT):
  The MEBT serves as matching section for the beam to the acceptance of the subsequent linac structures.
- H^- linac (tank I–III):
  The linac is a conventional Alvarez type with an end energy of $E_{\text{kin}} = 50$ MeV.
- high energy beam transport (HEBT):
  The HEBT serves as matching section for the beam to the acceptance of the injector synchrotron. Furthermore an integrated diagnostics beamline (indicated by $\Delta p/p$ in Fig. 6) is used to measure the beam properties during linac tuning.

– injection in synchrotron:
  An H^- multiturn injection scheme is applied, i.e., the hydrogen ions are converted to protons with a stripper foil.

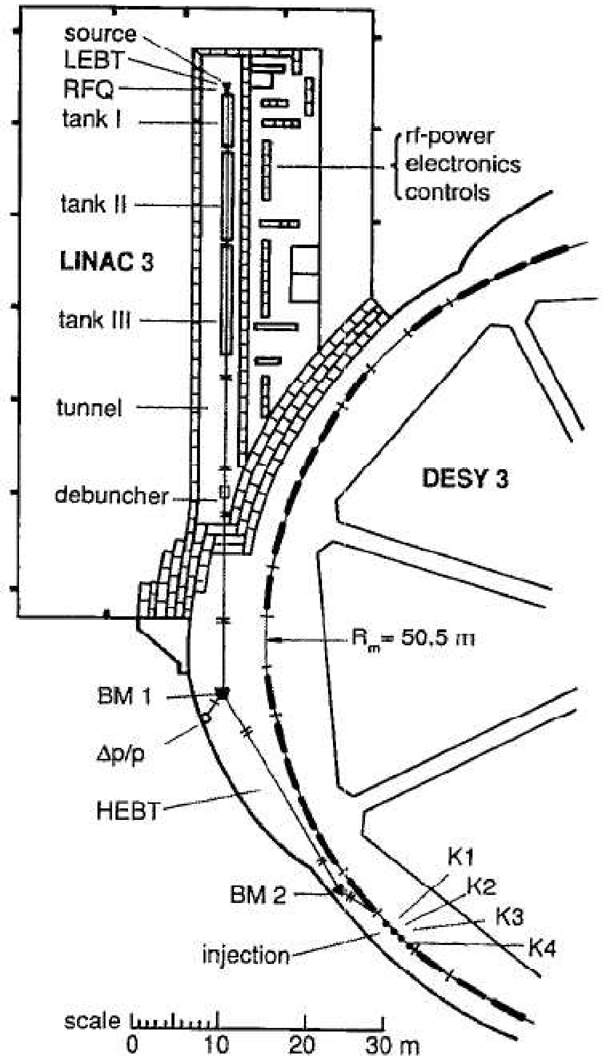

Fig. 6: Overview of the 50 MeV H^- injector linac for HERA

From the beam diagnostics point of view the injector linac needs key devices for the adjustment of the beam transport through the individual linac sections, for the setting of the RF system (i.e., the phases and amplitudes), and to indicate the operating status during standard operation. Apart from the beam monitors installed in the linac itself, several diagnostics instruments are usually grouped in a permanently installed diagnostics beamline behind the linac sections. In addition, during the commissioning phase sometimes a moveable diagnostics test bench is used which allows a full six-dimensional phase space characterization behind each linac section. As an example, Fig. 7 shows the test bench which was used during commissioning of the high current RFQ at the GSI in Darmstadt (Germany).

In the following the key instruments for linac diagnostics will be briefly described. More detailed descriptions about each monitor can be found in the dedicated articles in this CERN report. Further information and different examples of beam diagnostics in ion linacs can be found, for example, in Refs. [19–22].

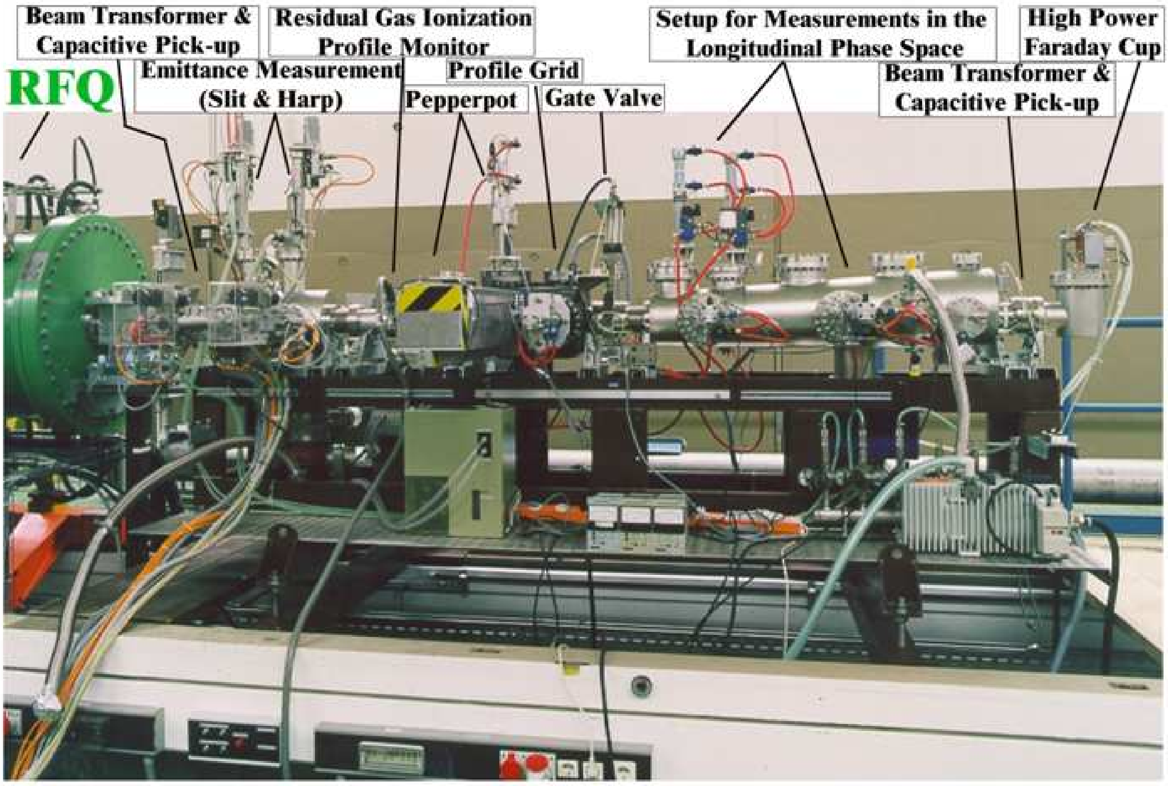

Fig. 7: Picture of the moveable test bench which was used during the commissioning of the high current RFQ at the GSI [23]. Most of the instruments indicated on the photograph will be explained in the following sections.

3.2.1 Current and transmission

Two different types of widely used monitors are shown in Fig. 8. Faraday cups are destructive monitors, i.e., they are beam stoppers which are isolated from the beam pipe ground potential and connected to a current meter. A Faraday cup allows one to measure very low intensities down to the pA region.

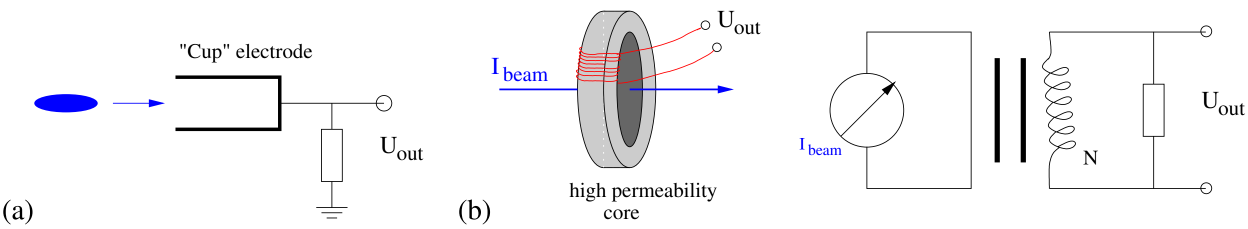

Fig. 8: (a) Sketch of the working principle of a Faraday cup. (b) Working principle of a passive beam current transformer (or AC current transformer, ACCT) together with the simplified equivalent circuit.

Beam current transformers determine the current in a non-destructive way. In this type of monitor the beam acts as single-turn primary winding of a transformer, and the AC component of the current is measured.

Besides the report in these proceedings [24] more information about beam current measurements can be found in the tutorials in Ref. [25] and in Ref. [26].

3.2.2 Beam position monitors

Position information can be gained via the electric, the magnetic, or the electromagnetic fields. Specifically for a hadron linac injector chain bunch lengths are rather large and acceleration frequencies are rather low. Therefore the corresponding beam spectrum contains only low frequencies (typically in the kHz up to the 100 MHz region). The provision of a precise determination of the beam position requires a high pick-up sensitivity at these frequencies.

Furthermore, the induced signals from the non-propagating fields are rather small because of the small Lorentz factor γ for particles at low energies with large rest masses. Therefore, in order to capture as many field lines as possible, the pick-ups have typically large electrodes.

Two beam position monitor types widely in use are depicted in Fig. 9. The capacitive pick-up relies on the interaction with the particle electric field, the inductive one on the interaction with the magnetic field.

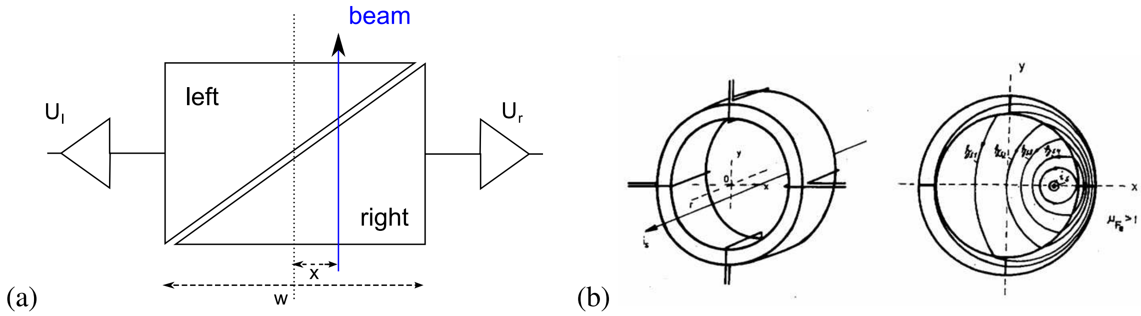

Fig. 9: (a) Capacitive pick-up of 'shoe-box' type geometry with the so-called linear cut. The position is determined as $x = \frac{w}{2}\frac{U_r-U_l}{U_r+U_l}$. (b) Working principle of an inductive pick-up together with the induced magnetic field distribution in the high permeability core [27].

Comprehensive review articles about BPMs can be found in Refs. [28–31] together with the report in these proceedings [32].

3.2.3 Transverse beam profiles

The determination of the transverse beam profile relies on the interaction of beam particles with matter. The method mostly applied is a destructive one where the particle beam hits a luminescent screen, cf. Fig. 10(a). A part of the deposited energy results in excited electronic states which de-excite partially via light emission. Therefore the beam profile can be observed via a CCD camera. Sometimes screens are even used instead of beam position monitors by analysing the centre of gravity of the measured light distribution. Care has to be taken because of the high energy deposition in material according to the Bethe–Bloch equation which is especially critical for heavy-ion machines. This may lead to a degradation of the screen material as shown in Fig. 10(b).

Less destructive methods are in use where the luminescent screen is replaced by a configuration of stretched wires or strips. If the particles hit the surface, secondary electrons are liberated. The secondary current from each individual wire or strip is converted to a voltage via a current-to-voltage amplifier, and the voltage distribution from all wires is a measure of the transverse beam profile. Configurations in use are the wire grid (i.e., stretched wires in both transverse planes), the harp (i.e., stretched wires in one transverse plane), or secondary emission monitors (SEMs) which consist of strips with a larger surface and therefore higher sensitivity.

A nearly non-destructive profile measurement relies on the creation of gas ions and free electrons in the beam interaction with residual gas in the beam pipe. The ionization products are accelerated via electrostatic guiding fields towards a microchannel plate for signal enhancement (secondary electron

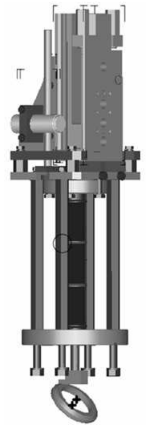

(a)

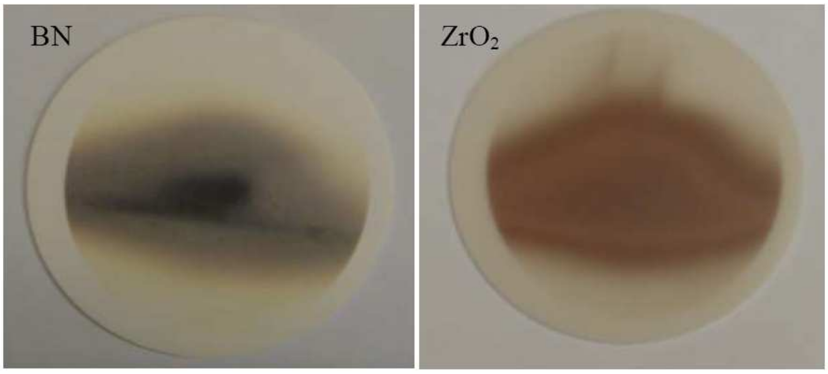

(b)

Fig. 10: (a) DESY-type luminescent screen used in the pre-accelerators (courtesy Ch. Wiebers, DESY). The viewing screen is mounted onto a pneumatically driven unit. (b) Radiation damaged screens from a scintillating screen study for the LEIR/LHC heavy-ion beams [33].

generation with multiplication factor of up to 10^7), and signal readout is performed either optically (phosphor screen together with CCD camera) or electronically (wire array with guiding field). A variation of this type of monitor is the residual gas fluorescence monitor.

Supplemental to the report in these proceedings [34], comprehensive review articles about the monitor types described in this section can be found in Refs. [35–37].

3.2.4 Transverse emittance

A method often applied in proton or heavy-ion linacs is the slit-grid measurement which is explained in Fig. 11. A slit formed by two metal blades produces a vertical slice in the transverse phase space. In the free-field drift space behind the slit (typical length between 10 cm and 1 m), the angular distribution of the slice is transformed into a spatial one which can be scanned with a moveable intensity detector. Moving the slit across the phase space ellipse and repeating the procedure described above, it is possible to scan the whole phase space. In order to reduce the number of measurements it is convenient to replace the moveable detector by a spatial resolving one like a SEM or profile grid. A further reduction of the measurements can be done with a pepper-pot scanner which offers even single shot capability. It uses a viewing screen to observe the trajectory-angle distribution of the individual beamlets sampled with a pepper-pot plate (matrix of small holes).

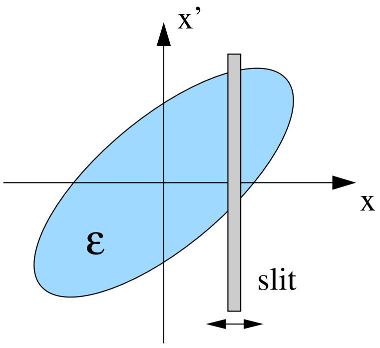

(a)

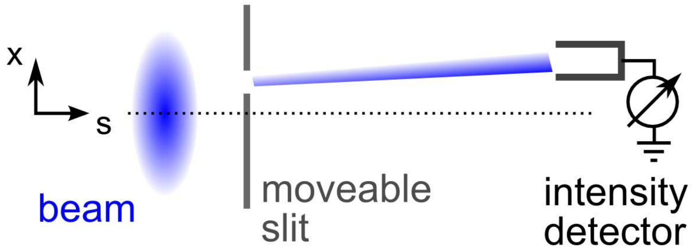

(b)

Fig. 11: (a) A moveable slit produces a vertical slice in the transverse phase space. (b) Simple scheme of a slit-grid emittance measuring device. In reality the moveable intensity detector is replaced by a spatial resolving one like a SEM or profile grid. This reduces the number of measurements required to scan the phase space.

Besides the report about emittance diagnostics and instrumentation in these proceedings [38], further information can be found, for example, in Refs. [39, 40].

3.2.5 Longitudinal plane

Reference [41] gives an introduction to the concept and a survey of measurement techniques in the longitudinal plane. The parameters of interest are particle energy, momentum and bunch length. Because of the small magnetic rigidity the determination of the particle momentum is usually done with a magnet spectrometer, where the dipole magnet of the permanently installed diagnostics beamline acts as spectrometer magnet. The spectrometer transforms the momentum (spread) into a position (spread) which is measured with a spatial resolving detector (screen, SEM, etc.) according to

$$\frac{\Delta x}{x_0} = \frac{\Delta p}{p_0} , \tag{8}$$

cf. also Fig. 12(a). In the case of non-relativistic energies even time-of-flight measurements are sometimes applied, see Refs. [7, 41] and the references therein.

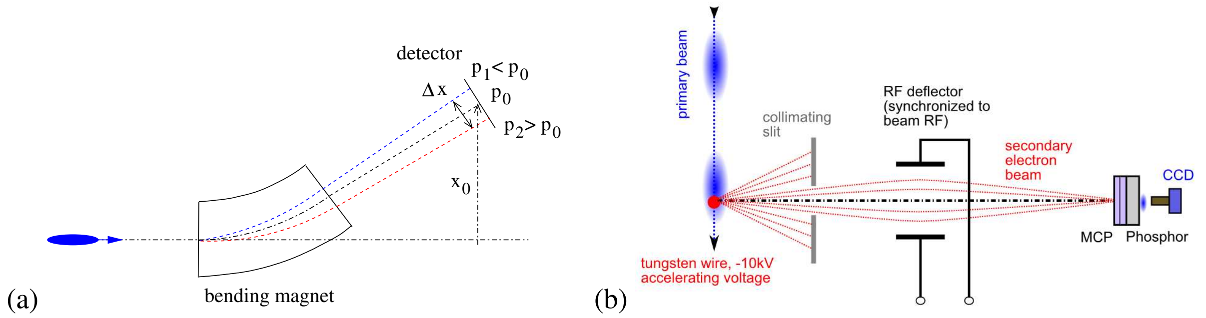

Fig. 12: (a) Principle of a magnet spectrometer for the energy or momentum determination. The energy spread is transformed into a position spread which is measured with a spatial resolving detector. (b) Scheme of a bunch shape monitor (BSM) for the determination of the longitudinal beam profile. The bunch charge distribution is converted into a low-energy secondary electron profile by a metallic wire (perpendicular to the paper plane) interacting with the beam. The secondary electron profile is streaked via a synchronized RF deflector and determined with a spatial resolving detector.

For the determination of the bunch length a so-called bunch shape monitor (BSM) is applied in various hadron accelerators, see, for example, Refs. [19, 42, 43]. The principle of operation depicted in Fig. 12 (b) is based on the analysis of secondary electrons produced by the primary beam hitting a 0.1 mm diameter tungsten wire, to which a potential of typically -10 kV is applied. The longitudinal charge distribution of the analysed beam is transformed into a spatial one of low-energy secondary electrons by synchronized transverse RF modulation. Readout can be performed electrically or optically via a CCD in combination with an MCP and a phosphor screen.

3.3 Injector synchrotron

After a description of the specific diagnostics needs of a hadron linac together with an overview of the typical instrumentation, this section briefly describes the peculiarities of hadron injector synchrotron instrumentation. The discussion is based on experience with the first proton synchrotron DESY III in the HERA injector chain, see Fig. 13.

DESY III used a H^- multiturn injection with a stripper foil for conversion to protons at an injection *energy* of 0.31 GeV$/c$. During acceleration up to the extraction *energy* of 7.5 GeV$/c$, the RF frequency increased from 3.27 MHz to 10.33 MHz. Further information about this machine can be found in Ref. [44].

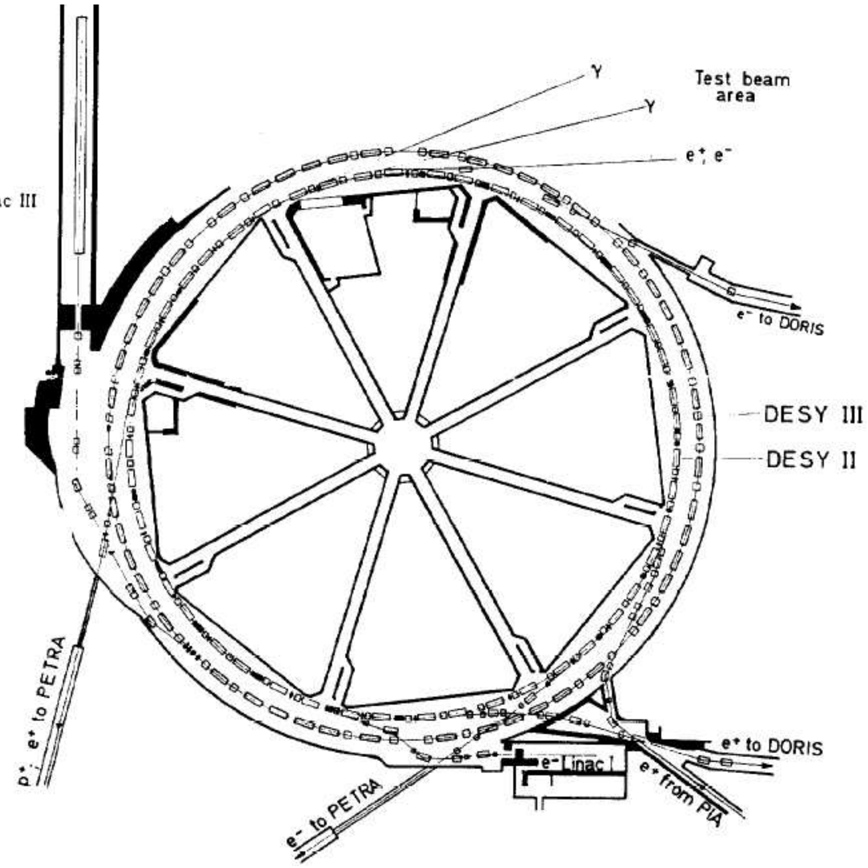

Fig. 13: Overview of the proton injector synchrotron DESY III (mean radius 50.42 m). The electron injector synchrotron DESY II is situated in the same tunnel. Further information about both machines can be found in Refs. [44, 45].

From the beam diagnostics viewpoint the requirements are threefold. Firstly beam instrumentation is required for parameter control during the beam acceleration. Then in the case of faulty operation monitors are required for fault finding. Furthermore, signals for beam optimization must be provided in specific critical places in the machine, especially for injection and extraction.

The main beam instrumentation used in the injector synchrotron is briefly described next.

3.3.1 Beam current

Beam current measurements are required for optimization of the injection efficiency, for the measurement of single bunch charge and average current, and for determination of the coasting beam.

A monitor typically used for bunch current measurements is the beam transformer as in the case of linac instrumentation.

For the determination of the average current, a parametric or DC current transformer (DCCT) is widely used. It relies on the extension of the transformer's bandwidth down to DC, typically realized in configuration of a zero flux magnetometer, see Fig. 14. Illustrative explanations about the monitor's working principle can be found in Refs. [46, 47] in addition to the references about beam current measurements listed before.

(a)

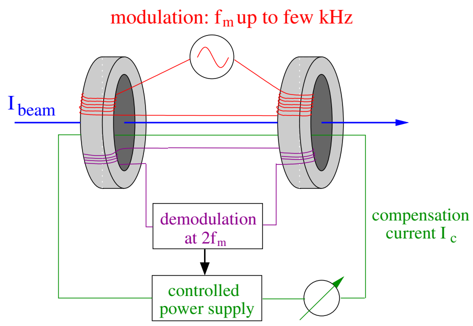

(b)

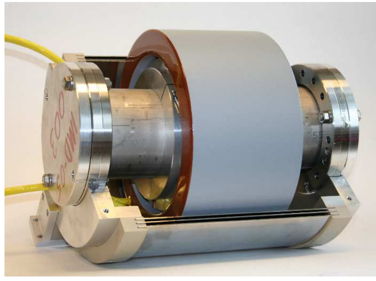

Fig. 14: (a) Working principle of a DC or parametric current comparator. (b) Photo of a DCCT with open shielding (courtesy K. Knaack, DESY).

3.3.2 Beam position

For the measurement of the beam orbit (closed orbit, position, oscillations, etc.) beam position monitors are required. In order to sample the closed orbit with sufficient accuracy, four monitors are typically used per betatron oscillation, i.e., they are located at a distance of about 90° phase advance. Owing to the large bunch lengths and the low acceleration frequencies, the beam spectrum contains only rather low frequencies, therefore a high pick-up sensitivity is required at these frequencies.

Inductive pick-ups were used for DESY III. Other schemes are capacitive ones such as the shoe-box types. At higher acceleration frequencies and beam energies, even stripline BPMs are sometimes used.

3.3.3 Tune measurements

The tune is the eigenfrequency of the betatron oscillations in a circular machine. It is a characteristic frequency of the magnet lattice, produced by the strength of quadrupole magnets. In addition to the report in these proceedings [48], Refs. [49, 50] give an introduction to the principles of tune diagnostics.

Figure 15 illustrates a simple scheme for a tune measurement. A coherent betatron oscillation is excited with a kicker, and the dipole moment due to the (coherent) transverse beam oscillation is observed with a pick-up. In order to have maximum sensitivity (betatron amplitude) the BPM is placed with a phase advance $\mu \approx 270^\circ$ from the kicker. The primary observable in this case is a time sequence of turn-by-turn beam positions, from which the tune can be deduced via a fast Fourier transform (FFT).

Owing to the strongly suppressed radiation damping for hadron beams, a permanent excitation with a kicker magnet may lead to an emittance blow-up. Therefore only very small excitations can be applied and the pick-up needs a very high sensitivity in order to detect small coherent beam oscillations. Furthermore, at injection energy, a hadron synchrotron is often space-charge dominated so that the acceptance is fully occupied. In this case a beam excitation will lead immediately to particle losses and has to be avoided.

DESY III, for example, was space-charge dominated at injection energy. For this machine it was decided to have no continuous tune measurement in standard operation. Tune measurements were performed only in dedicated machine studies in order to find a suitable working point in the tune diagram and a reproducible machine set-up.

3.3.4 Transverse profile and emittance

In a circular machine there exists a unique solution for particle orbit and Twiss parameters. Therefore the (absolute $1\,\sigma$) emittance ε can immediately be deduced with knowledge of transverse beam profile σ

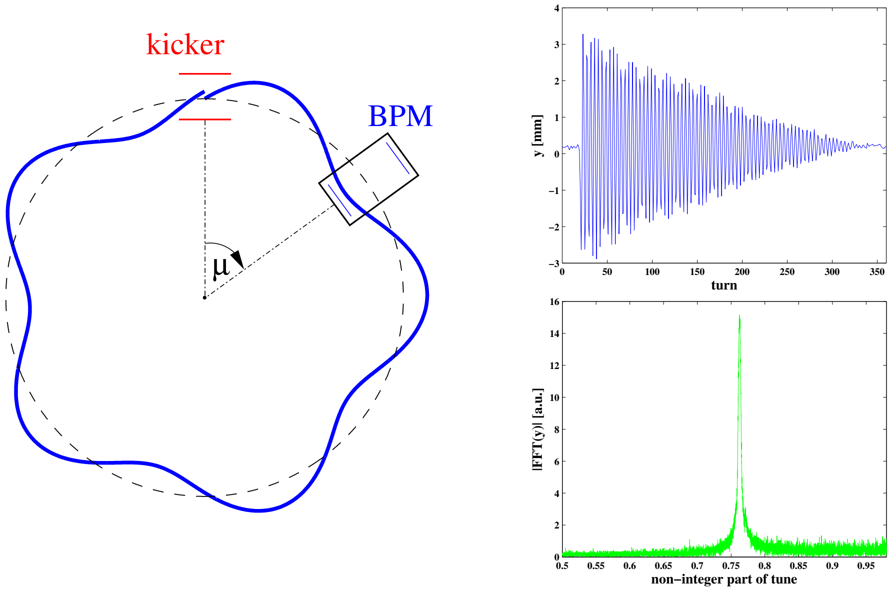

Fig. 15: Principle of a tune measurement. A kicker magnet excites a coherent betatron oscillation which is observed with a pick-up at fixed position. The BPM measures a sequence of turn-by-turn beam positions, an FFT of the position sequence gives the non-integer part of the tune. The turn-by-turn data were taken from a measurement at the positron storage ring DORIS at DESY. The fast oscillation damping is a result of the orbit feedback; for hadron machines the damping in the turn-by-turn displacement is much slower and caused by Landau damping.

and betatron function β in one location of the machine according to

$$\varepsilon = \frac{\sigma^2}{\beta} \, . \tag{9}$$

Equation (9) is simplified in the sense that the dispersion contribution to the beam size is neglected. Furthermore one should keep in mind that unfortunately several emittance definitions are in use, see e.g., Ref. [51]. However, in order to determine the emittance it is sufficient to perform a transverse profile measurement in one location. Therefore transverse emittance diagnostics can be reduced to the case of transverse profile diagnostics.

The simplest way to determine the transverse profile in an accelerator is to use a luminescent screen. In a circular machine, however, because of the multiple passages through the screen this method is completely destructive in the sense that the particle beam will be lost after several turns. Therefore this method is usually applied only during machine commissioning or in case of fault finding if there are doubts about signals from other monitors.

A less destructive method for transverse profile measurements is to use wire scanners. Here a thin wire is quickly moved through the beam with a speed of about 1 m/s. A simultaneous detection of the intensity of the particle shower outside the vacuum chamber with a scintillator/photomultiplier assembly gives an image of the beam profile.

However, in low energy machines there is a limitation to the application of the wire scanner principle as described before due to the fact that the intensity of the secondary particle shower strongly depends on the primary beam energy [21]. As can be seen in Fig. 16(a), at about 150 MeV there is a steep increase in the shower intensity. This energy corresponds to the pion threshold, i.e., the threshold required to produce the lightest shower particle. Below this energy it is more suitable to measure the secondary electron emission current of an electrically isolated wire, see the comparison of the signals in Fig. 16(b).

Finally, residual gas monitors are often used as transverse profile monitors in hadron machines.

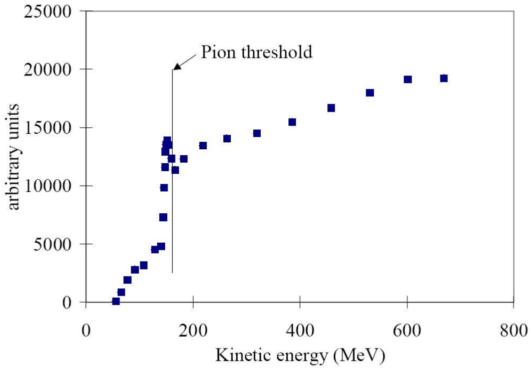

(a)

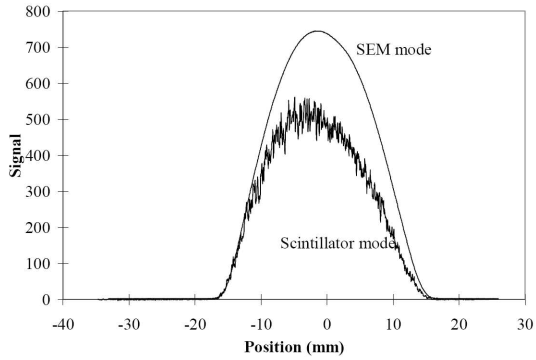

(b)

Fig. 16: (a) Secondary particle shower intensity as a function of the primary beam energy [21]. (b) Transverse beam profile, recorded with a scintillator/photomultiplier assembly and via the secondary emission current from an electrically isolated wire [21].

However, in a circular machine the vacuum pressure has to be much better (about 10^{-10} mbar) than in a linac or a transfer line (10^{-6}–10^{-8} mbar). Therefore the signal is much lower; this can be compensated by a local pressure bump.

3.3.5 Bunch length and time structure

Bunch length diagnostics are required to measure bunch lengths and to investigate longitudinal oscillations. A monitor widely used is the wall current monitor (WCM) as shown in Fig. 17. The working principle and the design of such monitors are described in Ref. [41]. A WCM offers typically a bandwidth up to a few GHz. However, in a recent publication the design of a monitor with up to 20 GHz bandwidth was reported [53].

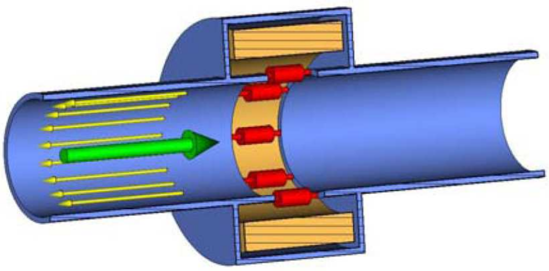

(a)

(b)

Fig. 17: (a) Working principle of a wall current monitor [52]. (b) Installation of a wall current monitor in the accelerator (courtesy R. Neumann and N. Wentowski, DESY).

3.3.6 Loss detection

Indications of beam losses are required in specific critical places, as for example at injection/extraction for optimization purposes. Therefore beam loss monitors are mandatory in a synchrotron.

Detailed information about beam loss detection can be found in Refs. [54, 55] together with the report in these proceedings [56].

3.3.7 *Comment on $\bar{p}$ and heavy-ion machines*

In an antiproton or heavy-ion machine the source emittance is worse compared to that in a proton accelerator, and the adiabatic shrinking of the emittance during acceleration is not sufficient to achieve the required final beam quality. In order to improve the emittance, electron cooling is often applied for bunched beams. However, one prerequisite for an efficient cooling process is a small cooling time which in the case of electron cooling is achieved at smaller beam energies. Therefore electron cooling is usually applied in a low-energy synchrotron in the injector chain. More information about beam cooling and related topics can be found in Refs. [57, 58].

Schottky diagnostics is an important tool to control the cooling process. It relies on the exploitation of the individual particle behaviour (Schottky noise) in the beam spectrum of a bunched or unbunched beam. The detection of these fluctuations with a very sensitive spectrum analyser allows a non-destructive measurement of a variety of beam parameters like momentum distribution, tune, transverse emittance, and chromaticity. As an example, Fig. 18 from Ref. [7] shows measurements of the momentum distribution where the momentum width of an ion beam has been reduced by two orders of magnitude via electron cooling.

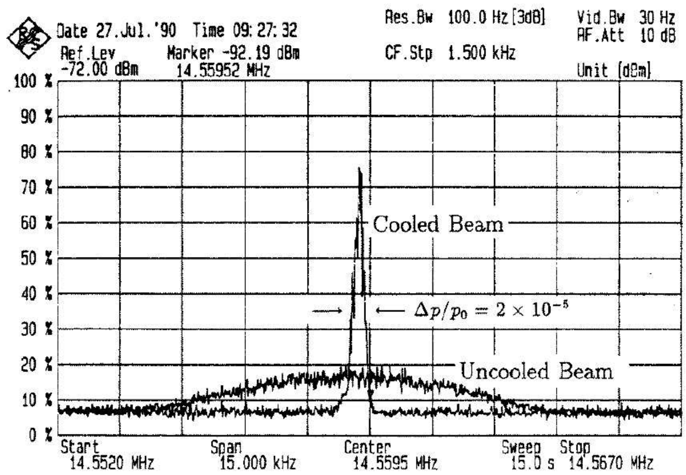

Fig. 18: Longitudinal Schottky scan for an Ar^{18+} ion beam at the GSI [7]. The broad curve is the frequency spectrum at injection with $\Delta p/p = 10^{-3}$, the narrow one that after the application of electron cooling.

Supplemental information to the report concerning Schottky diagnostics in these proceedings [59] can be found in Refs. [60, 61].

3.4 Transfer line

After the beam is ejected from the first synchrotron it has to be transported to the subsequent accelerator. A transfer line links both circular machines together while matching the optical beam parameters: owing to the imposed periodicity in a circular machine the Twiss parameters are determined uniquely. This holds for the injection/extraction points of both accelerators, and the transfer line has to map the extraction Twiss parameters from the preceding synchrotron correctly onto the injection parameters of the subsequent one. Therefore the line usually has a regular cell structure (FODO) over the majority of the length with matching sections at either end. From the diagnostics point of view, instrumentation is required for

- adjustment of the beam transport:
  This includes (i) control of the transfer efficiency via AC current transformers (at least at the entrance and the exit of the line), and (ii) the control of the beam position for orbit correction and steering via BPMs and/or luminescent screens.

– beam quality determination:
  The beam quality parameter of interest in a transfer line is mainly the transverse beam emittance. Similar to emittance measurements in a synchrotron, it is measured by determining the transverse beam profiles; luminescent screens are typically used for this purpose.
– machine protection:
  Beam loss monitors are required to control the beam losses and keep them as low as possible in standard operation. The loss monitor system can be connected to the machine interlock in order to prevent injection or extraction under faulty or irregular conditions.

General transfer line instrumentation is described in Ref. [62], a specific example is given in Ref. [63]. In the following, beam steering and emittance diagnostics will be discussed briefly with respect to their impact on the layout of a transfer line. More details and the specific features of a beam transfer line together with diagnostics requirements are described in Ref. [64], for example.

3.4.1 Beam steering

The usual philosophy used for beam steering in a transfer line is illustrated in Fig. 19 and will be explained according to Ref. [64].

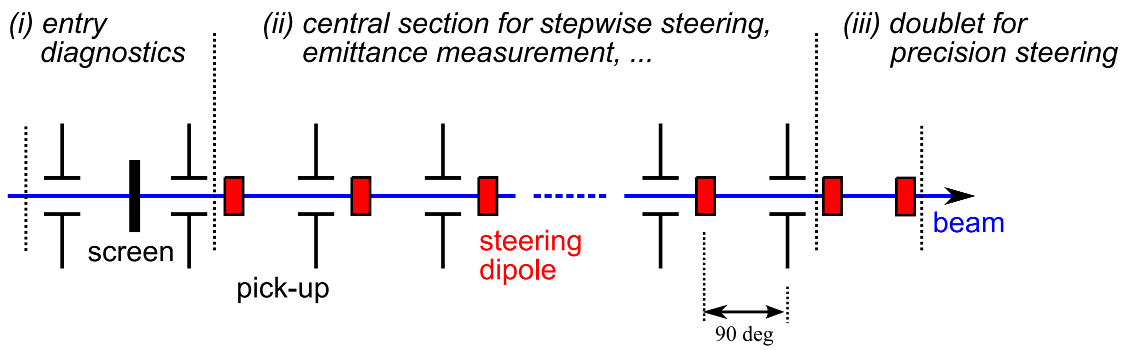

Fig. 19: Basic layout of transfer line diagnostics and correction elements for steering

(i) At the entry of the transfer line, it is useful to have information about the angle and position of the extracted beam together with qualitative information about the beam shape. Angle/position information are gathered with a pair of pick-ups. From a practical point of view the precision and reliability of such measurements are greatly improved by having only a drift space between them. For the beam shape determination a transverse profile monitor (e.g., luminescent screen) is used.
(ii) In the central section of the transfer line, each steering magnet is paired with a pick-up so that the trajectory can be corrected stepwise along the line. The phase advance between steerer and pick-up should be about 90° so that it is possible to reconstruct the betatron oscillation. However, in practice it is usual to have fewer pick-ups, especially if there are long straight sections.
  The beam emittance measurement is usually performed in the central part of the transfer line in a dispersion-free section, see Section 3.4.2.
(iii) At the line exit, the last two steering magnets are used as doublet to adjust beam angle and position to the values required for the uniquely determined closed orbit solution of the subsequent synchrotron. For maximum sensitivity, the steering magnets should be approximately a quarter betatron oscillation length apart.

Furthermore, horizontal and vertical planes should be independent for correction elements. Care has to be taken in positioning the elements for the best sensitivity for beam control and observation. The most sensitive points are the maxima of the beta function which are situated at the position of the quadrupoles. Therefore, both monitor and magnet should in general be located close to the quadrupoles.

3.4.2 Emittance measurement

Emittance diagnostics in circular machines and transfer lines is based on transverse profile measurements, cf. Eq. (9). However, in a circular machine the betatron function β is unambiguous and the emittance can be determined by a single profile measurement. In a transfer line the Twiss parameters (α, β, γ) are not known a priori and have to be determined together with the emittance ε. With the constraint $\gamma = \frac{1+\alpha^2}{\beta}$ there are three independent parameters, therefore an unambiguous determination can be achieved with at least three profile measurements.

There exist two common schemes for emittance diagnostics, (i) either the beam profile is varied by changing the focusing strength of a quadrupole upstream of a profile monitor, and the size is measured for each quadrupole setting, or (ii) the beam size is measured with different profile monitors for a fixed setting of the beam optics. The situation becomes even more complicated if the dispersion contribution to the beam size in Eq. (9) is taken into account. In order to avoid this additional complication, profile measurements should therefore be located in dispersion-free sections. More information about emittance diagnostics can be found in Ref. [38].

3.4.3 Final remarks on diagnostics for the injector chain

So far, diagnostics needs for accelerator subsections in a hadron injector chain have been discussed. Different monitors and diagnostics concepts have been presented with examples mainly from the DESY proton injector complex.

In addition, Fig. 20 shows an example for diagnostics in a hadron injector chain (including linac, transfer line, and circular accelerator): the Low Energy Ion Ring (LEIR) at CERN will be used to transform a series of long low-intensity pulses from Linac 3 into short high-density pulses, which are further accelerated in the PS and SPS ring before being injected into the LHC. The injected ion pulses will be stacked and phase space cooled via electron cooling before they are accelerated to the ejection energy of 72 MeV$/u$. As can be seen, the diagnostics needs and the instrumentation for the LEIR complex are similar to those described above. More information about the monitors in use at LEIR can be found in Refs. [65, 66]. Moreover, Ref. [67] gives an overview of diagnostics for hadron machines with special emphasis on heavy-ion machines.

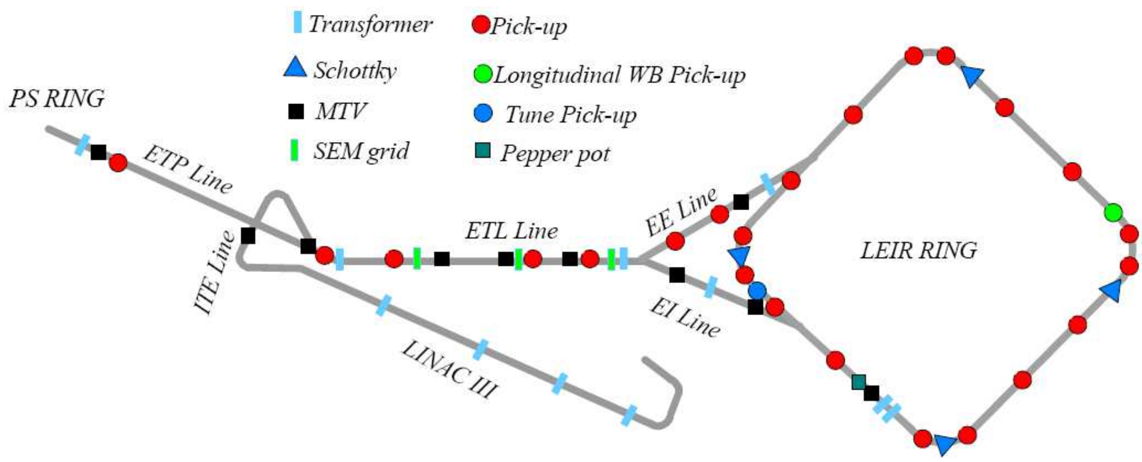

Fig. 20: Layout of the LEIR complex together with the beam instrumentation [65, 66]

After the beam is ejected from the first synchrotron it is transported via a transfer line to the next accelerator. This step may be repeated several times, cf. Fig. 5 for the HERA accelerator chain at DESY. From the diagnostics point of view, the requirements for beam monitors in the subsequent injector sections are the same, and the requirements for the final storage ring/collider will be considered in the following.

3.5 Storage ring diagnostics

As above, the description of hadron storage ring diagnostics will be based mainly on examples from the HERA proton ring at DESY. However, diagnostics overviews for other machines can be found, for example, in Refs. [68, 69] for the LHC at CERN, in Refs. [70, 71] for the FAIR project at GSI, in Refs. [72, 73] for the Tevatron at Fermilab, and in Refs. [74–76] for the RHIC at Brookhaven National Laboratory. For all these high energy machines it is common to use superconducting magnets to achieve the required magnetic dipole fields.

The following list summarizes the requirements for parameters and diagnostics systems which are needed to operate the storage ring/collider and which will be discussed in the subsequent sections:

- intensity (bunch and mean current)
- beam orbit
- tune, chromaticity, coupling
- beam distribution, emittance (longitudinal and transverse planes)
- luminosity
- beam energy
- machine protection to avoid quenches of superconducting magnets

Besides the needs of quench protection, the use of superconducting magnets has additional impact on the collider diagnostics as will be discussed in the following section.

3.5.1 Remarks on superconductivity

As mentioned above, in order to obtain superconductivity the magnets have to be cooled down to liquid helium temperatures. At HERA the operational temperature was 4.4 K, the LHC is to be operated at 1.8 K. The effects on beam diagnostics to operate the machine in a cold environment are listed below:

- Together with the magnets, a part of the beam diagnostics instrumentation has to be operated in the cold environment.
- For the design of the cold instrumentation, care has to be taken to minimize the heat transfer from the monitor to the cold environment (e.g., by higher order mode heating).
- No interceptive diagnostics can be used in or close to the cold sections since a particle shower may lead immediately to a magnet quench.
- Beam intercepting monitors must be protected against possible misuse, i.e., they have to be integrated in an interlock system.

In order to minimize the difficulties which arise because of the cold environment, the common strategy is to concentrate most of the beam instrumentation in warm sections, namely the straight insertions without need for particle bending (dipole magnets). Apart from the pick-ups which have to be installed all around the ring for closed orbit determination, the remaining monitors are located in warm sections.

3.5.2 Intensity

Intensity related parameters are bunch charge, fill pattern, and mean current. The bunch charge is monitored with an AC current transformer, the mean current with a DC or parametric current transformer. Figure 21 shows HERA intensity measurements as displayed in the control system.

Furthermore, additional parameters can be deduced from the current determination. DC current measurements performed in short time intervals result in the beam lifetime τ according to

$$\frac{1}{\tau(t)} = -\frac{1}{N}\frac{\mathrm{d}N}{\mathrm{d}t}\ . \tag{10}$$

(a) 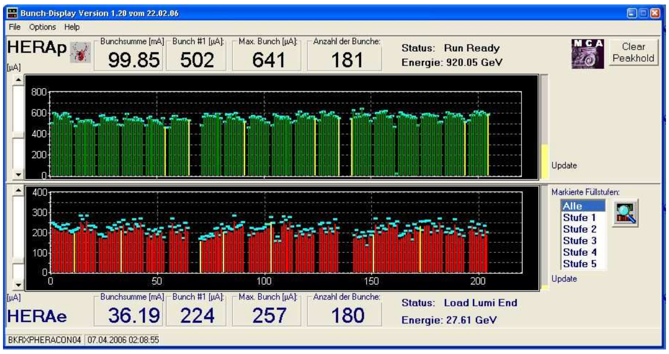

(b) 

Fig. 21: Screen shots of intensity measurements from the HERA control system. (a) Display of bunch charge and fill pattern: the charge is plotted as a function of the bunch position for both protons (top) and electrons (bottom), i.e., each bar represents an individual bunch together with its charge. (b) Mean current and lifetime display.

With knowledge of DC and bunch current, the coasting beam contribution I_{cb} (i.e., the number of beam particles leaking out of the RF buckets occupied by bunches) can be determined by subtracting the sum of all bunch currents from the DC current:

$$I_{\text{cb}} = I_{\text{DC}} - \sum_{i}^{\text{bunches}} I_{\text{AC},i}. \tag{11}$$

Careful monitor calibrations are mandatory for a reliable coasting beam indication.

3.5.3 Beam orbit

Position information is required for the determination of beam orbit related parameters. This includes a closed orbit measurement, from which the lattice parameters are deduced. This offers, for example, the possibility to compare the real machine with its design values. Additionally, single-turn information is required, especially for optimization of the injection. By minimizing injection orbit oscillations it is possible to eliminate mismatches of other parameters and related emittance blow-up, for example.

The beam position is measured with BPMs located in cold and warm environments. In order to reach maximum sensitivity for a measurement of the orbit deviation they are usually installed close to the quadrupoles where the β-function has its maximum.

The choice of pick-up type depends on linearity, dynamic range, and required resolution. While HERA was equipped with stripline monitors [77], cf. Fig. 22(a), cold button-type pick-ups have been installed in the LHC [69].

To give an example of the achievable position resolution, for the LHC at full intensity, 50 µm rms are required for a single turn, and 5 µm rms for the closed orbit (i.e., averaging over several turns) [78].

3.5.4 Tune, chromaticity, and coupling

For a circular accelerator the tune defines the working point of the accelerator. As for the injector synchrotron, the principle of the measurement relies on transverse beam excitations in combination with an FFT from a turn-by-turn position determined with a pick-up.

In order to minimize the emittance blow-up only small excitations are allowed. Therefore a very high sensitivity of the pick-up detector together with minimum disturbing excitation schemes are required. However, a recently developed base-band tune (BBQ) measurement system from CERN [79] based on an increase of the betatron frequency content in the base band allows less stringent demands on the pick-up sensitivity. The use of different pick-up types and measurement schemes at the Tevatron for protons and antiprotons are compared in Reference [80].

(a)  (b) 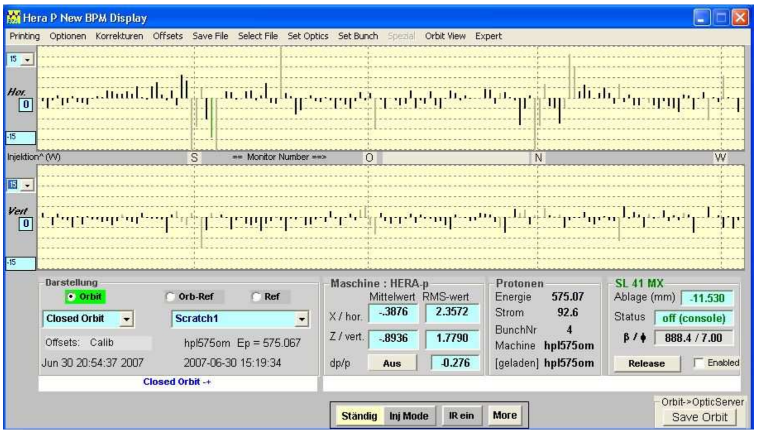

Fig. 22: (a) Photo of a HERA cold stripline monitor (courtesy S. Vilcins-Czvitkovits, DESY). (b) HERA proton orbit display for visualization of the horizontal (top) and vertical (bottom) orbit: the BPM reading is plotted as a function of the pick-up location in the ring, i.e., each bar represents a measured beam position with the pick-up.

Examples of widely used excitation schemes are

– tune kicker
  It is based on the traditional kick method. The principle is simple and robust and typically used for the commissioning stage.
– tune shaker
  The tune shaker relies on a continuous beam excitation. Therefore it can be used for continuous tune monitoring, and the signal can be integrated in a feedback loop for tune and chromaticity [81]. There exist a variety of excitation schemes like (i) single frequency excitation, (ii) single frequency locked on the tune (PLL mode), (iii) single or dual frequency with adiabatic rise and fall-off (AC dipole mode), (iv) band-limited excitation, or (v) repetitive chirp excitation [82].

Figure 23 shows screen shots from the HERA tune measurement system as displayed in the control room. The signals were produced with a repetitive chirp excitation and measured via a resonant 'Schottky type' pick-up [83]. The position of the signals indicates the fractional part of the tunes, the line widths are a measure of the chromaticity. As can be seen in Fig. 23 (b), the appearance of a second line in the spectrum is a hint for coupling which has to be corrected with skew quadrupoles.

(a) 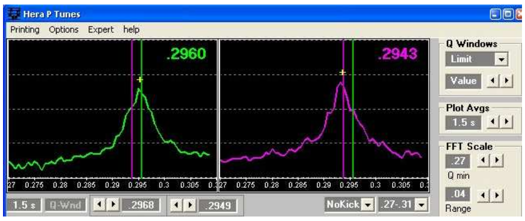

(b) 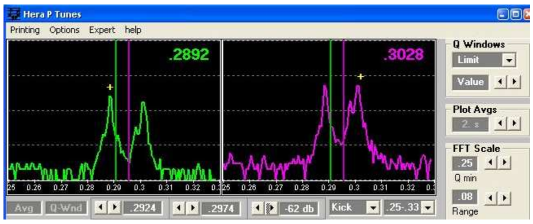

Fig. 23: Screen shots of the betatron tune measurement system from the HERA proton storage ring as displayed in the control room. (a) The position of the lines indicates the fractional parts of horizontal (left) and vertical (right) tune, the line widths are a measure of the chromaticity. (b) A second line in the spectrum of horizontal and vertical tune indicates coupling of both planes.

Apart from the methods described above, Schottky diagnostics can be used as passive method (i.e., without external excitation) to measure the (incoherent) tune and chromaticity.

However, the use of superconducting magnets has a strong impact on tune and chromaticity in the storage ring because of dynamic effects: superconducting eddy currents or persistent currents affect the multipole components of the dipole magnets especially at injection energy, and with it also the storage ring performance [84–86]. Furthermore, these persistent currents are not really persistent and decay with time. For HERA the most important contribution was the sextupole component, and with it the influence on the chromaticity. As an example, Fig. 24 shows a chromaticity measurement during injection energy at 40 GeV. As can be seen the chromaticity in both planes drifts away owing to persistent-current decay. In addition, the persistent currents are reinduced to their full strength on the first steps of the ramp, approaching the original magnet hysteresis curve. This 'snap-back' effect together with the persistent current decay needs correction in order to operate the accelerator under controlled conditions, i.e., a reliable control during the ramp is mandatory. Besides online measurements of magnetic multipole components and correction tables for the magnetic fields, a feedback on tune and chromaticity is highly recommended, see e.g., Refs. [48, 81].

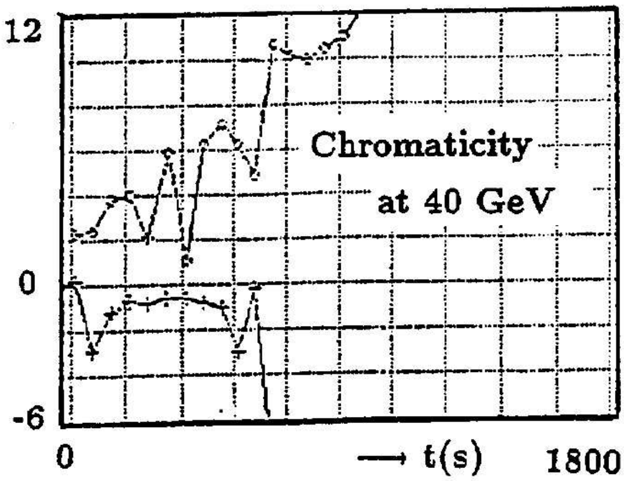

Fig. 24: Chromaticity measurement at HERA during injection energy [85]: owing to persistent-current decay the chromaticity drifts in both planes in opposite directions. Upper curve: horizontal chromaticity; lower curve: vertical chromaticity.

3.5.5 Transverse beam distribution and emittance

Owing to the unique solution for the beta function in the storage ring the emittance diagnostics can be reduced immediately to a transverse profile measurement. Depending on the extent of beam perturbations there exist three classes of transverse beam monitors.

Single pass monitors are simple and robust. They are used typically during the commissioning stage where beam operation is performed with only a single or few bunches. Therefore single pass monitors need a high sensitivity, but only modest demands on accuracy. A widely used monitor for this purpose is the luminescent screen.

Few pass monitors are used typically for the study of injection mismatch, i.e., for betatron and dispersion matching via observation of shape oscillations during the first turns. For this purpose turn-by-turn acquisition is required (typically 10–20 turns), and the demands on the accuracy are still moderate. However, only moderate beam blow-up is allowed and energy deposition in the screen material becomes a critical issue. Therefore optical transition radiation monitors are widely used because they require only thin foils for light generation. A description of such monitors can be found, for example, in Ref. [87]. A further option for turn-by-turn instrumentation is residual gas monitors [88, 89].

Circulating beam monitors are required to study the evolution of the rms beam size, for emittance diagnostics, and to determine the beam tilt owing to coupling between both transverse planes. These types of monitors can produce only a minimum beam blow-up, i.e., they have to rely on minimum, non-intercepting methods. Furthermore the demands on accuracy are high. Monitor principles in use are

- residual gas (luminescence) monitors
- flying wires
  Because of the partial beam intercepting signal generation, this type of monitor is sometimes used only for calibration of other transverse profile monitors. A limitation is high beam intensity combined with small beam sizes which can destroy the wire owing to high heat load. Therefore wire speeds of 1 m/s and even more are required.
- synchrotron radiation monitors
  In high energy proton machines the intensity of synchrotron radiation in the visible spectral region produced in the fringe field of a dipole magnet or from an undulator is sufficient to find applications in beam diagnostics. The first profile monitor based on this principle was realized at the SPS (CERN) [90], while later the Tevatron [91] and HERA [92] used monitors of this kind. For the LHC it is also foreseen to use synchrotron radiation based diagnostics. In order to optimize the performance over the whole energy range from 450 GeV up to 7 TeV, a superconducting undulator together with a separation dipole will act as radiation source [93].
  In Fig. 25 screen shots from the HERA proton synchrotron radiation monitor are shown for illustration.

(a) (b)

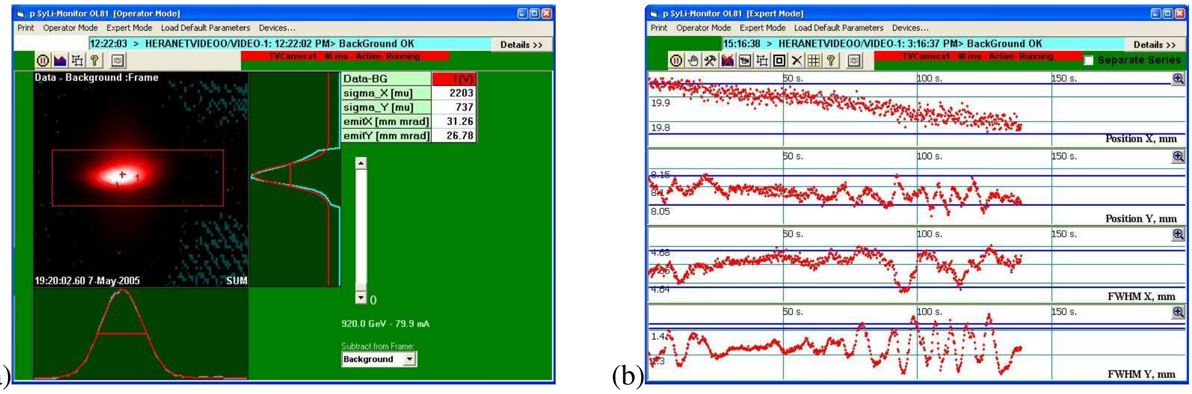

Fig. 25: Screen shots from the HERA proton synchrotron radiation monitor as displayed in the control system. (a) The transverse beam profile is continuously observed and analysed. (b) Time evolution of the horizontal (x) and vertical (y) beam position together with fitted beam sizes (FWHM) for the last 200 s. An oscillatory behaviour in vertical position and size was observed just after moving the proton collimators.

3.5.6 Longitudinal beam distribution and time structure

Longitudinal diagnostics serves mainly for the determination of the classical *longitudinal profile parameters*, i.e., bunch centre of gravity, rms bunch length, and core distribution. At HERA the bunch lengths (about 1.6 ns at 920 GeV) were monitored with a wall current monitor. The LHC with much shorter bunch lengths (in the order of 0.28–0.62 ns at 7 TeV) will use a synchrotron light diagnostics for this purpose.

Moreover, *abort gap monitoring* is essential for superconducting storage rings, i.e., a continuous monitoring to ensure that the rise time gap of the dump extraction kicker is free of particles. Particles located in this gap would not receive a proper kick when the dump system is fired, and this could lead immediately to damage of machine components. For this purpose synchrotron radiation based diagnostics is again a versatile tool [91].

Furthermore the *detection of ghost bunches* is of interest. They occur owing to diffusion of untrapped particles into nominally empty RF buckets. These ghost bunches may disturb the BPM system readout or physics data taking. Again synchrotron radiation diagnostics is often applied. As an illustration Fig. 26(a) shows the time structure of a number of HERA proton bunches as measured with optical synchrotron radiation from a magnetic fringe field and detected with a photomultiplier tube.

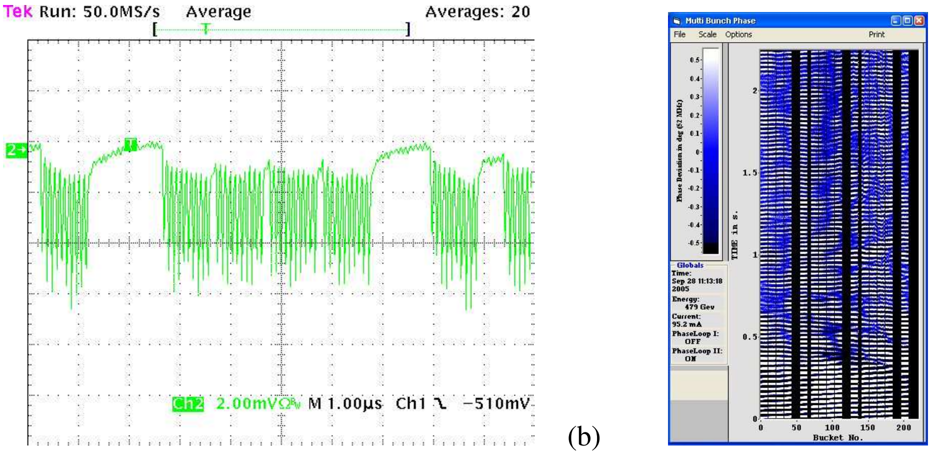

(a) (b)

Fig. 26: (a) Time structure of a number of proton bunches, measured with fringe field optical synchrotron radiation in HERA. (b) Multi bunch phase oscillation display in the HERA control room. The abscissa indicates the bucket number, the ordinate the time axis, and the color code is a representation of the deviation from the reference phase. The appearance of a pattern indicates the presence of a longitudinal instability.

Finally the *observation of longitudinal instabilities* is of interest to optimize the machine performance. At HERA coherent oscillations of the proton beam during acceleration led to an increase of the bunch length and a decrease of the luminosity. In order to investigate this effect a diagnostics system was developed to measure length and phase of every bunch together with the transient and accelerating RF voltages of all cavities [94, 95]. Figure 26(b) shows a screen shot of the longitudinal diagnostics as seen in the control room, indicating the onset of a longitudinal instability. Based on this diagnostics a broadband longitudinal coupled bunch feedback system was developed to counteract the instability and preserve the bunch length and luminosity [96].

3.5.7 Luminosity

Luminosity is the key parameter for determining the performance of a collider. Online luminosity diagnostics is important, e.g., for the optimization of beam collisions at the interaction point. The principle of a luminosity determination is based on measuring a count rate: a reaction channel with known cross-section σ_r is chosen and the corresponding event rate $\dot{N}_r$ is detected. According to Eq. (5) the luminosity is simply derived. Special care must be taken to suppress background contributions to the measured event rate since they falsify the luminosity value.

However, hadronic cross-sections are not precisely calculable because of the nature of the constituent particles. Therefore in hadron colliders reaction rates do not serve for absolute luminosity monitoring, but are mainly used for optimization purposes. The absolute luminosity determination, which is typically a complicated task, is often the duty of the experiments.

For the ep collider HERA the determination of an absolute online luminosity was straight forward. The reaction channel under investigation was the Bethe–Heitler process (bremsstrahlung)

$$e\,p \quad \rightarrow \quad \gamma\, e'\, p' \tag{12}$$

whose cross-section is well known. As an illustration Fig. 27 shows the HERA luminosity display at the

H1 experiment. Based on this information, position and angle of both colliding beams were tuned for maximum collision rate at this interaction point.

More information about luminosity measurements can be found in Refs. [97, 98] and in the report in these proceedings [99].

Fig. 27: Online luminosity display for the H1 experiment at HERA, just after adjustment of beam collisions for a new run. The luminosity count rate is plotted as a function of time. The lower curve indicates the absolute luminosity, the upper one the specific luminosity (i.e., normalized to the beam current).

3.5.8 Energy

In a hadron collider, the absolute energy determination is of less importance. The hadrons have a constituent nature (quarks and gluons), and these constituents share the beam momentum. Therefore the total energy in a reaction is only loosely related to beam energies. For the beam energy measurement the determination of the dipole magnet current is therefore sufficient. References [97, 100] contain additional information about energy diagnostics.

3.5.9 Machine protection system and loss monitors

A machine or quench protection system with integrated beam loss monitors is essential for the operation of superconducting accelerators. To emphasize this requirement, Fig. 28 shows the stored energy in the beam for different accelerators.

For HERA at 820 GeV beam energy, the He bath temperature was 4.4 K while the cable quench temperature was 5.2 K, i.e., a temperature rise of only 0.8 K in a magnet cable was sufficient to quench one of the superconducting magnets. For the LHC with about a factor of 200 more stored beam energy the situation is even more critical.

Therefore a very sensitive and reliable machine protection system is required which dumps the beam under controlled conditions to protect the equipment in case of component failure or non-tolerable background conditions, see also Ref. [101].

One of the most important parts of a machine protection system are beam loss monitors which have to detect irregular (uncontrolled, fast) losses. There are several considerations in selecting the

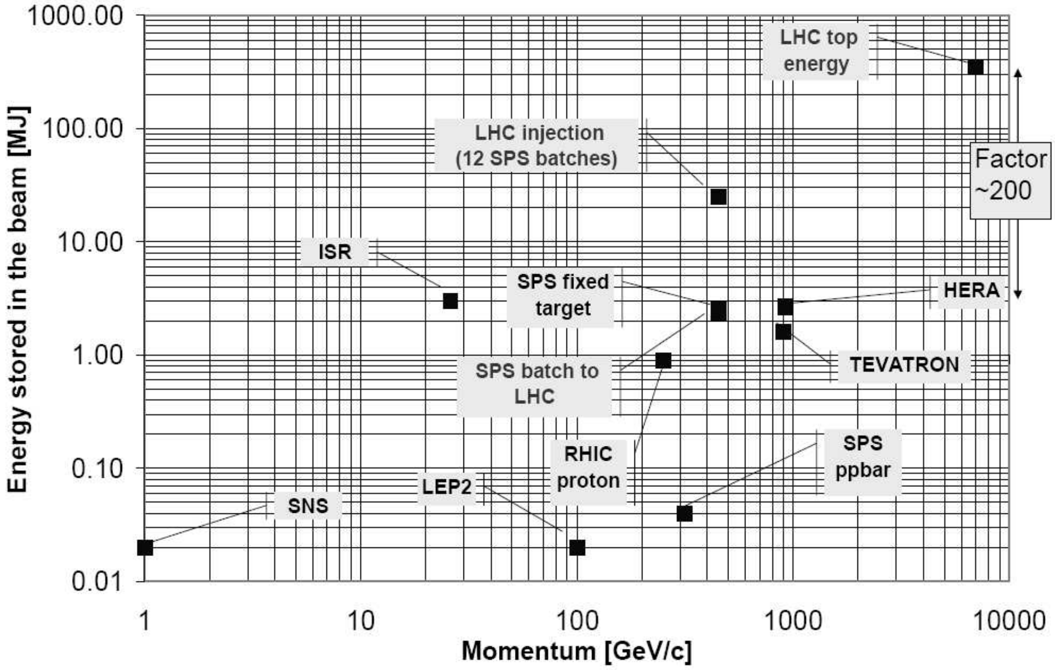

Fig. 28: Comparison of the stored beam energy for various accelerators [69]

appropriate type of beam loss monitor, see, for example, Ref. [55]. Monitors typically in use are gas ionization chambers, PIN diodes, photomultipliers with scintillators, and secondary emission tubes [56].

4 Additional examples for hadron accelerator diagnostics

So far the diagnostics needs for a hadron collider together with its injector chain have been discussed. This section presents two additional examples of hadron accelerators and their requirements for beam diagnostics: (i) a spallation neutron source and (ii) a hadron therapy accelerator. However, the discussion will be less extensive because most of the instruments in use are based on the same monitoring concepts described above. Therefore the description will be focused on the peculiarities of these accelerator concepts and the consequences for beam diagnostics.

4.1 Spallation neutron source

In a spallation source neutrons are produced by the interaction of a high energy proton beam with a heavy metal target. The neutrons are subsequently moderated to energies suitable for neutron scattering experiments (neV to eV). The number of neutrons produced by the protons depends on the primary beam energy in the range of 0.2–10 GeV. At a beam energy of about 1 GeV the neutron yield is ~ 30 neutrons per proton.

According to Refs. [102, 103] there exist three classes of spallation sources: (i) cw driven sources, (ii) sources with long (ms) pulses, and (iii) sources with short (µs) pulses. The subsequent discussion is based on the last category. The largest machine of this type, the Spallation Neutron Source (SNS) at Oak Ridge (Tennessee, USA), recently started operation [104]. Specific to this kind of machine is pulsed operation together with high beam power of up to 1.44 MW on the target. These conditions make possible time-resolved measurements with a high neutron flux.

Figure 29 shows a schematic view of a pulsed neutron source according to Ref. [105]. The principle set-up resembles that of a standard hadron linac and injector synchrotron, and with it also the concepts for beam instrumentation. However, the peculiarity of this accelerator type and the implications on beam diagnostics is the handling of high beam power. The following list gives an overview of the principle aspects:

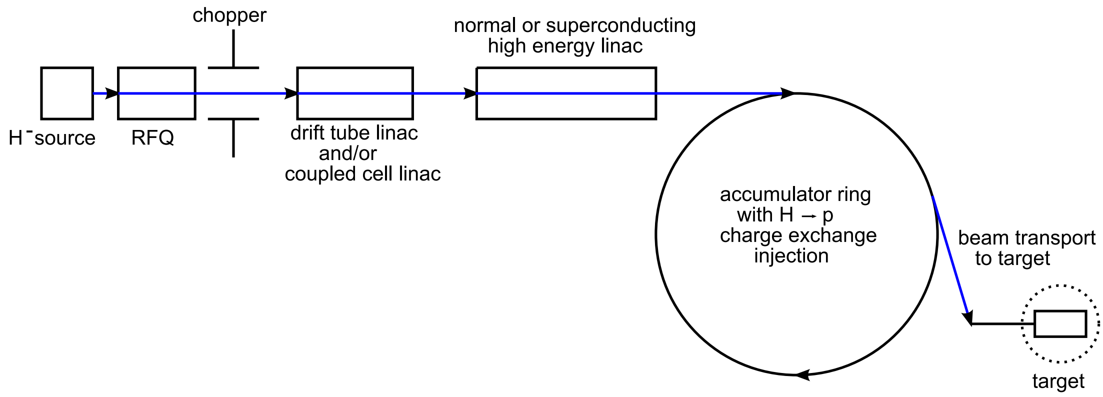

Fig. 29: Schematic view of a pulsed neutron source

1. Achieving high beam power:
   Diagnostics systems are required which help to understand the dynamics of intense beams. Examples are monitors to understand beam halo formation.
2. Measuring high power beams:
   Beam monitors have to measure the fundamental beam parameters during full power operation. Transverse beam profile monitors are especially challenging in this context because only non-interceptive principles can be used. Examples are ionization profile monitors or the laser profile monitor based on H^- photo neutralization [106].
3. Protecting the diagnostics:
   Beam monitors that cannot survive the interaction with high power beams have to be protected, e.g., the machine protection system needs interfaces for intercepting devices.
4. Protecting the facility:
   Diagnostics systems are required that protect the facility from beam induced damage or activation. Examples are loss monitors or beam-on-target diagnostics.

Figure 30 shows the layout of the SNS diagnostics systems. Further information about the monitors can be found in Refs. [107–109].

4.2 Hadron therapy accelerator

Nowadays a number of accelerator facilities are emerging for the medical treatment of tumor patients using proton or light-ion beams. Examples are the PROSCAN project at the Paul-Scherrer-Institute in Villigen (Switzerland), the CNAO project located in Pavia (Italy), and the Heidelberg Ion Therapy (HIT) facility in Heidelberg (Germany).

The radiobiological motivation for hadron therapy is to apply the energy of particles for the destruction of the DNA inside the nucleus of a tumor cell. The main requirements for this therapeutic method are illustrated in Fig. 31(a). These are (i) a constant and high dose profile at the location of the tumor, and (ii) a low dose profile at critical organs. The basic advantage of hadron therapy is that charged hadrons deposit the maximum energy density at the very end of their range (so-called Bragg peak), therefore the position where cells are damaged can be well localized in depth so that critical organs behind the tumor are safe. Furthermore, the use of carbon ions is advantageous because of the relative low radiation dose in the entry channel compared to protons, for example. More information about hadron therapy and its technological developments can be found in Ref. [110] and the references therein.

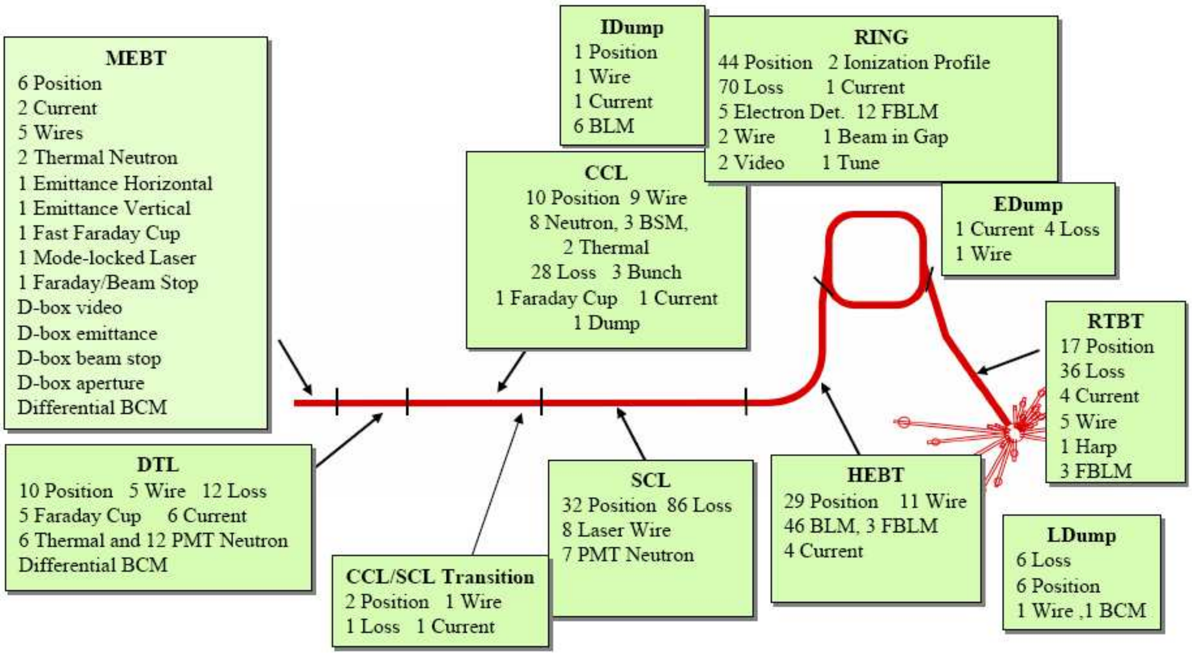

Fig. 30: Layout of the SNS diagnostics systems [109]

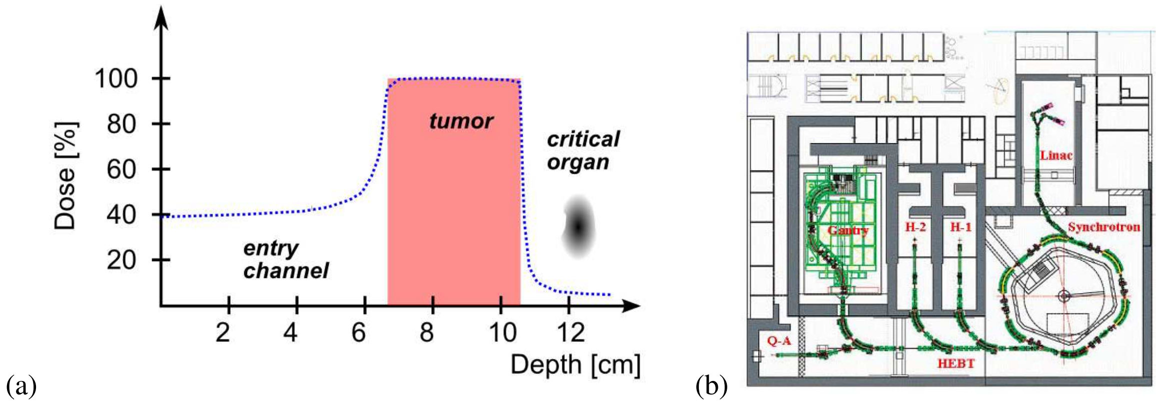

Fig. 31: (a) Dose profiles and the Bragg peak behaviour. (b) Layout of the HIT facility [114]. The complex consists of two ion sources, a linac (RFQ and DTL section), a synchrotron (64 m circumfence, $E = 48–220$ MeV$/u$ for protons and 88–430 MeV$/u$ for carbon), a high energy beam transport (HEBT) and transfer lines to the stations for patient treatment, and a diagnostics beamline for quality assurance (Q-A).

In order to scan the particle beam over the whole tumor region, scanning mechanisms are required for both transverse planes and the longitudinal one. As an example, the GSI pilot project for HIT developed an intensity-controlled rasterscan method which has been successfully applied in patients' treatment [111].

By this method the tumor is painted with a pencil-ion beam using an active variation of the beam properties. In transverse directions a two-dimensional scanner magnet excitation is applied in order to vary the beam position, i.e., a precise knowledge of beam position and beam size is mandatory. In the longitudinal direction the fact that the particle penetration depth is determined by the kinetic energy of the beam, i.e., the position of the Bragg peak can be controlled via the primary particle energy, is exploited. In contrast to the hadron accelerators described so far, for the hadron therapy accelerator an accurate knowledge of the particle beam energy is therefore mandatory. Moreover, to achieve a constant dose profile over the tumor region, the particle beam intensity has to be adjusted together with the beam energy. As consequence, the operation of a hadron therapy accelerator for patients' treatment requires precise diagnostics for the determination of beam size, beam position, energy, and intensity.

Figure 31(b) shows the layout of the HIT facility. The principle set-up resembles that of a standard hadron injector linac together with injector synchrotron and transfer lines. Therefore the monitors in use are similar to those discussed above. However, there are some peculiarities which are to be considered in view of beam instrumentation. Hence the diagnostic systems can be classified into three categories [112]:

(i) Non-destructive diagnostics systems that work online during patient treatment and in all other cases. These systems have to work reliably and must be easy to operate. Monitors of this type must be located in all important areas so that the operators can see at a glance if the accelerator is working correctly.
(ii) Destructive devices that are used for daily checks of the machine performance and the beam stability, and in addition to solve simpler machine problems. This kind of diagnostics is positioned more densely along the machine. Handling and data interpretation of these devices may be more complicated and require complex algorithms controlled by software.
(iii) Special devices that will be necessary during the machine commissioning and in the case of serious machine problems. Equipment of this kind will be used only by specialists and therefore can have a more complex user interface.

References [112–114] have more detailed information about specific diagnostics for medical hadron accelerators.

5 Diagnostics for lepton colliders

So far diagnostics needs for hadron accelerators have been considered. The present section is dedicated to the specific needs of lepton accelerators in general, and especially for high energy physics storage rings together with their injector chain. The description of the diagnostics instrumentation is mainly based on examples from the 27.5 GeV $e^+(e^-)$ ring of the ep collider HERA at DESY. Descriptions of beam instrumentation for other machines can be found, for example, in Ref. [115] for the 0.7 GeV collider DAΦNE (INFN Frascati, Italy), in Ref. [116] for the 2.2 GeV collider BEPC (IHEP Beijing, China), in Ref. [117] for the 6 GeV collider VEPP-4 (Budker Institute Novosibirsk, Russia), in Ref. [118] for the 9 GeV e^- / 3.1 GeV e^+ collider PEP-II (SLAC, USA), and in Refs. [119, 120] for the 100 GeV collider LEP (CERN). However, before starting with the description of the required instrumentation, the following subsection recalls the differences between lepton and hadron beams and their consequences for diagnostics.

5.1 Lepton properties and the consequences for diagnostics

The main differences between leptons and hadrons are that (i) leptons are simple point objects and have no constituent nature, and that (ii) their rest mass is much smaller than that of hadrons. The second aspect in particular has a strong impact on accelerator physics:

– Leptons are fully relativistic at a few MeV beam energy which is typically achieved early in the accelerator chain, behind the first accelerating sections.
– They produce a strong electromagnetic field which scales with the Lorentz factor $\gamma = E/m_0c^2$.

The γ scaling implies that non-propagating fields have a long transverse range, and especially that synchrotron radiation (SR) is emitted for bent particle motion. The emission of synchrotron radiation has a strong influence on both particle dynamics and beam diagnostics.

The SR emitted power can be estimated according to

$$P_\gamma = 8.85 \times 10^{-2} \, \frac{E^4[\text{GeV}^4]}{\rho[\text{m}]} \, I[\text{A}] \tag{13}$$

with E the beam energy, I the mean beam current, and ρ the mean bending radius. For HERA with $E = 27.5$ GeV, $I = 50$ mA, and $\rho = 550$ m the emitted power amounts to $P_\gamma = 4.6$ MW. This means that a huge level of radiation power is emitted from the beam which is deposited in the accelerator environment. Such a level may easily lead to damage of components, i.e., sensitive accelerator components have to be protected from direct SR illumination and cooling is required in places where the power is deposited.

Furthermore, the extracted beam power results in an energy loss per turn which is estimated as

$$\Delta E_\gamma = 8.85 \, \frac{E^4[\text{GeV}^4]}{\rho[\text{m}]} \, . \tag{14}$$

For the HERA parameters the energy loss per turn is $\Delta E_\gamma = 92$ MeV. Without restoration of this energy loss on every turn, a stable accelerator operation would be impossible. This is the duty of the RF system, i.e., cavities are required which have to provide sufficient voltage to bring the particles back to their nominal energy. Because of the large energy loss, a large number of cavities is usually necessary. HERA for example used 98 cavities, grouped in 8 section with 8 transmitter stations, each with 1.4 MW nominal power and fed by 2 klystrons.

In the following list the consequences of SR emission are summarized together with their impact on beam dynamics and beam diagnostics.

(i) A large number of cavities are required in order to restore the energy loss owing to the radiation emission. However, each cavity represents a high impedance for the beam. A higher impedance increases the possibility to excite (multibunch) instabilities which have to be be damped. Therefore circular lepton accelerators usually require a feedback system for stable operation.

(ii) The heat load on accelerator components owing to the high SR power becomes critical. Therefore the accelerator together with the instrumentation has to be protected, and cooling is required in locations where direct SR illumination cannot be avoided.

(iii) A high total cavity voltage V_r is required in order to compensate the energy losses and to guarantee sufficient lifetime. However, the cavity voltage is connected with the rms bunch length σ_t. Above transition energy the following relation holds:

$$\sigma_t = \frac{\alpha_c - 1/\gamma^2}{2\pi f_s} \, \sigma_\delta \quad \propto \quad 1/\sqrt{V_r} \tag{15}$$

with α_c the momentum compaction factor, f_s the synchrotron frequency, and σ_δ the relative energy spread. According to Eq. (15) a high cavity voltage implies smaller bunch lengths, i.e., the lepton beam spectrum contains much higher frequencies than the hadron spectrum.

(iv) In a lepton accelerator the SR emission leads to the formation of an equilibrium emittance due to the concurring processes of radiation damping and quantum excitation. Therefore the beam emittance in the final storage ring is determined by the ring itself and not by the injector chain, i.e., emittance blow-up is not critical and the injector chain has relaxed requirements.

As for the hadron collider, in the subsequent sections we take a 'walk' along the injector complex. The properties of the various accelerators in the chain together with their beam diagnostics are discussed.

5.2 Injector complex instrumentation

Figure 32 gives an overview of the e^+ / e^- injector complex of HERA. It consists of the following subsections:

- Thermionic gun (150 keV) which produces 3 µs long pulses at 50 Hz repetition rate.
- Chopper and collimator section for shortening of the long gun pulses (60/20 ns for e^+/e^-).
- Single cell 3 GHz pre-buncher cavity for matching to the linac RF.
- 450 MeV linac sections. These are 3 GHz (S-band) travelling wave structures which operate at a repetition rate of 50 Hz. After the linac the relative energy width is $\Delta E/E \approx 0.27\%$ for electrons and $\approx 1\%$ for positrons.
- Converter for e^+ production. The target consists of a 7 mm (2 radiation lengths) thick tungsten target which is located in a 1.8 T solenoidal field to enhance the collection efficiency [121].
- Positron Intensity Accumulator ring PIA. In addition to intensity accumulation, PIA is used for the re-formation of the time structure for the subsequent synchrotron which operates at 500 MHz [122]. It has two RF systems operating at 10.4 MHz and at 125 MHz.

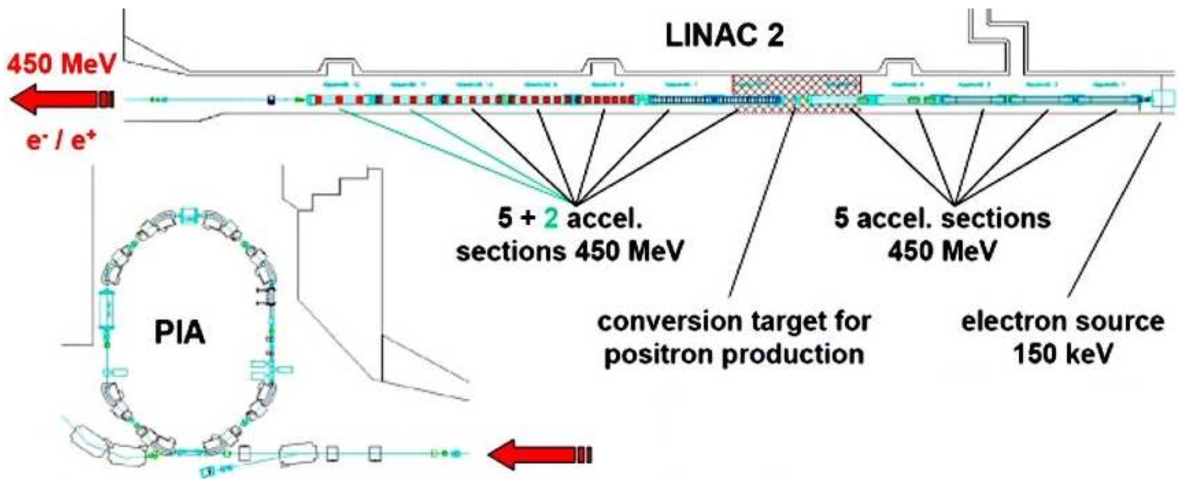

Fig. 32: The 450 MeV e^+/e^- injector linac for HERA together with the positron intensity accumulator ring PIA

A similar set-up was used for the LEP pre-injector (LPI), consisting of the LEP injector linac (LIL) and the electron positron accumulator (EPA) [123, 124].

As in the case for the hadron injector linac, the lepton injector complex needs beam instrumentation (i) for the adjustment of the beam transport through the individual accelerator sections, (ii) for the setting of the RF system, and (iii) to indicate the operating status during standard operation. The following list gives an overview of the standard instrumentation and the tasks involved:

- Intensity:
  Intensity diagnostics is required for determination of the transfer efficiency. Current transformers and/or wall current monitors are usually used.
- Beam position:
  Determination of the beam position is necessary for beam steering through various accelerator sections. Common devices for position determination are BPMs with sufficient sensitivity for the long linac bunch trains. However, luminescent screens are also used. Their use is less critical than for hadron beams because of the lower energy deposition in matter.
- Transverse beam profiles:
  The beam profile is an important prerequisite for emittance determination and beam optics matching. Typical beam monitors are fluorescent or OTR screens in straight sections and a synchrotron light monitor in the accumulator ring.
- Transverse emittance:
  Knowledge of the transverse emittance is required for the matching of different accelerator sec-

tions. It can be determined either via the multiscreen method or k-modulation of quadrupoles for transfer lines, or it is measured with synchrotron radiation diagnostics in the accumulator ring.

– Longitudinal plane:
  Magnet spectrometers are typically used for energy (-spread) measurements. As in hadron beam diagnostics the spectrometer magnet is normally the entrance magnet of a diagnostics beamline behind the linac. The time structure can be measured with an RF deflector, a wall current monitor, or via coherent radiation diagnostics.

The beam instrumentation required for a lepton injector complex is in principle the same as that for hadron machines. Therefore a detailed description of each monitor is not needed. An overview of the LEP injector linac instrumentation can be found in Ref. [125]. Further examples of synchrotron light source injector linac diagnostics are Ref. [126] for the APS (Argonne, USA) or Ref. [127] for the SLS (Villigen, Switzerland).

So far we have presented the lepton injector complex together with its instrumentation. Nevertheless, there are some peculiarities in the positron production which have an impact on the diagnostics. They will be discussed in the following subsection.

5.2.1 Comment on positron production

The principle of positron production is illustrated in Fig. 33 and explained according to Ref. [128]. A high-intensity electron beam of a few hundred MeV strikes a metal target. The resulting electromagnetic showers generate a mixture of secondary positrons and electrons with energies up to a few tens of MeV. A focusing system behind the target maximizes the collection efficiency of secondaries and guides them to the subsequent accelerator sections. Solenoids on the first accelerating sections together with quadrupoles on the sections further downstream provide focusing. At the end of the beam transfer, positrons and electrons are separated via a dipole.

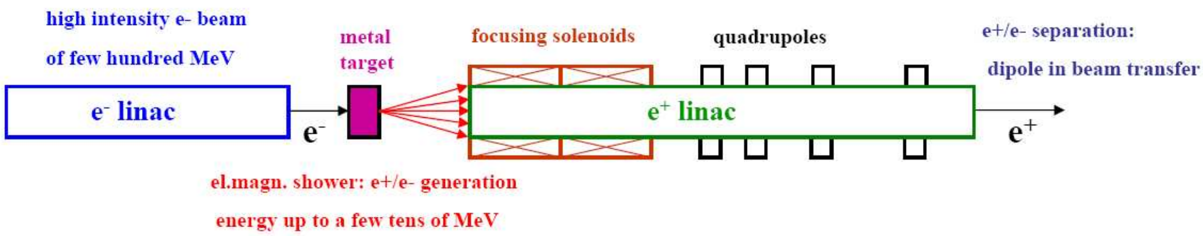

Fig. 33: Principle of positron generation

The positron production mechanism described above implies that the conversion target is located in a harmful radiation environment, and only radiation-resistant diagnostics can be applied close to the target.

Furthermore, for a high positron yield, a focus at the converter target is required. Therefore a transverse profile monitor close to the conversion target is desirable for beam size optimization. Luminescent screens cannot be used in such radiation-hard environments because of material degradation effects. As an example, two possible types of secondary emission monitors were discussed for LIL. More information about this can be found in Ref. [129].

Finally, the matching to the accumulator ring energy acceptance $\Delta E/E$ is of importance. As an example, for the LEP injector chain the EPA acceptance was $\pm 1\%$, and the energy spread was determined by three factors: the accepted momentum spread from the production target, the microbunch length, and beam loading [130]. In order to keep these effects under control, precise measurements of energy spread and bunch length are mandatory for a proper matching.

After the injector linac and accumulator ring the next elements in the injector chain are transfer line and booster synchrotron. However, there are no fundamental differences compared with hadron machines, and no fundamental differences in the instrumentation between an electron linac and a storage ring. Therefore the explicit description of diagnostics needs of these injector accelerators is not necessary and the discussion is continued with the description of the final storage ring instrumentation.

5.3 Storage ring diagnostics

The following list gives an overview of typical lepton storage ring instrumentation together with some comments concerning their usage.

- Current monitors (AC and DC):
  Current monitors are required for the determination of bunch charge and stored DC current. The monitor concepts in use are the same as those presented in the previous sections.
- BPMs:
  BPMs are necessary for the determination of beam orbit and associated parameters.
- Tune measurement:
  The tune defines the working point of the machine, its determination is therefore mandatory for machine operation.
- Feedback systems:
  Feedback systems are required in order to damp beam instabilities and to allow stable operation with high beam current.
- Synchrotron light diagnostics:
  This kind of diagnostics is used to measure longitudinal and transverse beam profiles and emittances and to study dynamical effects.
- Energy measurement:
  The beam energy is an important parameter for the experiments because it defines the cms energy for particle production.
- Luminosity monitor:
  The luminosity is a key parameter for colliders and is important for event rate optimization in the experiments. Leptons are simple point objects and their reaction cross-sections into final states are precisely calculable. Therefore the absolute luminosity determination is possible only after extensive off-line analysis.
- Beam loss monitors:
  Beam loss monitors are required for loss control and machine optimization. In a normal-conducting lepton machine the potential for damage of accelerator components in case of beam loss is less critical. Therefore loss monitors can be used not only for machine protection, but also for machine physics studies.
- Machine protection system:
  The machine protection system is necessary to protect sensitive and critical accelerator components, especially against excessive heat load. Therefore a reliable temperature control is essential for safe machine operation.

In the following sections selected instruments from this list will be presented and discussed and compared with those in hadron machines.

5.3.1 Beam position monitors

The bunch length in a lepton storage ring is much smaller than that in a hadron ring, typically of the order of 10–100 ps. Therefore button-type pick-ups are used. Owing to their high-pass characteristics they are suitable for small bunch lengths, but are also much simpler in construction and cheaper than a stripline monitor, for example.

The buttons are mounted out of the orbit plane to avoid direct synchrotron radiation illumination on them. Furthermore, in a lepton ring the vacuum chamber is not rotationally symmetric, see Fig. 34(a). There are two reasons for this, (i) the horizontal emittance is much larger than the vertical one because of synchrotron radiation emission in the horizontal plane, and (ii) injection oscillations in this plane due to off-axis injection allows intensity accumulation.

However, the symmetry distortion implies non-linear monitor position characteristics which must be corrected, cf. Fig. 34(b).

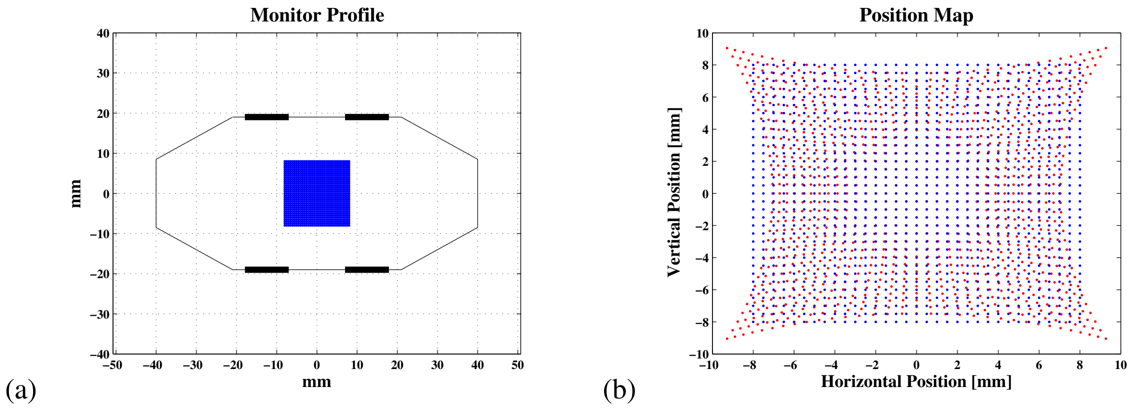

Fig. 34: (a) Cross-section of a lepton BPM vacuum chamber (PETRA III arc BPM). The button pick-ups are mounted on the top and the bottom of the chamber. (b) Position map of the arc BPM [131]. The blue dots correspond to the beam position inside the chamber [cf. figure (a)], the red ones are the reconstructed positions according to the Δ/Σ algorithm.

5.3.2 Tune and feedback

Because of radiation damping caused by emission of synchrotron radiation, beam blow up is not a critical issue. Therefore permanent beam excitation can be applied and an online tune control is possible.

In a high-energy lepton storage ring the particle's electromagnetic field has a long range and can act back on the beam itself via the environment. Owing to the short bunch lengths the beam spectrum has broadband characteristics, and instability excitations are possible over a wide frequency range. As a consequence the lepton storage ring has to be operated with a multibunch feedback system to damp coupled-bunch instabilities.

Figure 35 illustrates the components required for an electron feedback system. These are (i) a detection system to measure (longitudinal or transverse) beam oscillations, (ii) a signal processing unit to derive correction signals, and (iii) a broadband amplifier and beam deflector to act back on the beam. More information about feedback systems can be found in Refs. [132, 133].

5.3.3 Transverse profile and emittance

For transverse profile or emittance measurements, imaging with synchrotron radiation is widely used as non-destructive profile diagnostics. The imaging resolution of optical synchrotron radiation is usually sufficient. To give an example, the HERA horizontal and vertical beam sizes were about $\sigma_h = 1200$ µm and $\sigma_v = 250$ µm.

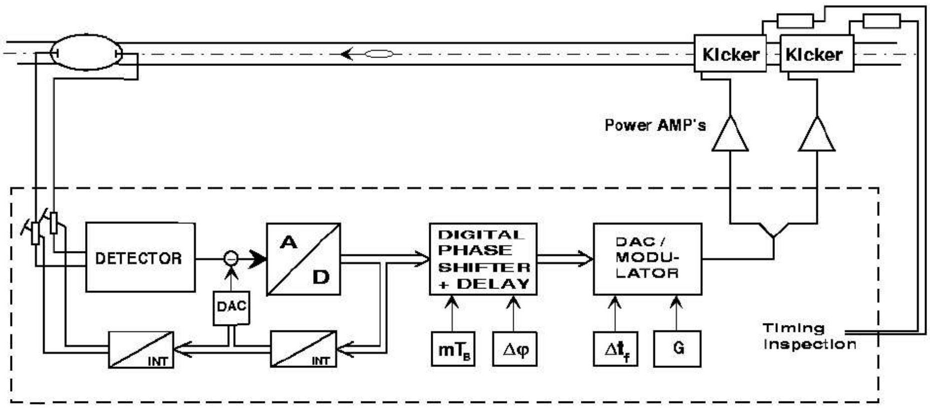

Fig. 35: Schematic view of the HERA transverse electron feedback system [132]

Figure 36(a) shows a schematic view of the HERA monitor set-up [134]. The light is extracted from the vacuum system by a mirror and the beam is imaged by a lens system onto the chip of a CCD camera. An interference together with a polarization filter serves for resolution improvement. Additional information about synchrotron radiation diagnostics in general can be found in Refs. [135, 136] and the references therein.

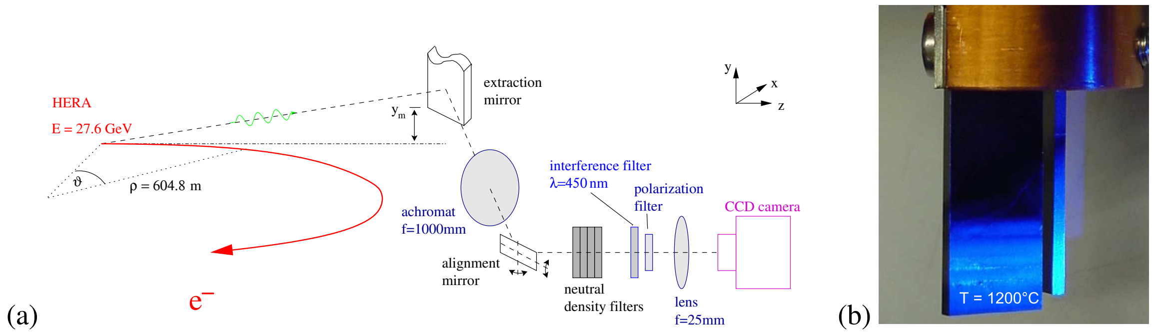

Fig. 36: (a) Schematic view of the HERA profile monitor set-up [134]. (b) Photo of the HERA extraction mirror. A surface deformation caused by the heat load is clearly visible close to the lower mirror edge.

A problem which often arises is the heat load on the first extraction mirror which leads to image distortion and resolution deterioration. This is caused by the X-ray part of synchrotron radiation absorbed in the mirror material. To keep the absorption to a minimum, materials with low absorption coefficients like beryllium are often used, and in addition the mirror is water-cooled. However, this is not sufficient to prevent image distortion and even destruction of the monitor components. Figure 36(b) shows a photo of the HERA extraction mirror which was in use for several years. A deformation of the surface caused by the heat load can be seen close to the lower mirror edge. Finite element calculations demonstrate that the mirror could heat up to a temperature of 1200°C in the region where the X-ray part of the synchrotron radiation fan hits the mirror.

There are different ways to overcome this problem, and a few selected solutions are included here. At HERA out-of-plane observation was used, i.e., the bottom edge of the extracting mirror was placed above the orbit plane [cf. Fig. 36(a)] so that the X-ray part of synchrotron radiation could not hit the mirror, and only optical synchrotron radiation emitted under larger angles was reflected out of the vacuum system. A drawback of this method was an increased diffraction-limited resolution contribution [134]. The LEP 2 synchrotron light telescopes used adaptive optics for correction, i.e., cylindrically deformable mirrors to compensate the cylindrical extraction mirror deformation together with moveable detectors to compensate spherical deformation [137]. At PEP-II a slotted mirror design together with an X-ray absorber was applied [138], but also with the drawback of increased diffraction-limited resolution. Finally, at SLS (Villigen, Switzerland) a thin absorber was inserted in front of the extraction mirror which blocks the radiation, and the measurement is performed with synchrotron radiation in π polarization [139].

5.3.4 Longitudinal profile

Synchrotron radiation based diagnostics is also widely applied for the investigation of the longitudinal profile. For illustration Fig. 37(a) shows the calculated transverse electric field in the orbit plane for a 27.5 GeV electron. As can be seen, the duration of the synchrotron radiation pulse is in the order of 10^{-2} as, i.e., it can resolve longitudinal beam profiles of the order of 10–100 ps.

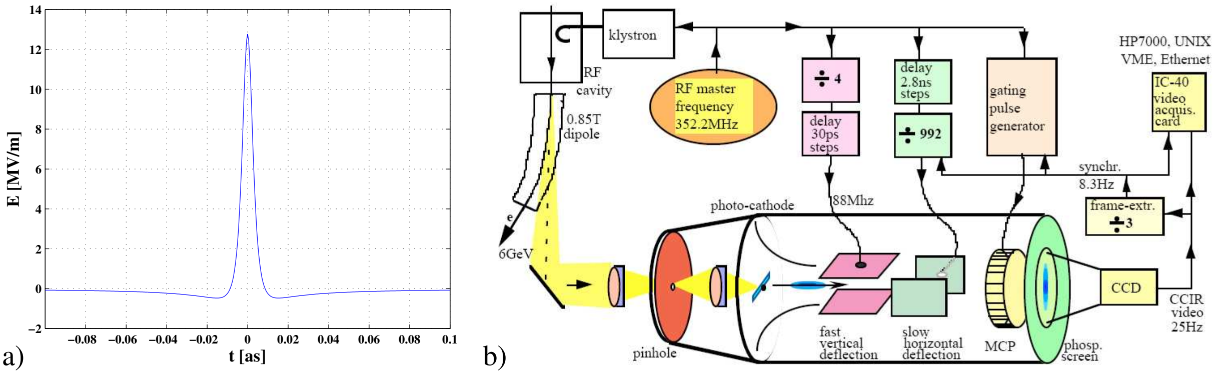

Fig. 37: (a) Calculation of the synchrotron radiation electric field component in the orbit plane. Parameters are for the HERA electron ring: $E = 27.5$ GeV, magnet bending radius $\rho = 604.81$ m. The zeroes of the field correspond to the reciprocal of the synchrotron radiation critical frequency. (b) Schematic view of a dual-sweep streak camera together with synchronization [140].

It is interesting to note that the zero-crossing of the field is given by the reciprocal of the characteristic synchrotron radiation frequency, i.e., the duration can be estimated by the time interval where the field is positive as

$$\Delta t = 2/\omega_c = \frac{4\rho}{3\gamma^3 c} \tag{16}$$

with ρ the bending magnet radius.

A standard device used for bunch length measurements at lepton storage rings is the streak camera. Its set-up together with the synchronization scheme is illustrated in Fig. 37(b). More information about streak cameras can be found in Refs. [141, 142].

5.3.5 Beam energy

Leptons are point-like objects, and in a lepton collider the total energy is of tremendous importance as it is a constraint on the final state detected in the experiment. Therefore the determination via the dipole current is not sufficient and more precise energy measurements are required.

One measurement technique in use is the resonant spin depolarization technique which is based on the destruction of the self-polarization arising from the Sokolov–Ternov effect [143]. The machine energy is varied until a $(g-2)$ resonance is excited which causes the beam to depolarize. Assuming the resonance is uniquely identified, the spin tune

$$\nu_s = \gamma(g-2)/2 \tag{17}$$

is determined, and with it the beam energy $E = \gamma m_0 c^2$. The g factor of the electron is known from precise quantum electrodynamical calculations, and the beam polarization is monitored by scattering a laser beam off the circulating beam and measuring the spin-dependent part of the Compton scattering by recording the angular distribution of the back-scattered γ rays. This method was successfully applied at LEP [100, 144].

Another scheme in use is the Compton backscattering technique which was originally implemented at the BESSY-I and BESSY-II storage rings [145], and also used at the VEPP-4M collider (BINP, Novosibirsk) [146].

6 Diagnostics for light sources

So far diagnostics needs for lepton accelerators with special emphasis on high energy physics colliders have been presented. This section is dedicated to a different class of electron accelerators, the light sources. In the first part, third-generation light sources based on a low emittance electron storage ring are treated. The second part presents the diagnostics needs for a linac (single pass) based fourth-generation light source (FEL).

6.1 Storage-ring-based light sources

In principle a storage-ring-based light source resembles a lepton collider with the difference that only one species of particle circulates in the machine. Figure 38 shows the typical layout of a light source, taken from the Diamond Light Source (Oxfordshire, UK) [147]. The storage ring of such a type of accelerator usually has an energy in the range 1–8 GeV and a circumference of the order of 100–2000 m. Most machines operate at fixed energy so special diagnostics to control the acceleration process is not required. The insertion devices (wigglers or undulators) are an integrated part of the machine located in straight sections, and user experiments are situated at the end of long photon beamlines which are typically 50–100 m away from the source point.

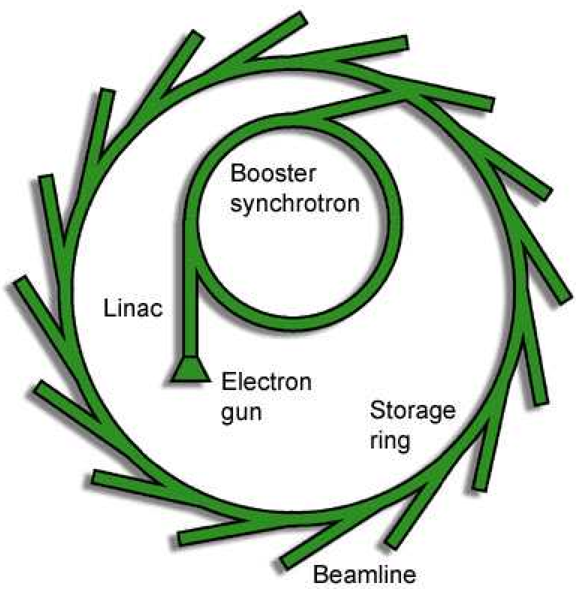

Fig. 38: Layout of a third-generation storage-ring-based light source [147]. The storage ring is densely equipped with user beamlines for transportation of the radiation from the source (bending magnet, wiggler or undulator) to the experimental huts where the user experiments are located. The injector chain is short and consists of the electron gun, the subsequent linac, a booster synchrotron, and a short transfer line.

The injector chain of a light source is much shorter than that of a collider, it consists of a linac, a booster synchrotron to cover the energy gap between linac and storage ring, and a short transfer line to the injection in the storage ring. The instrumentation required for operation and diagnostics in the injector chain consists of standard monitors already described above.

In the next section some general remarks concerning light source requirements are summarized.

6.1.1 Remarks on light sources

The key parameter of a light source is the spectral brilliance B which is defined as follows:

$$B = \frac{\text{Number of photons}}{[\text{s}]\,[\text{mm}^2][\text{mrad}^2][0.1\%\text{ bandwidth}]}\,. \tag{18}$$

Thus B is a measure of the phase space density of the photon flux. The user requirement is to have a high brilliance which means as many monochromatic photons as possible emitted from a minimum source region on the sample. The brilliance can be rewritten as a function of the accelerator parameters in the following form:

$$B \propto \frac{N_\gamma}{\sigma_x\,\sigma'_x\,\sigma_y\,\sigma'_y} \propto \frac{I_b}{\varepsilon_x\,\varepsilon_y} \tag{19}$$

with I_b the beam current, and $\varepsilon_{x,y}$ the horizontal and vertical beam emittance. According to Eq. (19) there are two requirements for the accelerator to achieve a high brilliance:

(i) High beam current. This has the following implications for beam diagnostics:
   (a) to achieve the high currents.
   Diagnostics is needed to detect and damp instabilities.
   (b) to cope with high heat load.
   Heat load changes may lead to a position drift of accelerator and beam line components which the user will see immediately as a change in the photon flux on the sample.

(ii) Small beam emittances. The implications are:
   (a) to achieve small emittances.
   The choice of the proper magnet lattice defines the minimum achievable emittance. Lattices in use are the Double Bend Achromat (DBA) or the Triple Bend Achromat (TBA), for example. However, this is a task for the lattice designer [148, 149] and will not be covered here.
   (b) to measure small emittances.
   If the accelerator is designed to have a small emittance, it is mandatory to have monitors which are capable of measuring this beam parameter. To measure a small transverse emittance in a storage ring means to be able to resolve small transverse beam sizes.
   (c) to preserve the emittance.
   There are various effects resulting in emittance growth and with it a deterioration of the beam quality. Examples are fast beam orbit motions as well as short-term and medium-term component position drifts, i.e., stability is again a critical issue.

As can be seen from this list, stability is crucial for the operation of a light source. Therefore in the following section stability issues and their implications on beam diagnostics will be addressed. Detailed discussions about this topic can be found in Refs. [150–152]. Further information about performance and trends of storage ring light sources in general can be found in Ref. [153] and the references therein.

6.1.2 Stability

Although stability issues are mutually dependent, they can roughly be classified into three categories.

(i) Energy stability and suppression of energy broadening effects:
These effects are mainly caused by (longitudinal) multibunch instabilities. They can result in a shift of the radiation harmonics from an undulator which the user sees as intensity fluctuations and line broadening. Examples for these effects can be found in Refs. [154, 155]. To combat such instabilities multibunch feedback systems are required.

(ii) Intensity stability:
A change in background conditions or thermal load on beamline and machine components due to intensity variations may affect position stability. Therefore it is desirable to keep the intensity at a constant level. Intensity fluctuations may be caused by transverse multibunch instabilities which have to be damped by a feedback system. However, a change in intensity due to the natural beam lifetime is also not tolerable for many applications. Therefore the trend is towards operating light sources in top-up mode, i.e., the natural losses are compensated by refilling small amounts of charge in short time intervals [156]. This implies a vast dynamic range that is required for the beam monitors, starting from the injector chain.

(iii) Position stability:
Instabilities in the beam position result in emittance growth and intensity fluctuations, i.e., in a reduction of the brilliance of the light source. In order to keep the orbit stable to a high level of precision, orbit feedback systems are required that include high-resolution electron BPMs in the storage ring together with photon BPMs in the user beamlines. Reference [157] gives an actual overview of state-of-the-art fast beam position feedback systems.

In the following sections diagnostics instrumentation is presented which is specific for the operation of light sources. These are beam position monitors and devices for emittance diagnostics. A general overview of diagnostics for third-generation light sources and recent developments can be found in Refs. [158, 159]. Additional information about beam instrumentation can be found in diagnostics overview articles for light sources. Examples are Ref. [160] for the APS (Argonne, USA), Ref. [161] for Diamond (Oxfordshire, UK), Ref. [162] for Soleil (Gif-sur-Yvette, France), and Refs. [163, 164] for PETRA III (DESY, Germany).

6.1.3 Beam position monitoring

The typical stability requirement for a light source is to keep the intensity fluctuations constant to a level of 0.1%. This can be translated into a maximum allowed emittance growth of 20% owing to short-term orbit fluctuations, which is equivalent to an orbit stability requirement of 10% of the $(1\,\sigma)$ beam size and beam divergence [165]. For the new synchrotron light source PETRA III at DESY, the beam sizes close to insertion devices are $\sigma_h = 20$ µm and $\sigma_v = 3$ µm, i.e., the corresponding stability requirements are 2 µm and 0.3 µm.

High-resolution button-type pick-ups are used to monitor the electron beam orbit. As an example, Fig. 39 shows a drawing of a PETRA III BPM which is installed in sections between two canted undulators. Because of the small undulator gaps the chamber height is only 7 mm, and the chamber width is 83.5 mm and asymmetric in order to avoid heat load owing to direct synchrotron radiation illumination. Both the strong ellipticity and the asymmetry of the vacuum chamber profile result in strong non-linearities in the beam position determinations that have to be corrected.

Besides the electron BPMs, additional X-ray BPMs are installed in the photon beamlines. Usually two XBPMs are used per beamline in order to correct photon beam angle and position. These parameters are often included in the orbit feedback system. A monitor type widely used is the gapped photoemission blade monitor. It probes the outer fringes of the photon beam with metal electrodes, permitting the central

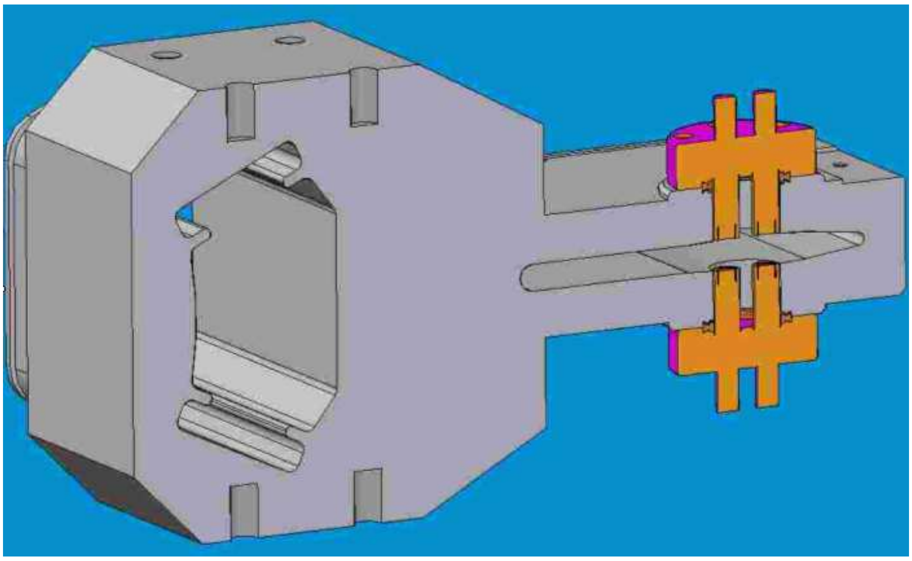

Fig. 39: PETRA III vacuum chamber between canted undulators with flanged BPM (cut). The pump channel on the left side is used for the mounting of NEG-strip pumps (courtesy A. Brenger, DESY).

core of the beam to pass through to a downstream experiment [166, 167]. However, gapped monitors suffer from the fact that they sample only the lower energy tails of the photon beam. Any asymmetry in illumination of the electrodes owing to occlusion from upstream apertures, low-energy scattered or reflected photons, or in the case of undulator radiation beamlines from nearby bending magnet radiation, leads to an error in determining the centroid beam position [158]. In order to overcome this drawback, at PETRA III residual gas X-ray BPMs are foreseen which probe also the central core of the photon beam distribution [168]. Further information about XBPMs can be found in Ref. [158] and the report in these proceedings [169].

6.1.4 Emittance diagnostics

Modern light sources need to achieve horizontal emittances in the order of 1 π nm rad and even less with emittance coupling of about 1%. Therefore a precise measurement especially of the small vertical emittance is a challenge. As usual in a storage ring, synchrotron-based diagnostics is used to measure a photon spot which contains information about the emittance.

The most common way is to make a beam image with an appropriate light optics, i.e., the photon spot is a measure of the transverse beam profile. However, in the imaging process there exists a principle limitation which is given by Heisenberg's uncertainty relation. In this specific case it can be reformulated as

$$\Delta\sigma \approx \frac{\lambda}{2\Delta\Psi} \tag{20}$$

with $\Delta\sigma$ the resolution broadening owing to diffraction, λ the wavelength of observation, and $\Delta\Psi$ the opening angle of the emitted photon as measured from the orbit plane. While the horizontal emission angle is large owing to the particle motion on a curved trajectory, the vertical one is small and thus imposes the fundamental resolution limit. For a typical optical wavelength of observation $\lambda = 500$ nm and an opening angle $\Delta\Psi = 1$ mrad, the resolution would amount to $\Delta\sigma = 250$ µm. Considering that the vertical beam size in a modern light source is of the order of a few tens of microns and even less, such a monitor would have a totally diffraction-limited resolution. In order to overcome this limit there exist different concepts which will be briefly addressed in the following. More information can be found in Ref. [170] and the references therein.

The most straightforward way to overcome this limitation is imaging at smaller wavelengths in the VUV, soft or even hard X-ray region, cf. Eq. (20). In this case the discussion about a monitor concept is reduced to the question of the appropriate imaging optics. This can be a focusing optics like a reflective one (Kirkpatrick–Baez mirrors), a diffractive one (Fresnel zone plate or Bragg–Fresnel lens), or a refractive one (compound refractive lens). Beside these, focus-free imaging with X-ray pinhole cameras is widely used in many accelerator laboratories. Furthermore, the wave optics features of the emitted radiation can be exploited [139]. Finally, in a recent publication an approach based on coded-aperture imaging was reported [171], a technique well-developed among X-ray astronomers. However, in any case, a necessary prerequisite for X-ray imaging as emittance diagnostics is to have a dedicated diagnostics beamline, at least with synchrotron radiation from a bending magnet as the source.

Another concept used in some laboratories is an interferometric approach [172] which is adapted from the stellar interferometer of Michelson used for the determination of the extent of stars. It is based on the investigation of the spatial coherence properties of the radiation by measuring the blurring of the interferogram which depends on the particle beam size in a double-slit interferometric set-up, cf. Fig. 40. The fundamental limit of this monitor principle is again Heisenberg's uncertainty relation which can be reformulated for an interferometric measurement as $\Delta n \Delta\Phi \sim 1$, with $\Delta\Phi$ the relative phase difference between the wave trains passing the two individual slits and Δn the number of required photons [173]. As a consequence, in order to measure the phase difference with high accuracy, the intensity must be sufficient. For the determination of the beam size in both transverse directions each plane requires a dedicated interferometric set-up. The measurement is performed such that the slit distance D is varied and the interference pattern is recorded with a CCD in the image plane.

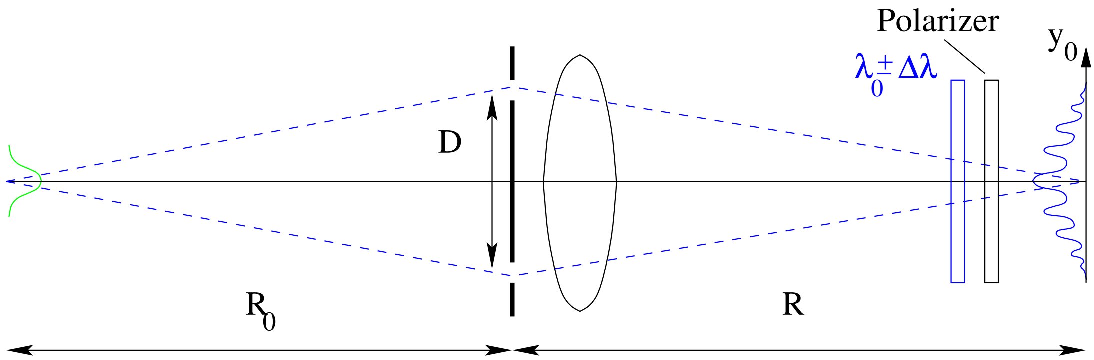

Fig. 40: Principle set-up for interferometric beam-size measurements

A less used consept is the projection method which exploits the angular divergence instead of the beam size. However, on account of the horizontal fan of bending magnet radiation, only the vertical emittance can be determined. The principle of this method relies on the fact that only a tiny fraction of very hard X-rays can fully penetrate the dipole crotch absorber and enter in the free air space behind. These X-rays are detected by a simple, compact and low-cost device, consisting of a $\mathrm{CdWO_4}$ scintillator and a standard CCD camera system. With knowledge of the measured photon spot size $\sigma_{\gamma,y}$, the mean square photon emission angle $\langle\vartheta_\gamma^2\rangle$, the distance between source and image plane L, and the accelerator Twiss parameters at the emission point, the emittance can be derived as

$$\varepsilon_y = \frac{\sigma_{\gamma,y}^2 - \langle\vartheta_\gamma^2\rangle L^2}{\beta_y + 2\alpha_y L + \gamma_y L^2} \,. \tag{21}$$

So far the peculiarities of storage-ring-based synchrotron light sources have been pointed out. The next section is devoted to the diagnostics needs of a new class of fourth-generation light source, the linac (single-pass) based FEL.

6.2 Free electron lasers

The discussion covers FELs which are based on the principle of self-amplified spontaneous emission (SASE), and relies especially on experience with the operating FLASH facility [174,175] and the planned European XFEL project [176], both situated at DESY (Germany). However, from the diagnostics viewpoint the type of linac-based FEL is not important.

Figure 41 illustrates the working principle of a SASE FEL. It makes use of the fact that a high quality electron beam, passing a long undulator magnet, exponentially amplifies an initially existing radiation field. A prerequisite for this effect is that the photon wavelength λ_r matches the resonance condition

$$\lambda_r = \frac{\lambda_u}{2\gamma^2}(1 + K^2) \tag{22}$$

which is determined by the Lorentz factor γ, the undulator period λ_u, and the undulator parameter K which is a measure of the magnetic field. The intensity amplification results from the modulation of the electron bunch with the undulator radiation field emitted by the bunch itself. This leads to a density modulation (microbunching) in the bunch so that more and more electrons radiate in phase until saturation is reached. Further information about the theory of FELs can be found in the textbook by Saldin *et al.* [178].

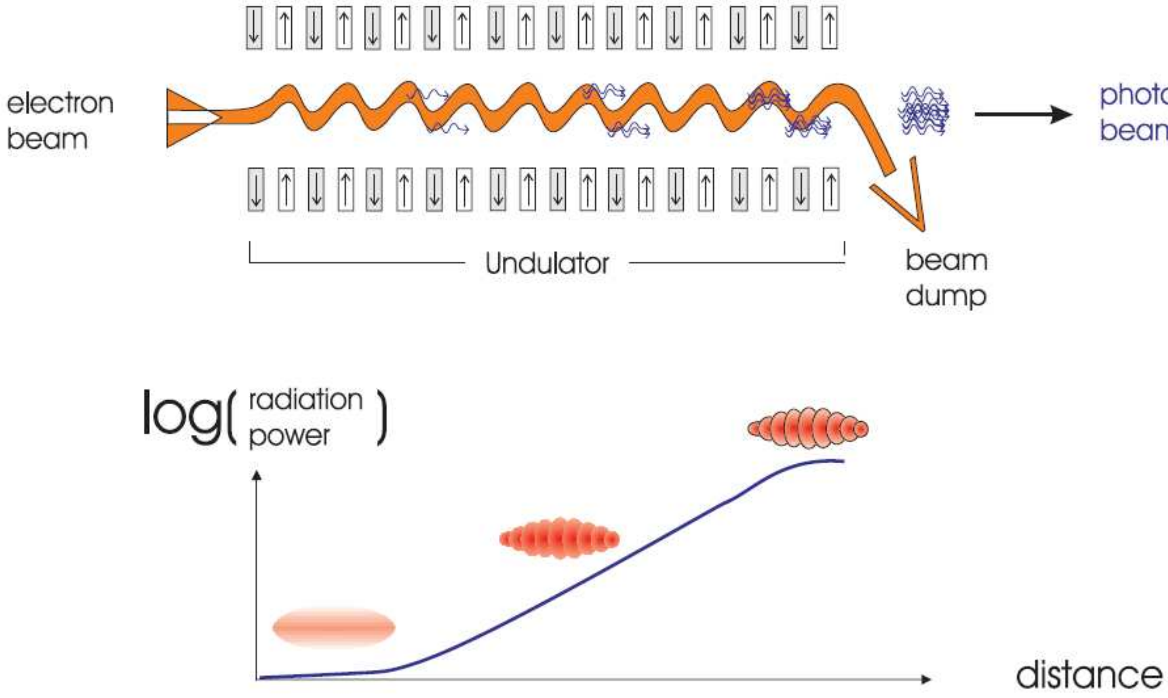

Fig. 41: Working principle of a single-pass Free Electron Laser (FEL) operating in the self-amplified spontaneous emission (SASE) mode. The lower plot shows the bunch density modulation (microbunching), developing in parallel to the radiated power [177].

There exist a number of SASE FEL projects in different accelerator laboratories worldwide. Besides the FLASH and XFEL facilities at DESY, further examples are the SPARC/X projects in Frascati (Italy) [179, 180], the LCLS facility at SLAC (USA) [181], and the SCSS facility at SPring8 (Japan) [182]. In the next subsection the requirements for the FEL operation are addressed and their impact on beam diagnostics is pointed out.

6.2.1 FEL requirements

A high current density is mandatory in order to have sufficient energy transfer from the electron beam to the radiation field. For a rough current estimation the number of electrons per wavelength

$$N_{e,\lambda} = \frac{I\lambda_r}{ec} \tag{23}$$

is considered as natural scale. According to Eq. (23) the current in a slice of a microbunched beam containing a single electron is calculated as

$$N_{e,\lambda} = 1 \quad \Rightarrow \quad I = \begin{cases} 0.5\ \mu\text{A} & \text{for}\ \ \lambda_r = 100\ \mu\text{m}, \\ 0.5\ \text{A} & \text{for}\ \ \lambda_r = 0.1\ \mu\text{m}. \end{cases}$$

However, the energy transfer from a single electron to the radiation field is not sufficient and very high peak currents are required depending on the wavelength. At FLASH, for example, the peak current of the uncompressed bunch amounts to about 70 A, but a peak current exceeding 1 kA is required for laser operation. In order to achieve these currents, additional longitudinal bunch compression is required for this increase of the current density. For this purpose a correlation between particle energy deviation and longitudinal position is introduced with an RF system. In the following dispersive beam line section, particles with different energies have different path lengths. With the proper parameter settings, the bunch tail has a shorter path and can catch up to the head so that the bunch is effectively compressed. At FLASH the bunch compression using magnetic chicanes is done in two steps at different energies, and the resulting bunch lengths are of the order of much less than 100 fs which is about three orders of magnitude smaller than in a lepton storage ring.

Together with the requirements of extremely short bunches, a very good electron beam quality is essential to sustain the lasing. In order to have resonant energy exchange from the beam to the radiation field, the demands on the beam energy spread are

$$\frac{\sigma_E}{E} \approx 10^{-4}\ .$$

In addition, the radiation field and electron beam must have a good overlap which defines constraints on the transverse beam emittance:

$$\varepsilon \leq \frac{\lambda}{4\pi} \quad \text{with} \quad \varepsilon = \varepsilon_n/\beta\gamma\ ,$$

i.e., a high beam energy is helpful to achieve this condition.

The FEL working principle relies on the fact that the electrons slip back in phase with respect to the photons by one radiation wavelength λ_r each undulator period, i.e., the FEL integrates over the slippage length. As a consequence it is the slice emittance and not the projected one which is of primary concern, see also Fig. 42.

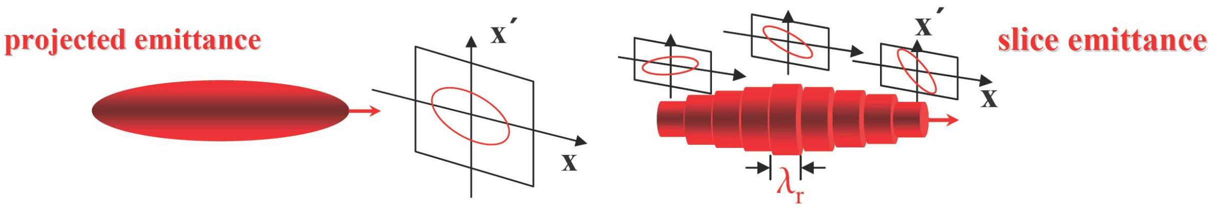

Fig. 42: Difference between projected and slice emittance of a bunch

To conclude, the operation of a SASE FEL requires very high demands on the full six-dimensional phase space. But in contrast to a circular accelerator, in a linac-based accelerator there exists no radiation damping and the beam quality is determined from the gun. This implies the necessity of careful diagnostics and control of the relevant beam parameters starting from the gun along the whole linac.

Besides the demands on the phase space, stability is a critical issue. This includes

(i) the energy stability which translates directly into a wavelength stability as

$$\frac{\Delta\lambda}{\lambda} = -2\,\frac{\Delta E}{E}$$

according to Eq. (22), i.e., energy jitter causes wavelength jitter. Because of the use of magnetic chicanes the energy stability also defines the stability of the photon arrival time which is of importance for the users, especially in pump–probe experiments.

(ii) Position stability is crucial because the overlap between electron and photon beam in the undulators has to be maintained. To give an example, the length of the undulator sections for the European XFEL is in the order of 100–150 m with a transverse rms beam position stability requirement of 10% of the $\sim$ 30 μm beam size ($1\,\sigma$). In order to be sensitive to small orbit variations in the micron region, high-resolution BPMs are required. In the case of the XFEL, cavity BPMs with a (single-bunch) resolution of about 1 μm are planned for the intersections between the undulator segments [176]. For linac-based FELs which can produce long bunch trains (which is usually the case for FELs using superconducting accelerating structures such as the XFEL with up to 3250 bunches) it is even possible to stabilize the beam orbit with an intra-bunch-train feedback system which damps harmful beam position perturbations [183, 184].

To achieve a high average power in a SASE FEL, some of the accelerators will use or already use superconducting accelerating structures. Examples are FLASH and XFEL with their nine-cell standing wave structures of about 1 m length and fundamental TM mode at 1.3 GHz. These cavities are identical to the so-called TESLA cavity [185], made from solid niobium, and bath-cooled by superfluid helium at 2 K. The use of superconducting accelerator structures requires again that parts of diagnostics components be operated in the cold environment, especially the pick-ups. These components must additionally be suitable for an assembly in a particle-free environment. For illustration, Fig. 43 shows the cold BPMs for the XFEL together with their environment.

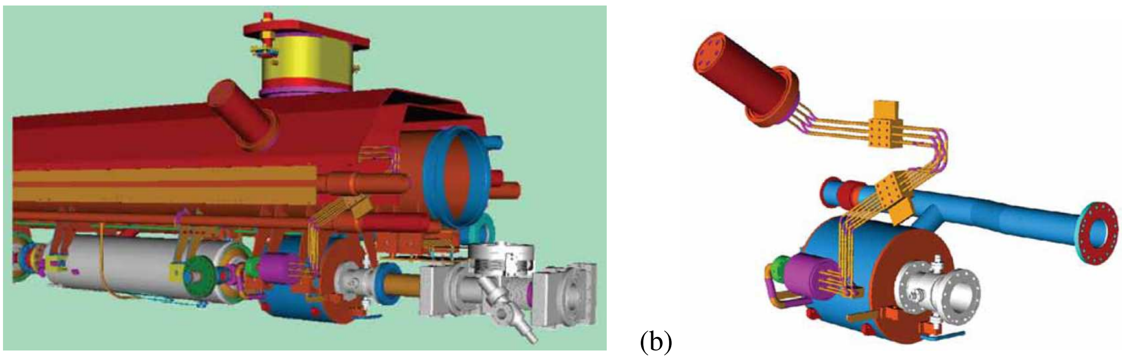

(a) (b)

Fig. 43: (a) Schematic view of a cryomodule for the XFEL: cold mass with (from left) cavity, magnet, BPM, and HOM-absorber beam pipe valve. (b) Detailed view of the BPM together with magnet and current leads which are located at the downstream end of each XFEL accelerator module [176].

6.2.2 Comments on FEL diagnostics

This section gives an overview of general diagnostics which are essential for FEL operation and some peculiarities which will be addressed later. The discussion is based on the experience with the operating FLASH facility at DESY. A general overview of beam instrumentation and diagnostics strategies for FLASH can be found in Ref. [186], further developments are summarized in Ref. [175].

Because of the nonlinear and stochastic FEL process, the accelerator, the electron beam parameters along the FEL undulator, and the user beamlines with experiments are strongly coupled. To operate the FEL under controlled conditions, diagnostics systems are required for all sections. The stochastic nature of the radiation requires additionally an event-oriented data acquisition system for machine operation and user experiments so that parameters can be correlated. According to Ref. [186] the required diagnostics systems can be arranged in three categories:

(i) *Standard electron beam diagnostics to operate the linac.*
Instrumentation is required to measure the necessary beam parameters. These are the electron beam orbit, the bunch charge, the beam size, and the beam phase (with respect to the RF).
Fast protection systems with response time in the μs range are mandatory to shut off the beam in case of high losses in order to prevent damage to the undulators (demagnetization) and to the vacuum system (leakage). Such systems are essential for the operation of superconducting linacs owing to the large amount of transported energy.

(ii) *Diagnostics needed to control and optimize the FEL.*
For this purpose the phase space of both the electrons and the photons have to be measured and controlled. This includes the determination of the transverse emittance, bunch length and bunch shape (i.e., compression), and energy as well as energy spread.
For the determination of beam size and transverse emittance, the transverse beam profile has to be measured at different positions along the machine with a resolution of 10 μm and better. Instruments in use for this purpose are OTR screens and/or wire scanners.
Bunch lengths smaller than 100 fs have to be measured. The lasing process is typically supported by only a small fraction of the charge in a narrow spike produced by the strong bunch compressor, so that it is not sufficient to determine only the first moment of the charge distribution. As a consequence a measurement is required which allows the full reconstruction of the bunch shape.
As described above, it is the slice emittance and the slice energy spread that determines the performance of the FEL, and a measurement of these parameters is required with a longitudinal resolution less than a radiation pulse length for complete characterization of the electron phase space distribution.
An online signal is needed for the optimization of the SASE process that can be used to determine the optimal phase for bunch compression with a precision of about 0.1°.

(iii) *Diagnostics needed for user experiments.*
The FEL is a pulsed radiation source, and user experiments will be pulse resolved. Since the SASE process starts from noise, every radiation pulse is different, and all relevant photon beam parameters have to be measured with single-pulse resolution. The characterization of each radiation pulse requires the determination of photon energy and spectral distribution.
Time-resolved experiments need information on duration and temporal structure of the radiation pulse. They require a precise determination of the arrival time which is especially important in pump–probe experiments, i.e., beam synchronous timing is crucial.

Figure 44 shows an overview of the FLASH diagnostics in the different machine sections. In the following, some of the monitor concepts that are specific for control and optimization of the FEL will be presented. This includes bunch length diagnostics, slice emittance diagnostics, and bunch compression monitors. While standard instrumentation for linac operation has already been covered in the preceding sections, further information about monitors for the characterization of radiation pulses can be found in Ref. [186] and the references therein. The topic of beam synchronous timing is covered in Refs. [187, 188]. More information about diagnostics in general for FEL operation can be found in Ref. [189].

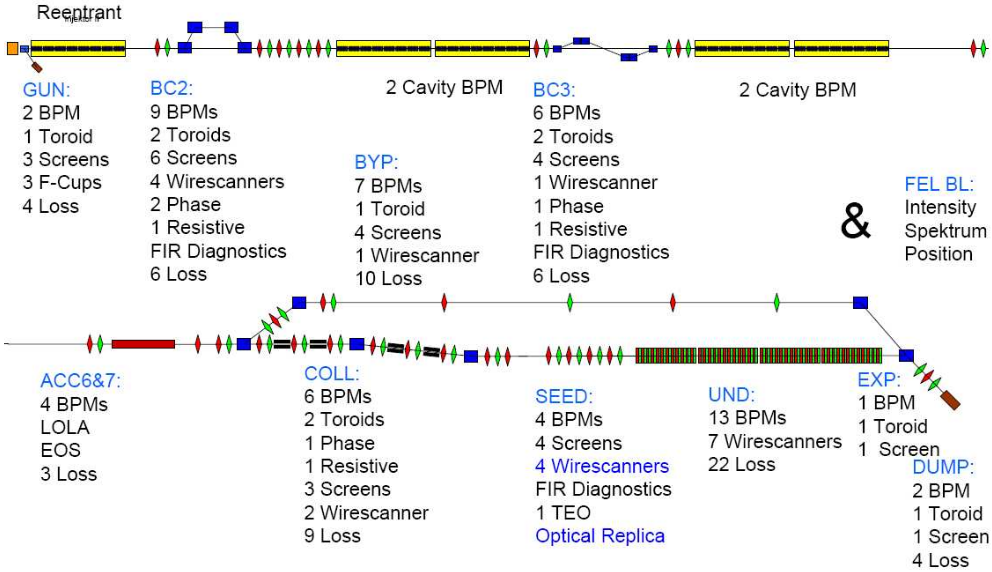

Fig. 44: Overview of FLASH diagnostics systems (courtesy D. Nölle, DESY)

6.2.3 Bunch length and bunch profile diagnostics

The resolution limit of a streak camera is typically of the order of a picosecond. In order to resolve time distributions in the femtosecond region new diagnostics concepts are required. Two new schemes have been applied for the measurements of sub-ps longitudinal charge distributions. These are coherent radiation diagnostics (CRD) and electro-optical sampling (EOS), and they will be briefly described in the following. More information can be found in Ref. [190].

Radiation is emitted coherently if the wavelength is of the order of the bunch length, i.e., information about bunch length and shape is encoded in the emission spectrum which is exploited in CRD. In the case of coherent emission the spectral intensity is strongly amplified which can be expressed in the following form:

$$\frac{\mathrm{d}U}{\mathrm{d}\lambda} = \left(\frac{\mathrm{d}U}{\mathrm{d}\lambda}\right)_1 \left(N + N(N-1)|F(\lambda)|^2\right) \; . \tag{24}$$

Here $(\mathrm{d}U/\mathrm{d}\lambda)_1$ is the single-particle emission spectrum, N the number of particles in the bunch, and $F(\lambda)$ the bunch form factor. It is related to the normalized bunch profile $S(z)$ via a Fourier transform:

$$F(\lambda) = \int_{+\infty}^{+\infty} \mathrm{d}z \; S(z) \; e^{-2\pi i z/\lambda} \; . \tag{25}$$

According to Eq. (24), from a measurement of the spectral intensity and with knowledge of the single-electron spectrum together with the bunch charge, the form factor can be determined. Inverting the Fourier transform Eq. (25) results in the reconstructed bunch profile $S(z)$. However, the situation is more complicated because it is the magnitude $|F(\lambda)|$ of the form factor which is determined rather than the complex form factor itself. Reconstruction is possible only if both amplitude and phase are available. Although a strict solution of this phase-reconstruction problem is not possible, a so-called minimal phase can be constructed with the Kramers–Kronig relation. A detailed treatment of this problem can be found in Ref. [191].

In principle any kind of coherent radiation can be used as a radiation source. Measurements have been performed with coherent synchrotron radiation, transition radiation, diffraction radiation, and Smith–Purcell radiation. Figure 45 shows a measurement with coherent synchrotron radiation together with the reconstructed bunch shape. As can be seen from the comparison with an independent streak camera measurement, CRD allows fine details of the bunch shape to be resolved.

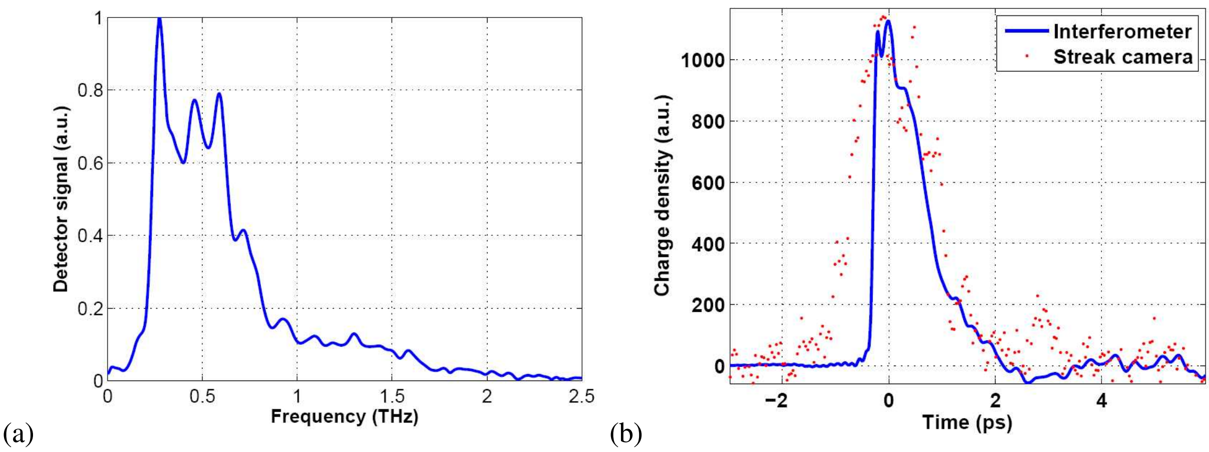

Fig. 45: Example of a bunch shape reconstruction with coherent radiation diagnostics at FLASH. (a) Measured synchrotron radiation spectrum. (b) Reconstructed charge distribution together with a streak camera measurement, performed at the same location using visible light (courtesy L. Fröhlich, DESY).

EOS can be applied for ultrarelativistic charged electrons where the particle Coulomb field is purely transversal, i.e., the field strength of the non-propagating particle field is a measure of the longitudinal bunch profile. If the bunch passes close to an electro-optical crystal, its Coulomb field induces a change in the crystal refractive index (so-called Pockels effect). The information about the longitudinal profile is therefore encoded in a refractive index change which can be converted into an intensity variation by means of a laser together with polarizers. Figure 46 illustrates a simple EOS set-up using a variable delay.

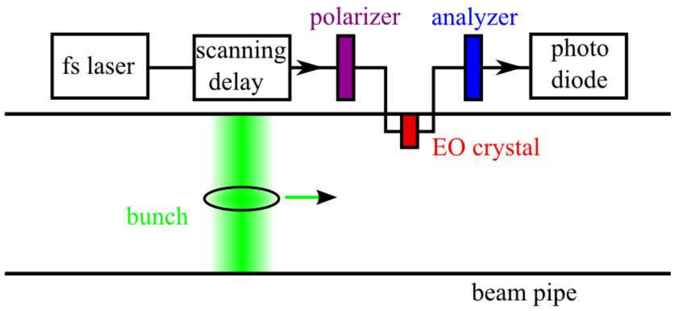

Fig. 46: Schematic drawing of an EOS sampling set-up using crossed polarizers. The laser pulse passes through the polarizer and the electro-optical crystal in the beampipe. In the presence of an electrical field induced by the particle bunch the polarization becomes elliptical. The analyser turns the elliptical polarization into an intensity change which is measured by a photodiode. By changing the delay of the laser pulse, a different longitudinal position of the Coulomb field along the bunch can be probed.

In this scheme a polarized laser beam is scanned along the bunch, and the change in intensity is recorded as a function of the time delay. There exist even more sophisticated schemes with the capability of single-shot resolution like spectrally [192], temporally [193] or spatially [194] resolved detection. More information can be found in Ref. [195].

6.2.4 *Slice emittance diagnostics*

The most state-of-the-art tool for measurement of the slice emittance (and even more) is travelling-wave transverse-deflecting RF structures [196, 197]. Their working principle resembles that of an *intra beam streak camera*.

At FLASH a 3.66 m long vertical-deflecting RF structure (S-band at 2.865 GHz) is operated at zero crossing: a single bunch inside the bunch train, traversing the structure at an appropriate RF phase, experiences a vertical kick which depends linearly on time and vanishes in the bunch centre. As a result of the vertical deflection, the vertical position of the electrons inside this bunch are linearly correlated to their longitudinal coordinates. A fast horizontal kicker deflects the bunch onto an off-axis OTR screen. Figure 47 shows the scheme of the set-up together with measurements.

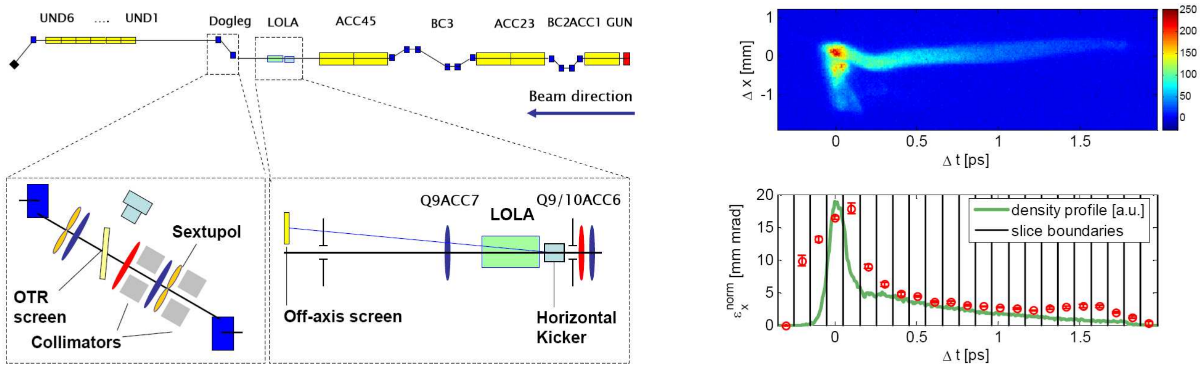

Fig. 47: Left side: Schematic view of the FLASH beamline and a zoom in regions used for measurements. Longitudinal profile and slice emittance are measured with a transverse deflecting RF structure (LOLA) in combination with a horizontal deflecting kicker and an off-axis screen. Right side: Longitudinal phase space distribution measured at FLASH (top) and 1 σ slice emittance (bottom) together with slice boundaries and density profile [198].

The spot at the OTR screen in the vertical direction (in Fig. 47 rotated by 90°) is again a measure of the longitudinal bunch profile. In addition, the OTR image in the horizontal direction contains information about the horizontal beam size, but now for each longitudinal position (Δt) inside the bunch. If the quadrupoles upstream of the structure are scanned and the horizontal beam size in each slice is determined as a function of the quadrupole settings, this technique gives access to the horizontal slice emittance.

In addition, with an OTR screen located in a horizontally dispersive section behind the deflecting structure (left insert in Fig. 47) it is possible to measure the longitudinal phase space distribution directly. More information about this technique can be found in Ref. [198].

6.2.5 *Bunch compression monitor*

For optimization and stabilization of the compression in bunch compressors it is sufficient to detect trends in the bunch lengths rather than to perform precise longitudinal bunch profile measurements. According to Eq. (24) the total radiation intensity increases for shorter bunches, and therefore a frequency-integrated intensity measurement is sufficient for relative measurements of the bunch length for purposes of online optimization.

A simple monitor set-up used in FLASH is shown in Fig. 48(a). Transition or diffraction radiation from a screen is extracted from the vacuum system and transported to a pyroelectric detector via suitable far-infrared optics. The degree of bunch compression is adjusted by changing the acceleration phase of the accelerator module in front of the bunch compressor. A scan of the phase as a function of the intensity measured with the pyroelectric detectors is routinely used to establish the phase set-point as shown in Fig. 48(b). For compression stabilization the detector output signal is even used as input for a feedback

(a) (b)

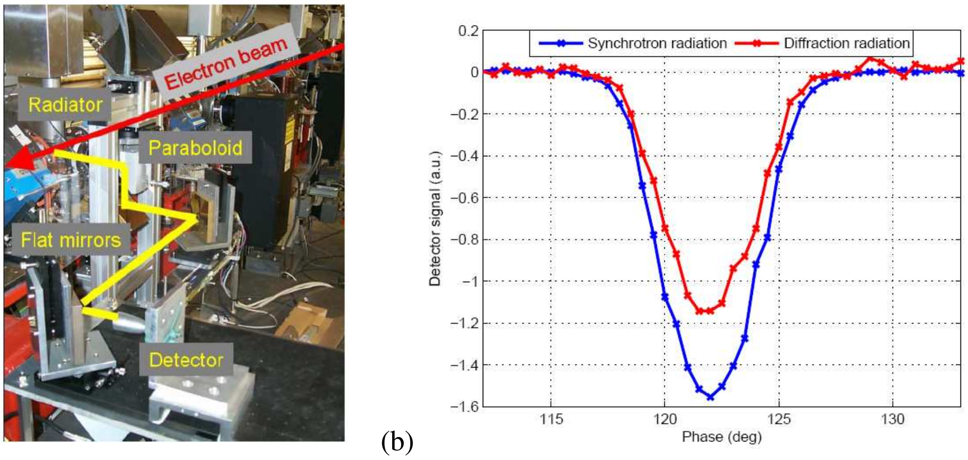

Fig. 48: (a) Bunch compression monitor set-up and (b) phase scan with two bunch compression monitors at FLASH [190]

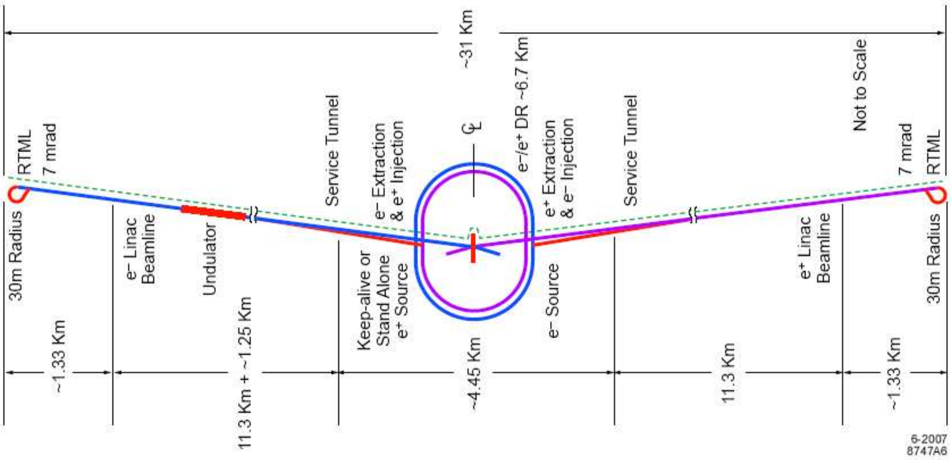

Fig. 49: Schematic layout of the ILC complex for 500 GeV centre-of-mass energy [199]

on the accelerator phase. Reference [190] contains further information about the bunch compression monitor.

7 Outlook

So far diagnostics needs for different hadron and lepton accelerators have been presented. The description covered accelerators in use, machines recently commissioned or at the beginning of their commissioning phase such as the LHC, accelerators still under construction or shortly before, such as the European XFEL, or even machines already shut down, such as LEP and HERA. However, from the beam diagnostics viewpoint each new accelerator represents a new challenge. Therefore, although the LHC is not yet in routine operation, a short insight into future projects will be given: the next accelerator is already appearing on the horizon, namely, the International Linear Collider (ILC).

The ILC will be a linear e^+/e^- collider as was the Stanford Linear Collider, SLC. According to the baseline design [199], the ILC will have a maximum centre-of-mass energy of 500 GeV, peak luminosity of 2×10^{34} cm^{-2} s^{-1} and an overall length of about 31 km. Figure 49 shows a schematic view of the layout together with the major sub-systems. These are

– a polarized electron source based on a photocathode DC gun;

- an undulator-based positron source, driven by the 150 GeV main electron beam;
- 5 GeV electron and positron damping rings with 6.7 km circumference;
- beam transport from the damping rings to the main linacs, followed by a two-stage bunch compressor system prior to injection into the main linac;
- two 11 km long main linacs with 1.3 GHz superconducting RF cavities which operate at an average gradient of about 31.5 MV/m;
- a 4.5 km long beam delivery system which brings both beams under 14 mrad crossing angle into collision, the single interaction point can be shared by two detectors.

To get an impression about beam diagnostics requirements for this machine, Table 2 summarizes the nominal values of the key parameters at the interaction point. As can be concluded from Table 2, beam position stability (i.e., BPMs and feedbacks) and beam profile monitoring systems are particularly challenging. In many cases, individual devices have been built that satisfy the minimum requirements, but these must be integrated into large, highly reliable systems to achieve the required levels of beam monitoring and control. Reference [200] includes a discussion about ILC diagnostics aspects in greater depth.

Table 2: Nominal values of ILC beam parameters at the interaction point [199]

bunch population	2×10^{10}
number of bunches per train	2625
linac bunch interval	369 ns
train repetition rate	5 Hz
train length	~ 970 µs
normalized emittance at IP $\gamma\varepsilon_{x,y}$	10 / 0.04 [mm mrad]
rms beam size at IP $\sigma_{x,y}$	640 / 5.7 [nm]
rms bunch length σ_z	300 µm
power per beam at IP	10.5 MW
luminosity $\mathfrak{L}$	2×10^{34} cm^{-2} s^{-1}

Button or stripline BPMs will be used for applications requiring medium or low resolution of about 10–30 µm rms (single bunch). Cavity BPMs are used for higher resolution applications where few- or sub-micron resolution is required. Three different types operating in C-band, S-band and L-band will be used depending on the needs of different beam pipe apertures, and the L-band cavity monitors must even be operated in the cold environment. There are a variety of research and development activities for ILC BPMs at different laboratories worldwide. Warm cavity BPMs studied at the KEK Accelerator Test Facility (ATF) in Japan have already achieved position resolutions of 8.7 nm for a bunch with 0.68×10^{10} particles over a dynamic range of 5 µm [201].

Different types of beam profile monitors will be used throughout the machine. These include conventional wire scanners, optical beam monitors like OTR or YAG screens, and X-ray synchrotron light diagnostics, e.g., in the damping rings. Most of these instruments rely on the beam interaction with matter, but in the damping rings and downstream areas of the machine, the low emittance would destroy the monitor. Therefore non-invasive profile diagnostics has to be applied. A monitor concept under discussion is the laser wire scanner [202] where a finely focused beam of laser light is scanned across the bunches. The resulting rate of Compton scattered photons is measured downstream in a detector as a function of the laser beam position. Prototype laser wire scanners have been developed at PETRA [203] and ATF [204, 205]. Another non-invasive technique is based on the generation of optical diffraction radiation (ODR). The mechanism is similar to OTR: when a charged particle passes through a slit in a metallic foil, radiation is emitted owing to the interaction of the charge electromagnetic field with the screen surface. Experimental studies of ODR have been performed or are still in progress at ATF [206], APS [207], and at FLASH [208].

To conclude this report the various beam instrumentation systems for the ILC accelerator complex are listed in Table 3 together with their number and some basic requirements according to Ref. [199].

Table 3: Beam instrumentation system installations in the ILC complex [199]. DR: damping rings; RTML: beam transport from damping rings to main linacs; ML: main linacs; BDS: beam delivery systems to IP.

Instrument requirements (e.g., resolution)	**Area** e^- source	e^+ source	DR	RTML	ML	BDS
button/stripline BPM	69	400	2×747			120
resolution (μm)	10–30	10–30	<0.5			<100
C-band cavity BPM (warm)		109		2×649		262
resolution (μm)		<0.1–0.5		<0.1–0.5		<0.1–0.5
S-band cavity BPM (warm)						14
resolution (μm)						<0.1–0.5
L-band cavity BPM (warm)				2×27		42
resolution (μm)				<1–5		<1–5
L-band cavity BPM (cold)				2×28	2×280	
resolution (μm)				∼0.5–2	∼0.5–2	
laser-wire IP	8	20	2×1	2×12	2×3	8
resolution (μm)	<0.5–5	<0.5–5	<0.5–5	<0.5–5	<0.5–5	<0.5–5
wire scanner	12	8				
optical monitor	6	17	2×2	2×8		11
transv. deflecting structure	3	4		2×2		2 (cold)
beam current monitor	7	11	2×1	2×2	2×3	10
beam phase monitor	4	2		2×3		2
BLM	62	420	2×44	2×77	2×335	110
feedback system	5	10	2×2	2×1	2×10	12

Acknowledgements

Many thanks to my DESY colleagues K. Balewski, W. Decking, B. Holzer, M. Hüning, M. Lomperski, J.R. Maidment, D. Nölle, and K. Wittenburg for their stimulating discussions and their help in the preparation of this lecture, and also to A. Peters (Heidelberg Ionenstrahl-Therapie Centrum) for providing me with information on hadron therapy accelerators.

References

[1] U. Amaldi, *The importance of particle accelerators*, Proc. EPAC'00, Vienna, Austria, 2000, p. 3.

[2] G. Amsel, M. Menu, J. Moulin, and J. Salomon, *Nucl. Instrum. Methods Phys. Res.* **B 45** (1990) 296.

[3] W. Wieszczycka and W.H. Scharf, *Proton Radiotherapy Accelerators* (World Scientific, Singapore, 2001).

[4] R. Aymar, *World-wide perspectives in accelerators and the role of CERN*, Proc. EPAC'04, Lucerne, Switzerland, 2004, p. 1.

[5] M.G. Minty and F. Zimmermann, *Measurement and Control of Charged Particle Beams* (Springer Verlag, Berlin, 2003).

[6] P. Strehl, *Beam Instrumentation and Diagnostics* (Springer Verlag, Berlin, 2006).

[7] P. Forck, *Lecture notes on beam instrumentation and diagnostics*, Joint Universities Accelerator School 2006, Archamps, January–March 2006.

[8] A. Hofmann, *The Physics of Synchrotron Radiation* (Cambridge University Press, Cambridge, 2004).

[9] A. Hofmann, *Dynamics of beam diagnostics*, these proceedings.

[10] C. Amsler *et al.*, *Phys. Lett.* **B 667** (2008) 1.

[11] National Institute for Standards and Technology (NIST), *Stopping-power and range tables for electrons, protons, and helium ions*, `http://physics.nist.gov/PhysRefData/Star/Text/contents.html`.

[12] O. Klein and Y. Nishina, *Z. Phys.* **52** (1929) 853.

[13] J.T. Broad and W.P. Reinhardt, *Phys. Rev.* **A 14** (1976) 2159.

[14] V. Danilov, *First steps toward laser stripping implementation*, Proc. EPAC'08, Genoa, Italy, 2008, p. 2955.

[15] G.-A. Voss and B.H. Wiik, *Annu. Rev. Nucl. Part. Sci.* **44** (1994) 413.

[16] R.P. Walker, *Radiation damping* and *Quantum excitation and equilibrium beam properties*, Proc. CERN Accelerator School, Jyväskylä, Finland, 1992, CERN 94-01, Vol 1, pp. 461–80 and pp. 481–498.

[17] L. Rivkin, *Introduction to dynamics of electrons in rings in the presence of radiation*, Proc. CERN Accelerator School, Grenoble, France, 1996, CERN 98-04, p. 45.

[18] L. Criegee *et al.*, *Rev. Sci. Instrum.* **62** (1991) 867.

[19] P.N. Ostroumov, *Review of beam diagnostics in ion linacs*, Proc. LINAC'98, Chicago, IL, 1998, p. 724.

[20] P. Forck, A. Peters, and P. Strehl, *Beam diagnostic for the upgraded UNILAC at GSI*, Proc. EPAC'98, Stockholm, Sweden, 1998, p. 1500.

[21] U. Raich, *Instrumentation in small low energy machines*, Proc. DIPAC'05, Lyon, France, 2005, p. 1.

[22] J.B. Lallement *et al.*, *Measurement strategy for the CERN LINAC4 chopper-line*, Proc. 39th ICFA Advanced Beam Dynamics Workshop, Tsukuba, Japan, 2006, CARE Conf-06-038-HIPPI (2006).

[23] P. Forck and P. Strehl, *Measurements with a versatile test bench for the commissioning of the new GSI high current linac*, Proc. DIPAC'99, Chester, UK, 1999, p. 45.

[24] J.-C. Denard, *Beam current monitors*, these proceedings.

[25] R.C. Webber, *Charged particle beam current monitoring tutorial*, Proc. Beam Instrumentation Workshop BIW'94, Vancouver, Canada, 1994, AIP Conf. Proc. **333**, p. 3, and *Tutorial on beam current monitoring*, FERMILAB-Conf-00-119, June 2000.

[26] G. Gelato, *Beam current and charge measurements*, in CERN-PE-ED 001-92 (revised Nov. 1994), p. 185.

[27] W. Kriens and W. Radloff, *Induktive Lagemessung des umlaufenden Elektronenstrahls im Synchrotron von DESY unter Ausnutzung der 1 MHz-Umlaufstruktur*, DESY S-1 68/1.

[28] G.R. Lambertson, *Electromagnetic detectors*, Proc. 3rd US–CERN School on Particle Accelerators, Anacapri, Isola di Capri, Italy, 1988, Lecture Notes in Physics 343 (Springer Verlag, Berlin, 1989), p. 380.

[29] R.E. Shafer, *Beam position monitoring*, Proc. Accelerator Instrumentation Workshop, Upton, NY, 1989, AIP Conf. Proc. **212**, p. 26.

[30] E. Schulte, *Beam position monitors (pick-ups) and Q measurement*, in CERN-PE-ED 001-92 (revised Nov. 1994), p. 129.

[31] S.R. Smith, *Beam position monitor engineering*, Proc. of Beam Instrumentation Workshop BIW'96, Argonne, IL, 1996, AIP Conf. Proc. **390**, p. 50.

[32] P. Forck, *Beam position monitors*, these proceedings.

[33] C. Bal *et al.*, *Scintillating screens study for LEIR/LHC heavy ion beams*, Proc. DIPAC'05, Lyon, France, 2005, p. 57.

[34] E. Bravin, *Transverse beam profiles*, these proceedings.

[35] R. Jung, *Beam intercepting monitors*, Proc. 3rd US–CERN School on Particle Accelerators, Anacapri, Isola di Capri, Italy, 1988, Lecture Notes in Physics 343 (Springer Verlag, Berlin, 1989), p. 403.

[36] R. Jung, *Beam profile monitors*, in CERN-PE-ED 001-92 (revised Nov. 1994), p. 245.

[37] M. Plum, *Interceptive beam diagnostics – signal creation and materials interactions*, Proc. of Beam Instrumentation Workshop BIW'04, Knoxville, TN, 2004, AIP Conf. Proc. **732**, p. 23.

[38] H. Braun, *Emittance diagnostics*, these proceedings.

[39] K.T. McDonald and D.P. Russell, *Methods of emittance measurement*, Proc. 3rd US–CERN School on Particle Accelerators, Anacapri, Isola di Capri, Italy, 1988, Lecture Notes in Physics 343 (Springer Verlag, Berlin, 1989), p. 122.

[40] M.P. Stockli, *Measuring and analyzing the transverse emittance of charged particle beams*, Proc. of Beam Instrumentation Workshop BIW'06, Batavia, IL, 2006, AIP Conf. Proc. **868**, p. 25.

[41] R.C. Webber, *Longitudinal emittance: An introduction to the concept and survey of measurement techniques including design of a wall current monitor*, Proc. of Accelerator Instrumentation Workshop, Upton, NY, 1989, AIP Conf. Proc. **212**, p. 85.

[42] S.K. Esin *et al.*, *A three dimensional bunch shape monitor for the CERN proton linac*, Proc. LINAC'96, Geneva, Switzerland, 1996, p. 193.

[43] A.V. Feschenko *et al.*, *Bunch shape monitors for the DESY* H^- *linac*, Proc. PAC'97, Vancouver, Canada, 1997, p. 2078.

[44] G. Hemmie and J.R. Maidment, *DESY III, the new proton injector for HERA*, Proc. PAC'87, Washington, D.C., 1987, p. 172.

[45] G. Hemmie *et al.*, *Status of the DESY II project*, Proc. PAC'87, Washington, D.C., 1987, p. 851.

[46] R. Jones and H. Schmickler, *Introduction to beam instrumentation and diagnostics*, Proc. CERN Accelerator School, Zeuthen, Germany, 2003, CERN 2006-002, p. 75.

[47] U. Raich, *Beam diagnostics*, Proc. CERN Accelerator School, Zeegse, The Netherlands, 2005, CERN 2006-012, p. 297.

[48] R. Steinhagen, *Tune and chromaticity diagnostics*, these proceedings.

[49] M. Serio, *Transverse betatron tune measurements*, Proc. 3rd US–CERN School on Particle Accelerators, Anacapri, Isola di Capri, Italy, 1988, Lecture Notes in Physics 343 (Springer Verlag, Berlin, 1989), p. 65.

[50] M. Serio, *Tune measurements*, Proc. CERN Accelerator School, Jülich, Germany, 1990, CERN 91-04, p. 136.

[51] O.R. Sander, *Transverse emittance: Its definition, applications, and measurements*, Proc. of Accelerator Instrumentation Workshop, Upton, NY, 1989, AIP Conf. Proc. **212**, p. 127.

[52] U. Raich, *Beam diagnostics*, Proc. CERN Accelerator School, Sigtuna, Sweden, 2007, CERN-2008-003, p. 361.

[53] A. D'Elia, R. Fandos, and L. Søby, *High bandwidth wall current monitor for CTF3*, Proc. EPAC'08, Genoa, Italy, 2008, p. 1092.

[54] K. Wittenburg, *Beam loss detection*, Proc. 1st European Workshop on Beam Diagnostics and Instrumentation for Particle Accelerators, Montreux, Switzerland, 1993, CERN PS-93-35-BD, pp. 11–20.

[55] R.E. Shafer, *A tutorial on beam loss monitoring*, Proc. of Beam Instrumentation Workshop BIW'06, Upton, NY, 2006, AIP Conf. Proc. **648**, p. 44.

[56] K. Wittenburg, *Beam loss monitors*, these proceedings.

[57] Workshop on *Beam Cooling and Related Topics*, Montreux, Switzerland, 1993, CERN 94-03.

[58] J. Bosser, *Electron cooling*, Proc. CERN Accelerator School, Rhodes, Greece, 1993, CERN 95-06, Vol. 2, p. 673.

[59] F. Caspers, *Schottky signals for longitudinal and transverse bunched-beam diagnostics*, these proceedings.

[60] S. van der Meer, *Diagnostics of Schottky noise*, Proc. 3rd US–CERN School on Particle Accelerators, Anacapri, Isola di Capri, Italy, 1988, Lecture Notes in Physics 343 (Springer Verlag, Berlin, 1989), p. 423.

[61] T. Linnecar, *Schottky beam instrumentation*, in CERN-PE-ED 001-92 (revised Nov. 1994), p. 161.

[62] U. Raich, *Beam-line instrumentation*, in *Beam Measurement*, Proc. of the Joint US–CERN–Japan–Russia School on Particle Accelerators, Montreux, Switzerland, 1998, Eds. S.-i. Kurokawa, S.Y. Lee, E. Perevedentsev, and S. Turner (World Scientific, Singapore, 1998), p. 263.

[63] L. Jensen, *The instrumentation of the TI8 SPS to LHC transfer line*, Proc. DIPAC'05, Lyon, France, 2005, p. 147.

[64] P.J. Bryant, *Beam transfer lines*, Proc. CERN Accelerator School, Jyväskylä, Finland, 1992, CERN 94-01, Vol. 1, pp. 219–38.

[65] C. Bal *et al.*, *LEIR beam instrumentation*, Proc. DIPAC'05, Lyon, France, 2005, p. 258.

[66] C. Bal *et al.*, *Commissioning the beam diagnostics systems for the CERN Low Energy Ion Ring*, Proc. of Beam Instrumentation Workshop BIW'06, Batavia, IL, 2006, AIP Conf. Proc. **868**, p. 445.

[67] P. Strehl, *Diagnostics in heavy-ion machines*, Proc. DIPAC'99, Chester, UK, 1999, p. 28.

[68] R. Jones, *LHC beam instrumentation: Status and challenges*, Proc. of Beam Instrumentation Workshop BIW'06, Batavia, IL, 2006, AIP Conf. Proc. **868**, p. 85.

[69] O.R. Jones, *LHC beam instrumentation*, Proc. PAC'07, Albuquerque, NM, 2007, p. 2630.

[70] A. Peters and P. Forck, *Beam diagnostics challenges in the FAIR project at GSI*, Proc. of Beam Instrumentation Workshop BIW'06, Batavia, IL, 2006, AIP Conf. Proc. **868**, p. 98.

[71] A. Peters and P. Forck, *Innovative beam diagnostics for the challenging FAIR project*, Proc. EPAC'06, Edinburgh, Scotland, 2006, p. 1016.

[72] R.E. Shafer, *Beam Diagnostics at the Fermilab Tevatron*, Proc. PAC'85, Vancouver, Canada, 1985, p. 1862.

[73] V.D Shiltsev, A. Jansson, and R. Moore, *Tevatron instrumentation: Boosting collider performance*, Proc. of Beam Instrumentation Workshop BIW'06, Batavia, IL, 2006, AIP Conf. Proc. **868**, p. 65.

[74] T.J. Shea and R.L. Witkover, *RHIC instrumentation*, Proc. of Beam Instrumentation Workshop BIW'98, Stanford, CA, 1998, AIP Conf. Proc. **451**, p. 145.

[75] P. Cameron *et al.*, *Overview of RHIC beam instrumentation and first experience from operation*, Proc. DIPAC'01, Grenoble, France, 2001, p. 41.

[76] M. Bai *et al.*, *Nucl. Instrum. Methods Phys. Res.* **A 499** (2003) 372.

[77] W. Schütte, M. Wendt, and K.-H. Meß, *The new directional-coupler pick-up for the HERA proton beam position monitoring system*, Proc. PAC'87, Washington, D.C., 1987, p. 1725.

[78] J.-P. Koutchouk *et al.*, *Measurement of the beam position in the LHC main rings*, Functional Specification, LHC-BPM-ES-0004 rev 2.0, 2002.

[79] M. Gasior and R. Jones, *High sensitivity tune measurement by direct diode detection*, Proc. DIPAC'05, Lyon, France, 2005, p. 312.

[80] C.Y. Tan, *Novel tune diagnostics for the Tevatron*, Proc. PAC'05, Knoxville, TN, 2005, p. 140.

[81] R.J. Steinhagen, *Feedbacks on tune and chromaticity*, Proc. DIPAC'07, Venice, Italy, 2007, p. 43.

[82] S. Fartoukh *et al.*, *On the measurement of the tunes, coupling & detuning with momentum and amplitude in the LHC*, Functional Specification, LHC-B-ES-0009 rev 1.0, 2004.

[83] S. Herb, *Betatron tune measurement system for the HERA proton storage ring*, Proc. PAC'91, San Francisco, CA, 1991, p. 1222.

[84] K.-H. Mess, P. Schmüser, and S. Wolff, *Superconducting Accelerator Magnets* (World Scientific, Singapore, 1996).

[85] B.J. Holzer, *Impact of persistent currents on accelerator performance*, Proc. CERN Accelerator School, Hamburg, Germany, 1995, CERN 96-03, p. 123.

[86] F. Willeke and F. Zimmermann, *The impact of persistent current field errors on the stability of the proton beam in the HERA proton ring*, Proc. PAC'91, San Francisco, CA, 1991, p. 2483.

[87] O.V. Afanasyev *et al.*, *A beam shape oscillation monitor for HERA*, Proc. of Beam Instrumentation Workshop BIW'06, Batavia, IL, 2006, AIP Conf. Proc. **868**, p. 534.

[88] P. Forck *et al.*, *Advanced residual gas profile monitor for high current synchrotrons and cooler rings*, Proc. DIPAC'03, Mainz, Germany, 2003, p. 134.

[89] A. Jansson *et al.*, *The Tevatron ionization profile monitors*, Proc. of Beam Instrumentation Workshop BIW'06, Batavia, IL, 2006, AIP Conf. Proc. **868**, p. 159.

[90] R. Bossart *et al.*, *Nucl. Instrum. Methods* **164** (1979) 375.

[91] R. Thurman-Keup, *Proton synchrotron radiation at Fermilab*, Proc. of Beam Instrumentation Workshop BIW'06, Batavia, IL, 2006, AIP Conf. Proc. **868**, p. 364.

[92] G. Kube *et al.*, *Proton synchrotron radiation diagnostics at HERA*, Proc. of Beam Instrumentation Workshop BIW'06, Batavia, IL, 2006, AIP Conf. Proc. **868**, p. 374.

[93] L. Ponce, R. Jung, and F. Méot, *LHC Proton Beam Diagnostics Using Synchrotron Radiation*, CERN-2004-07 (2004).

[94] E. Vogel, *Real time measurements of single bunch phase and length at the HERA proton storage ring and observation of multi bunch oscillations*, DESY Report, DESY-HERA-00-08 (2000).

[95] V. Soloviev *et al.*, *Diagnostic system of longitudinal proton beam dynamics in HERA*, Proc. ICALEPCS'03, Gyeongju, Korea, 2003, p. 480.

[96] M. Hoffmann *et al.*, *The longitudinal coupled bunch feedback for HERA-p*, Proc. EPAC'06, Edinburgh, Scotland, 2006, p. 2985.

[97] R. Johnson, *Absolute luminosity and energy determination in bunched colliding-beam machines*, Proc. 3rd US–CERN School on Particle Accelerators, Anacapri, Isola di Capri, Italy, 1988, Lecture Notes in Physics 343 (Springer Verlag, Berlin, 1989), p. 167.

[98] K. Potter, *Luminosity measurements and calculations*, Proc. CERN Accelerator School, Jyväskylä, Finland, 1992, CERN-94-01, Vol. 1, p. 117.

[99] J. Wenninger, *Luminosity diagnostics*, these proceedings.

[100] A.S. Müller, *Measurements of beam energy*, these proceedings.

[101] R. Schmidt, *Machine protection*, these proceedings.

[102] G.H. Rees, *Overview of future spallation neutron sources*, Proc. PAC'93, Washington, D.C., 1993, p. 3731.

[103] P.J. Bryant, *Synchrotron-driven spallation sources*, Proc. PAC'95, Dallas, TX, 1995, p. 322.

[104] S. Henderson, *Status of the Spallation Neutron Source: machine and science*, Proc. PAC'07, Albuquerque, NM, 2007, p. 7.

[105] A.W. Chao and M. Tigner, *Handbook of Accelerator Physics and Engineering* (World Scientific, Singapore, 2002).

[106] W. Blokland *et al.*, *SNS laser profile monitor progress*, Proc. EPAC'04, Lucerne, Switzerland, 2004, p. 2852.

[107] T.J. Shea *et al.*, *SNS diagnostics*, Proc. of Beam Instrumentation Workshop BIW'00, Cambridge, MA, AIP Conf. Proc. **546**, p. 132.

[108] T.J. Shea *et al.*, *SNS accelerator diagnostics: progress and challenges*, Proc. PAC'01, Chicago, IL, 2001, p. 512.

[109] P. Cameron *et al.*, *Spallation Neutron Source ring diagnostics*, Proc. PAC'03, Portland, OR, 2003, p. 2444.

[110] P.J. Bryant, *Rev. Sci. Instrum.* **73** (2002) 688.

[111] G. Kraft *et al.*, *First patients' treatment at GSI using heavy-ion beams*, Proc. EPAC'98, Stockholm, Sweden, 1998, p. 212.

[112] A. Peters and P. Forck, *Beam diagnostics for the heavy-ion cancer therapy facility*, Proc. of Beam Instrumentation Workshop BIW'00, Cambridge, MA, AIP Conf. Proc. **546**, p. 519.

[113] M. Schwickert and A. Peters, *Computer controlled beam diagnostics for the HICAT facility*, Proc. EPAC'04, Lucerne, Switzerland, 2004, p. 2547.

[114] M. Schwickert and A. Peters, *Diagnostic instrumentation for medical accelerator facilities*, Proc. DIPAC'07, Venice, Italy, 2007, p. 381.

[115] M.E. Biagini *et al.*, *Overview of DAΦNE beam diagnostics*, Proc. EPAC'94, London, UK, 1994, p. 1503.

[116] L. Ma *et al.*, *BEPC beam instrumentation system and its upgrade for BEPC-II*, Proc. APAC'01, Beijing, China, 2001, p. 698.

[117] V. Smaluk, *Accelerator physics issues of the VEPP-4M at low energy*, Proc. EPAC'04, Lucerne, Switzerland, 2004, p. 749.

[118] A.S. Fisher, *Instrumentation and diagnostics for PEP-II*, Proc. of Beam Instrumentation Workshop BIW'98, Stanford, CA, 1998, AIP Conf. Proc. **451**, p. 95.

[119] C. Bovet, *Beam diagnostics for LEP*, CERN/LEP-BI/86-16.

[120] J. Borer, *Instrumentation and diagnostics used in LEP commissioning, with accent on the LEP beam orbit measurement system*, Proc. Accelerator Instrumentation, Batavia, IL, 1990, AIP Conf. Proc. **229**, p. 1.

[121] G. Stange, *IEEE Trans. Nucl. Sci.* **NS-26** (1979) 4146.

[122] G. Mülhaupt, *Ein Kleinspeicherring als Zwischenspeicher für die Positronen-Injektion in PETRA*, DESY Technical Note H2 -76/11 (1976).

[123] J.H.B. Madsen *et al.*, *First experience with the LEP pre-injector (LPI) by the LPI beam commissioning team*, Proc. PAC'87, Washington, D.C., 1987, p. 298.

[124] J.H.B. Madsen *et al.*, *Status report on the LEP pre-injector (LPI) and the proton synchrotron (PS) as e^+e^- accelerator*, Proc. EPAC'88, Rome, Italy, 1988, p. 386.

[125] S. Battisti *et al.*, *Beam instrumentation in the LEP pre-injector*, Proc. PAC'87, Washington, D.C., 1987, p. 570.

[126] A.H. Lumpkin *et al.*, *Results of prototype particle-beam diagnostics tests for the Advanced Photon Source (APS)*, Proc. PAC'93, Washington, D.C., 1993, p. 2112.

[127] V. Schlott, *SLS linac and transfer line diagnostics*, SLS Annual Report, 1999.

[128] K. Hübner, *Hyperfine Interactions* **44** (1988) 167.

[129] *LEP Design Report*, Vol. 1, CERN-LEP/TH/83-29, CERN/PS/DL-83-31, CERN/SPS/83-26, LAL/RT/83-09 (1983).

[130] J.-C. Godot and L. Rinolfi, *A new front-end for the LEP injector linac*, Proc. PAC'91, San Francisco, CA, 1991, p. 2964.

[131] G. Kube, *Sensitivity estimation for the PETRA III beam position monitors based on a boundary element method*, DESY Technical Note 2007-01, 2007.

[132] K. Balewski, *Review of feedback systems*, Proc. EPAC'98, Stockholm, Sweden, 1998, p. 169.

[133] M. Lonza, *Multi-bunch feedback systems*, Proc. CERN Accelerator School, Sigtuna, Sweden, 2007, CERN-2008-003, p. 285, and M. Lonza, these proceedings.

[134] G. Kube *et al.*, *Detailed resolution studies of the synchrotron radiation profile monitor for the HERA electron beam*, DIPAC'05, Lyon, France, 2005, p. 202.

[135] A. Hofmann, *Diagnostics with synchrotron radiation*, Proc. CERN Accelerator School, Brunnen, Switzerland, 2003, CERN-2005-012, p. 295.

[136] M. Wilke, *Optical and X-ray imaging of electron beams using synchrotron emission*, Proc. 6th workshop on beam instrumentation, Vancouver, Canada, 1994, AIP Conf. Proc. **333** (1995), p. 128.

[137] G. Burtin *et al.*, *Adaptive optics for the LEP 2 synchrotron light monitors*, Proc. DIPAC'99, Chester, UK, 1999, p. 77.

[138] A.S. Fisher *et al.*, *Design of the synchrotron-light monitors for PEP-II*, Proc. EPAC'96, Sitges, Spain, 1996, TUP098L, p. 1734.

[139] Å. Andersson *et al.*, *Electron beam profile measurements with visible and X-ray synchrotron radiation at the Swiss Light Source*, Proc. EPAC'06, Edinburgh, Scotland, 2006, p. 1223.

[140] K. Scheidt *et al.*, *Dual streak camera at the ESRF*, Proc. EPAC'96, Sitges, Spain, 1996, TUP031L, p. 1624.

[141] K. Scheidt, *Review of streak cameras for accelerators: Features, applications and results*, Proc. EPAC'00, Vienna, Austria, 2000, p. 182.

[142] B. Yang, *Streak camera 101: Visualizing charged-particle beam dynamics*, Proc. Beam Instrumentation Workshop BIW'06, Batavia, IL, 2006, AIP Conf. Proc. **868**, p. 124.

[143] A.A. Sokolov and I.M. Ternov, *Sov. Phys. Dokl.* **8** (1964) 1203.

[144] L. Arnaudon *et al.*, *Z. Phys.* **C 66** (1995) 45.

[145] R. Klein *et al.*, *Nucl. Instrum. Methods* **A 384** (1997) 293.

[146] A. Bogomyagkov *et al.*, *Precise energy measurements in experiments on VEPP-4M collider*, Proc. PAC'05, Knoxville, TN, 2005, p. 1138.

[147] `http://www.diamond.ac.uk/AboutDiamond/Diamondstep-by-step/default.htm`

[148] A. Ropert, *Lattices and emittances*, Proc. CERN Accelerator School, Grenoble, France, 1996, CERN 98-04, p. 91.

[149] A.Streun, *Lattices for light sources*, Proc. CERN Accelerator School, Brunnen, Switzerland, 2003, CERN 2005-012, p. 55.

[150] C.J. Bocchetta, *Lifetime and beam quality*, Proc. CERN Accelerator School, Grenoble, France, 1996, CERN 98-04, p. 221.

[151] L. Farvacque, *Beam stability*, Proc. CERN Accelerator School, Grenoble, France, 1996, CERN 98-04, p. 287.

[152] G. Decker, *Beam stability in synchrotron light sources*, DIPAC'05, Lyon, France, 2005, p. 233.

[153] R. Bartolini, *Performance and trends of storage ring light sources*, Proc. EPAC'08, Genoa, Italy, 2008, p. 993.

[154] M. Furman, J. Byrd, and S. Chattopadhyay, *Beam instabilities*, in *Synchrotron Radiation Sources - A Primer*, edited by H. Winick (World Scientific, Singapore, 1994), p. 306.

[155] C. Kim, A. Jackson, and A. Warwick, *Beam Lifetime and Beam Brightness in ALS*, Proc. PAC'95, Dallas, TX, 1995, p. 198.

[156] H. Ohkuma, *Top-up operation in light sources*, Proc. EPAC'08, Genoa, Italy, 2008, p. 36.

[157] D. Bulfone, *Overview of fast beam position feedback systems*, Proc. EPAC'08, Genoa, Italy, 2008, p. 1021.

[158] P. Kuske, *Beam diagnostics*, in *Synchrotron Radiation Sources - A Primer*, edited by H. Winick (World Scientific, Singapore, 1994), p. 244.

[159] G. Rehm, *Recent development of diagnostics on 3rd generation light sources*, Proc. EPAC'08, Genoa, Italy, 2008, p. 1016.

[160] A. Lumpkin *et al.*, *Overview of charged-particle beam diagnostics for the Advanced Photon Source (APS)*, Proc. 4th Accelerator Instrumentation Workshop, Berkeley, CA, 1992, AIP Conf. Proc. **281**, p. 150.

[161] G. Rehm and M. Abbott, *Performance of global diagnostics systems during the commissioning of Diamond*, Proc. EPAC'06, Edinburgh, Scotland, 2006, p. 1109.

[162] A. Nadji *et al.*, *Commissioning of the SOLEIL synchroton radiation source*, Proc. PAC'07, Albuquerque, NM, 2007, p. 932.

[163] K. Balewski *et al.*, *The beam diagnostic instrumentation of PETRA III*, Proc. Beam Instrumentation Workshop BIW'08, Lake Tahoe, CA, 2008, to be published.

[164] G. Kube *et al.*, *Overview of the diagnostic systems of PETRA III*, Proc. EPAC'08, Genoa, Italy, 2008, p. 1323.

[165] J.N. Galayda, Y. Chung, and R.O. Hettel, *Orbit stabilization and multibunch feedback systems*, in *Synchrotron Radiation Sources - A Primer*, edited by H. Winick (World Scientific, Singapore, 1994), p. 344.

[166] E.D. Johnson and T. Oversluizen, *Rev. Sci. Instrum.* **60** (1989) 275.

[167] F. Loyer, *X-ray beam position monitors for the ESRF front ends: Design and first results*, Proc. of the First European Workshop on Beam Diagnostics and Instrumentation for Particle Accelerators, DIPAC 1993, Montreux, Switzerland, 1993, CERN-PS-93-35-BD, p 156.

[168] P. Ilinski *et al.*, *Residual gas X-ray beam position monitor development for PETRA III*, Proc. Ninth International Conference on Synchrotron Radiation Instrumentation, Daegu, Korea, 2006, AIP Conf. Proc. **879**, p. 782.

[169] S. Hustache-Ottini, *Photon beamline diagnostics*, these proceedings.

[170] G. Kube, *Review of synchrotron radiation based diagnostics for transverse profile measurements*, Proc. DIPAC'07, Venice, Italy, 2007, p. 6.

[171] J.W. Flanagan *et al.*, *X-ray monitor based on coded-aperture imaging for KEKB upgrade and ILC damping ring*, Proc. EPAC'08, Genoa, Italy, 2008, p. 1029.

[172] T. Mitsuhashi, *Beam profile and size measurement by SR interferometers*, in *Beam Measurement*, Proc. of the Joint US–CERN–Japan–Russia School on Particle Accelerators, Montreux, Switzerland, 1998, Eds. S.-i. Kurokawa, S.Y. Lee, E. Perevedentsev, and S. Turner (World Scientific, Singapore, 1998), p. 399.

[173] S.G. Lipson, H.S. Lipson, and D.S. Tannhauser, *Optical Physics* (Cambridge University Press, Cambridge, 1995).

[174] V. Ayvazyan *et al.*, *Eur. Phys. J.* **D 37** (2006) 297.

[175] H. Schlarb *et al.*, *FLASH upgraded - preparing for the European XFEL*, Proc. FEL'07, Novosibirsk, Russia, 2007, p. 211.

[176] M. Altarelli *et al.* (eds.), *The European X-Ray Free-Electron Laser Technical Design Report*, DESY 2006-097 (2006), `http://xfel.desy.de`.

[177] F. Richard *et al.* (eds.), *TESLA Technical Design Report*, Part 1: Executive Summary, DESY 2001-011 (2001), `http://flash.desy.de/tesla/tesla_documentation/#e1509`.

[178] E.L. Saldin, E.A. Schneidmiller, and M.V. Yurkov, *The Physics of Free Electron Lasers* (Springer Verlag, Berlin, 2000).

[179] M. Ferrario *et al.*, *Recent results and future perspectives of the SPARC project*, Proc. EPAC'08, Genoa, Italy, 2008, p. 2169.

[180] L. Palumbo *et al.*, *Status of the SPARX project*, Proc. EPAC'08, Genoa, Italy, 2008, p. 121.

[181] J. Arthur *et al.* (eds.), *Linac Coherent Light Source (LCLS) Conceptual Design Report*, SLAC-R-593 (2002).

[182] T. Shintake *et al.*, *Status of the SCSS & X-ray FEL project in Japan*, Proc. FEL'07, Novosibirsk, Russia, 2007, p. 216.

[183] V. Schlott *et al.*, *Intra bunch train feedback system for the European X-FEL*, Proc. EPAC'06, Edinburgh, Scotland, 2006, p. 3017.

[184] B. Keil *et al.*, *Design of an intra-bunch-train feedback system for the European X-ray FEL*, Proc. DIPAC'07, Venice, Italy, 2007, p. 232.

[185] R. Brinkmann *et al.* (eds.), *TESLA Technical Design Report*, Part 2: The Accelerator, DESY 2001-011 (2001), `http://flash.desy.de/tesla/tesla_documentation/#e1509`.

[186] J. Feldhaus and S. Nölle, *Beam diagnostics at the VUV-FEL facility*, Proc. EPAC'04, Lucerne, Switzerland, 2004, p. 262.

[187] R. Wilcox *et al.*, *Optical synchronization systems for femtosecond X-ray sources*, Proc. PAC'05, Knoxville, TN, 2005, p. 3958.

[188] J. Kim *et al.*, *An integrated femtosecond timing distribution system for XFELs*, Proc. EPAC'06, Edinburg, Scotland, 2006, p. 2744.

[189] K. Jordan, *FEL-accelerator related diagnostics*, in Proc. Eighth International Topical Meeting on Nuclear Applications and Utilization of Accelerators, AccApp'07, Pocatello, ID, 2007 (American Nuclear Society, La Grange Park, IL, 2007).

[190] O. Grimm, *Coherent radiation diagnostics for short bunches*, Proc. PAC'07, Albuquerque, NM, 2007, p. 2653.

[191] O. Grimm and P. Schmüser, *Principles of longitudinal beam diagnostics with coherent radiation*, TESLA FEL Note 2006-03 (2006).

[192] I. Wilke *et al.*, *Phys. Rev. Lett.* **88** (2002) 124801.

[193] G. Berden *et al.*, *Phys. Rev. Lett.* **93** (2004) 114802.

[194] A.L. Cavalieri *et al.*, *Phys. Rev. Lett.* **94** (2005) 114801.

[195] B. Steffen, *Electrooptic Methods for Longitudinal Bunch Diagnostics at FLASH*, doctoral dissertation, University of Hamburg, Germany, 2007.

[196] G.A. Loew and O. H. Altenmueller, *Design and application of RF separator structures at SLAC*, SLAC Technical Report SLAC-PUB-135 (1965).

[197] P. Emma, J. Frisch, and P. Krejcik, *A transverse RF deflecting structure for bunch length and phase space diagnostics*, LCLS Technical Report LCLS-TN-00-12 (2000).

[198] M. Röhrs, Ch. Gerth, and H. Schlarb, *Investigation of the longitudinal electron bunch structure at the FLASH linac with a transverse deflecting RF-structure*, Proc. FEL'06, Berlin, Germany, 2006, p. 300.

[199] N. Phinney, N. Toge, and N. Walker (eds.), *International Linear Collider Reference Design Report*, Part 3: Accelerator, ILC Global Design Effort and World Wide Study (2007), `http://www.linearcollider.org/cms/?pid=1000437`.

[200] P. Tenebaum, *Beam instrumentation challenges at the International Linear Collider*, Proc. Beam Instrumentation Workshop BIW'06, Batavia, IL, AIP Conf. Proc. **868**, p. 138.

[201] Y. Inoue *et al.*, *Phys. Rev. ST Accel. Beams* **11** (2008) 062801.

[202] I. Agapov, G.A. Blair, and M. Woodley, *Phys. Rev. ST Accel. Beams* **10** (2007) 112801.

[203] A. Bosco *et al.*, *Nucl. Instrum. Methods Phys. Res.* **A 592** (2008) 162.

[204] S.T. Boogert *et al.*, *A laser-wire system at the ATF extraction line*, Proc. EPAC'06, Edinburgh, Scotland, 2006, p. 738.

[205] Y. Honda *et al.*, *Nucl. Instrum. Methods Phys. Res.* **A 538** (2005) 100.

[206] P. Karataev *et al.*, *Phys. Rev. Lett.* **93** (2004) 244802.

[207] A.H. Lumpkin *et al.*, *Phys. Rev. ST Accel. Beams* **10** (2007) 022802.

[208] E. Chiadroni *et al.*, *Nucl. Instrum. Methods Phys. Res.* **B 266** (2008) 3789.